order of 50 degC, e.g. Co in Cu–Co[2] and Ni_3Al in Ni–Al.[11] However, in most systems the structure of the equilibrium precipitate is so different from that of the matrix that heterogeneous nucleation still predominates at undercoolings of the order of several hundred degrees, e.g. $MgZn_2$ in Al–Zn–Mg where only heterogeneous nucleation is apparent at an undercooling of $\sim$ 170 deg C (Fig. 2). Unless the dislocation density is exceptionally high, heterogeneous nucleation leads to a coarse dispersion of precipitates and poor age-hardening properties. Similar arguments apply to many transition precipitates where ΔG_e may again be high. It appears that the majority of alloys are only able to be heat-treated to give a fine " homogeneous " distribution of precipitates because of the role played by G.P. zones. Before considering this role in detail, the components of ΔG_e^{β} must be re-examined. The free-energy change when a β particle is formed in an α matrix is composed of the algebraic sum of the volume free-energy change ΔG_V, the surface free-energy change ΔG_S, and the strain free-energy change ΔG_E

$$\Delta G^{\beta} = \Delta G_V + \Delta G_S + \Delta G_E \qquad \ldots (2)$$

When the alloy is supersaturated, ΔG_V is negative and ΔG_S and ΔG_E are positive. It is possible to consider ΔG^{β} and its components to be made up of two parts: that associated with the bringing together of sufficient B atoms to give the required composition of the β phase and that associated with the change in crystal structure from α to β. The former can be approximately equated with the free-energy change occurring during the formation of G.P. zones $\Delta G^{\text{G.P.}}$, and the latter will be equal to the difference between ΔG^{β} and $\Delta G^{\text{G.P.}}$ which we shall call $\Delta G^{\text{Tr.}}$.

We now consider the application of classical nucleation theory to G.P. zone formation. This is best accomplished using the concept of the metastable solvus line on an equilibrium diagram (Fig. 3). This idea has been discussed extensively by Borelius and his co-workers[12,13] and by Gerold[14] and has been used empirically for the interpretation of many phenomena in precipitation-hardening.[15] For G.P. zones, the metastable phase boundary is identical to the coherent phase boundary derived theoretically by Cahn.[16] A given alloy therefore has a solvus temperature, T_{β}, below which the solid solution becomes metastable with respect to the β phase and a G.P. zone solvus temperature, $T_{\text{G.P.}}$, below which the solid solution is also metastable with respect to G.P. zones. The nucleation rate for G.P. zones is given by

$$I_{\text{G.P.}} = K_2 \exp\left(-\frac{\Delta G^{\text{G.P.}}}{kT}\right) \exp\left(-\frac{Q_m}{kT}\right) \qquad \ldots (3)$$

where K_2 again includes the vacancy concentration (which will depend sensitively on the quenching treatment). Since $\Delta G^{\text{G.P.}} < \Delta G^{\beta}$, nucleation is easier than for the β precipitate and a detectable rate of homogeneous nucleation will occur at undercoolings below $T_{\text{G.P.}}$ of the order of 10–20 degC. Heterogeneous nucleation of G.P. zones is therefore unimportant. Cahn[16] has shown that spinodal decomposition occurs at the spinodal line to the coherent phase boundary and it is possible that G.P. zone formation occurs by spinodal decomposition. However, whether G.P. zones form by spinodal decomposition or by nucleation and growth is not important in the present situation, since even in the former case Rundman and Hilliard[17] have shown that some undercooling is necessary before the transformation occurs at an appreciable rate and hence the rate of formation of G.P. zones will be qualitatively similar in both cases. There are two models for G.P. zone formation due to Gerold[18] and to Guinier[19] (Fig. 4). Most of the experimental evidence supports Gerold's model[15] and we shall use it in the present paper. However, the results are not affected qualitatively by the adoption of the Guinier model.

We now consider the relation between G.P. zone formation and the nucleation of the β precipitate. There are many references in the literature concerning the possible nucleation of β precipitates by G.P. zones, e.g. Hardy[20] and Rosenbaum and Turnbull,[21] but the present ideas are believed to be original in the sense that this point is now considered in relation to the ageing temperatures and the G.P. zone solvus temperature. If an alloy is quenched and aged for a time t_1 at a temperature T_1, below $T_{\text{G.P.}}$, G.P. zones will form and grow and their size distribution will be a time- and temperature-dependent function $N(d)_{T_1,t_1}$. If the Gerold model of G.P. zones is correct (and this is consistent with the kinetic results of Turnbull[22]), the size distribution will be determined by the process of particle coarsening (Ostwald ripening[23]) and the number of zones will decrease while their average size increases (Fig. 5).

If the alloy is now up-quenched to a temperature T_2 above $T_{\text{G.P.}}$, the G.P. zones are unstable with respect to the α solid solution and will dissolve in the same way that β particles dissolve when the temperature is raised above T_{β}. However, there is some hysteresis in the phase change because of the necessity for diffusion to occur to disperse the solute-rich G.P. zones. During this period the alloy contains a number of solute-rich clusters (the dissolving G.P. zones) which are far larger than the transient segregates expected in the quasi-steady-state distribution used for the determination of equation (1). Those segregates that exceed the critical nucleus size can therefore act as nuclei for the β precipitate, requiring only part of the normal activation energy $\Delta G^{\text{Tr.}}$ since the change in composition has already been carried out under equilibrium conditions at T_1; the remaining zones which do not exceed the critical size will dissolve. The resulting nucleation rate is of the form

$$I_{\beta} = K_3 f[N(d)_{T_1,t_1}] \exp\left(-\frac{\Delta G_e^{\text{Tr.}}}{kT}\right) \exp\left(-\frac{Q_m'}{kT}\right) f(t_2/\tau) \qquad \ldots (4)$$

where K_3 again contains the vacancy concentration and $f[N(d)_{T_1,t_1}]$ is some function of the G.P. zone size distribution. The parameter $\exp(-Q_m'/kT)$ arises because atom movement is required within the G.P. zone for the atoms to take up the required crystal structure; Q_m is the activation energy for this process, which is probably similar to the activation energy for solute migration. The parameter $f(t_2/\tau)$ describes the limited period of existence of the alloy in the segregated condition when it is above $T_{\text{G.P.}}$; τ is a temperature-dependent constant and t_2 is the time at T_2. When t_2 is small, i.e. immediately after up-quenching, $f(t_2/\tau) \sim 1$ and equation (4) predicts a nucleation rate which is far greater than that given by equation (1), since $\Delta G_e^{\text{Tr.}}$ is probably of the order of $\Delta G_e^{\beta}/2$. The G.P. zones have effectively " seeded " the transformation to β. As the time at T_2 increases, the nucleation rate declines to that given by equation (1), but all the particles nucleated previously will grow to give a fine dispersion which appears " homogeneous " but is, in fact, dependent on the previous distribution of G.P. zones and

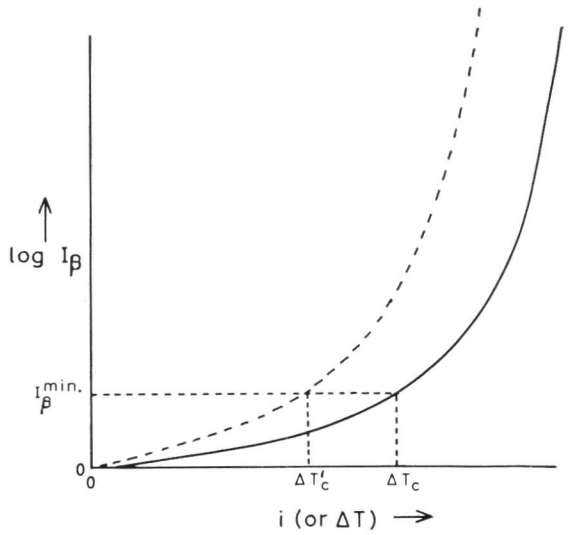

Fig. 1 A schematic illustration of the variation in nucleation rate of the β phase with undercooling. The full line is for a material with the equilibrium concentration of vacancies and the broken line for an alloy with excess vacancies introduced by quenching. The same curves are applicable to $I_{G.P.}$ for undercooling below $T_{G.P.}$

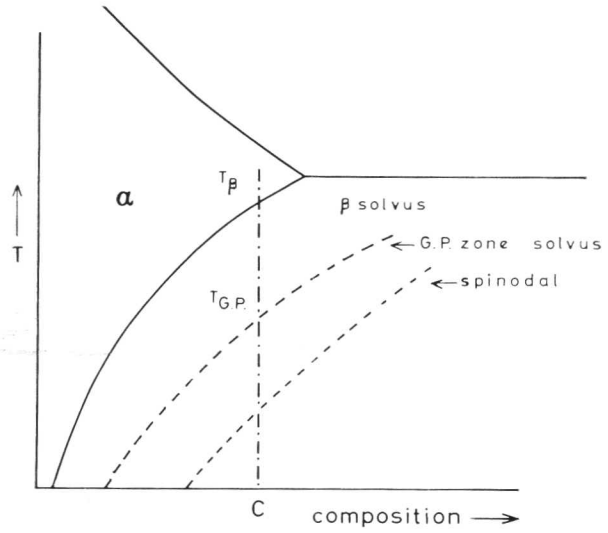

Fig. 3 Showing the β solvus, the G.P. zone solvus, and the coherent spinodal lines for the hypothetical system A–B.

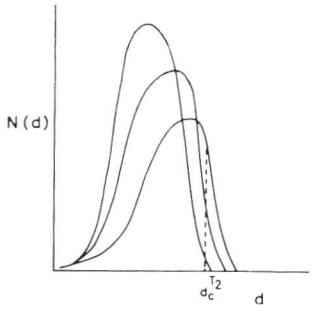

Fig. 5 Showing the variation of G.P. zone-size distribution with ageing time (schematic).

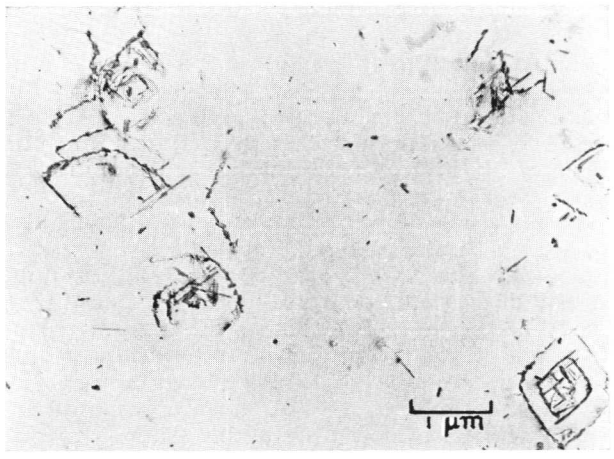

Fig. 2 Micrograph showing only heterogeneous nucleation of the η($MgZn_2$) phase in an Al–Zn–Mg alloy with an undercooling of ~ 170 degC.

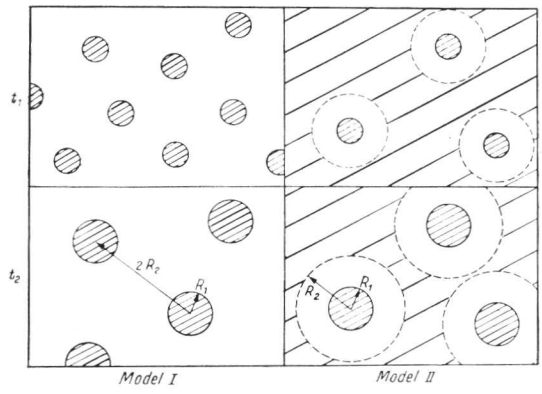

Fig. 4 A schematic illustration of the variation of G.P. zone size with ageing time for Model I (Gerold[18]) and Model II (Guinier[19]).

might more accurately be called " homogeneously distributed ".

In the present paper it is necessary to make a series of simplifying assumptions concerning the use of equation (4). The value of $\Delta G_c^{Tr.}$ for a particular size of G.P. zone and hence the probability of forming a β precipitate from the zone is likely to be a function of the zone size and composition; equally Q_m' may well depend on the defect concentration in the zone. However, we will assume that only zones with a size greater than a certain critical diameter $d_e^{T_2}$ at the first ageing temperature T_1 are able to transform and grow into β precipitates at the second ageing temperature T_2. Furthermore, $d_e^{T_2}$ will be equated with the critical nucleus size at T_2 according to the classical nucleation theory expressed in equation (1). Then the number of β nuclei N_β will be given by

$$N_\beta = \sum_{d_c^{T_2}}^{\infty} N(d)_{T_1,t_1} \cdot \Delta d \qquad \ldots (5)$$

where $N(d).\Delta d$ is the number of G.P. zones having sizes in the range $d \pm \Delta d/2$. As T_2 is increased above $T_{G.P.}$ towards T_β, $d_e^{T_2}$ will become larger and hence the number of β nuclei for a given treatment at T_1 will become fewer. Equally, as the time at T_1 is increased or as T_1 is increased while re-

maining below $T_{G.P.}$, $\sum_{d_c^{T_2}}^{\infty} N(d)_{T_1,t_1}\,\Delta d$ increases and hence the density of precipitates on up-quenching to T_2 increases (Fig. 5).

Clearly the transformation of a G.P. zone to a β precipitate is not a process that is confined to temperatures above $T_{G.P.}$ This reaction can occur isothermally with a nucleation frequency given by equation (4), except that the term $f(t_2/\tau)$ is no longer required since the G.P. zones are stable at the transformation temperature. However, isothermal transformation is difficult because of the lower value of $\exp(-Q'_m/kT)$. If the alloy is up-quenched, the atomic rearrangement process becomes increasingly easy but $d_c^{T_2}$ becomes larger, and above $T_{G.P.}$ there is only a limited time for the nucleation of β to take place by this mechanism before the zones dissolve. There is therefore an optimum temperature for β nucleation (Fig. 6) which is normally above $T_{G.P.}$.

In summary, therefore, the proposed model has the following important characteristics:

(1) G.P. zones that have formed below $T_{G.P.}$ can act as β precipitate nuclei above $T_{G.P.}$ if they are larger than $d_c^{T_2}$.

(2) Isothermal transformation of G.P. zones to β precipitates can take place below $T_{G.P.}$.

(3) The time required for isothermal transformation to β below $T_{G.P.}$ is normally longer than that needed to grow G.P. zones to a size greater than $d_c^{T_2}$ so that they can act as β precipitate nuclei above $T_{G.P.}$.

(4) The longer the treatment below $T_{G.P.}$, the larger will be the number of G.P. zones that achieve $d_c^{T_2}$ and can act as nuclei at a given ageing temperature T_2 above $T_{G.P.}$. Quenched-in vacancies play an important role since they determine the total diffusive flux below $T_{G.P.}$ and hence the G.P. zone-size distribution before up-quenching.

(5) The higher the second ageing temperature T_2 (above $T_{G.P.}$), the fewer will be the number of G.P. zones that reach a sufficient size to act as precipitate nuclei.

(6) Since only a small proportion of G.P. zones act as nuclei and the remainder will dissolve, the hardness of the alloy falls corresponding to the well-known phenomenon of reversion.[15,24]

Most alloys are given a simple treatment of the following type: solution-treat above T_β → quench to a low temperature and hold for a variable time at that temperature → age at a high temperature below T_β. On the basis of the proposed model it is worth while classifying alloys into three types:[7] (*a*) alloys in which the quench-bath temperature and the ageing temperature are both above $T_{G.P.}$, e.g. Al–Mg; (*b*) alloys in which the quench-bath temperature and the ageing temperature are both below $T_{G.P.}$, e.g. Cu–Co, Ni–Al, Al–Mg–Si; (*c*) alloys in which $T_{G.P.}$ lies between the quench-bath temperature and the ageing temperature. Although our model is applicable to all three cases, we shall concentrate on class (*c*) in the present paper.

Results

The Determination of $T_{G.P.}$

$T_{G.P.}$ was determined for the Al–Cu alloy by direct quenching to the ageing temperature by heat-treatment (*a*) in Fig. 7. The rapid increase in homogeneously distributed θ″ precipitate as T_2 is decreased is shown in Fig. 8. Figs. 8(*b*), (*c*), and (*d*) correspond to ageing at increasing undercooling below $T_{G.P.}$ (Fig. 1) leading to an increasing rate of nucleation of G.P. zones followed by their isothermal transformation to θ″. $T_{G.P.}$ was identified as 160° C.

A similar experiment was carried out for Al–Ge alloy (Fig. 9) and $T_{G.P.}$ was identified as 80° C. However, if the quenching rate was increased by quenching into water, appreciable homogeneous nucleation occurred on quenching to 100° C, indicating some quench-rate-dependence of the apparent value of $T_{G.P.}$ This is readily explained by reference to equation (4) and Fig. 1. The parameter K_2 in equation (3) depends on the vacancy concentration. The more rapid the quenching rate, the greater the number of excess vacancies retained and the larger the value of K_2; hence the value of $I_{G.P.}$ is greater at a given undercooling (Fig. 1). Since we are measuring the undercooling at which a given nucleation rate occurs, this will depend on the quenching rate. We are able to approach the true value of $T_{G.P.}$ only by faster and faster quenching and the values quoted above are effectively values of $T'_{G.P.}$, which is $T_{G.P.}$ less an unspecified amount of undercooling ΔT_c of the order of 10–20 degC. This is consistent with the value of $T'_{G.P.}$, 160° C for Al–Cu, which is 15 degC less than the value of 175° C given by Beton and Rollason[24] from reversion experiments. A similar variation of $T'_{G.P}$ with quenching rate has been found by Pashley *et al.*[8] for Al–Mg–Si. This explanation in terms of the effect of excess vacancies on the pre-exponent in equation (3) is equally applicable if G.P. zone formation occurs by spinodal decomposition, since the position of the C curve on the time axis will also be determined by the atom mobility.[17]

An attempt to measure $T_{\theta''}$ in Al–Cu by the direct-quenching technique was not successful because θ″ apparently cannot be nucleated homogeneously above $T_{G.P.}$, i.e. the critical undercooling for θ″ is greater than $T_{\theta''} - T_{G.P.} \simeq 50$ degC. If the alloy was given heat-treatment (*a*) (Fig. 7) at any temperature above $T_{G.P.}$, only heterogeneous nucleation of θ′ was observed (Fig. 8(*a*)).

Multiple-Ageing Treatments

If heat-treatment (*b*) (Fig. 7) is used, the number of precipitates that nucleate and grow at T_2 increases for increasing time t_1 at T_1. This has been shown for Al–Zn–Mg alloys[7] and Fig. 10 shows the same effect for Al–Ge. This type of treatment leads to the highest density of Ge precipitates.

Similar results were obtained for the G.P. zone → θ″ transformation in Al–Cu and an attempt was made to perform the same experiment for the θ″ → θ′ transformation after first nucleating the θ″ precipitate with G.P. zones. However, specimens up-quenched from < 210° C ($T_{\theta''}$) to higher temperatures showed complete reversion, with all the θ″ precipitates dissolving followed by heterogeneous nucleation of θ′ on dislocations. This is presumably due to the fact that none of the θ″ particles reached $d_c^{T_2}$ during the treatment at T_1. If the specimens were held at T_1 for a longer time in an attempt to reach $d_c^{T_2}$, isothermal transformation of θ″ → θ′ took place. We interpret this result as indicating that the maximum nucleation frequency for the θ″ → θ′ transformation (Fig. 6) occurs below $T_{\theta''}$.

Grain-Boundary Effects

The structure near grain boundaries is affected by the vacancy concentration gradient caused by quenching from the solution-treatment temperature. This causes a diffusivity gradient which, as already mentioned, leads to a variation of the G.P. zone-size distribution $N(d)$ with distance from the grain boundary.[7,10,26] At a certain point for given values of t_1, T_1, and T_2, $\sum_{d_c^{T_2}}^{\infty} N(d)_{T_1,t_1}\,\Delta d \simeq 0$ and no precipitates will be nucleated at T_2. This point corresponds to the edge

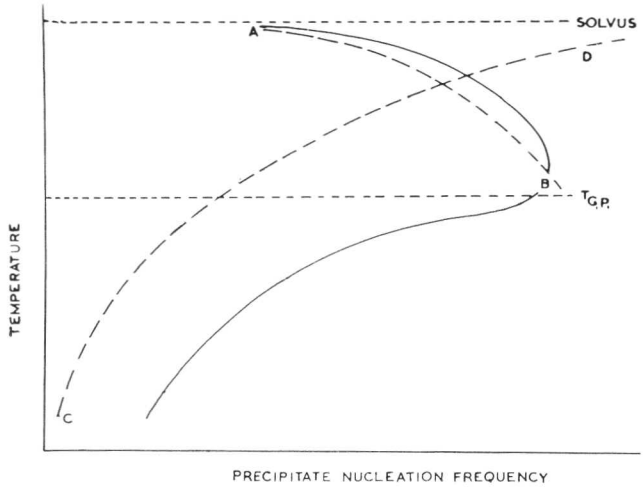

Fig. 6 A schematic illustration of the overall variation of β nucleation frequency as a function of temperature. The shape of the curve is compounded of the line AB indicating a decreasing frequency due to the increasing value of $d_c^{T_2}$ with increasing T_2, and a line CD indicating the increasing ease of the G.P. zone → β transformation as the atom mobility increases.

of the precipitate-free zone (P.F.Z.), (Fig. 11(*a*)) and approaches the grain boundary as t_1 and T_1 are increased.[7,10] G.P. zones formed within the P.F.Z. will dissolve when the

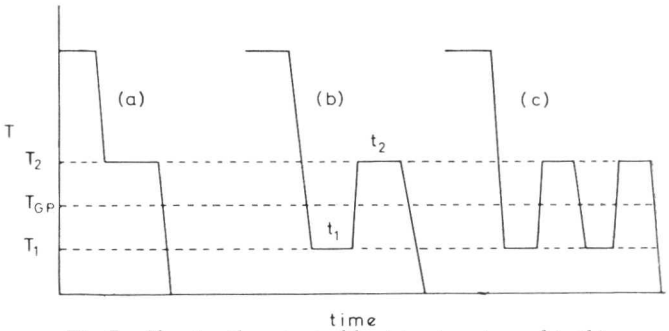

Fig. 7 Showing three typical heat-treatments used in this investigation.

temperature is raised to T_2 and hence a supersaturated solid solution will be re-formed. However, a further ageing period below $T_{G.P.}$, (treatment (*c*), Fig. 7) will cause the G.P. zones to form again and if this treatment is sufficiently prolonged, $d_c^{T_2}$ will be exceeded within the P.F.Z. and new precipitates are nucleated.[5,7] A similar type of treatment is illustrated in Fig. 11(*b*) for Al–Cu.

Comparison with Other Theories

The present theory is consistent with the ideas of Taylor[4] and Holl[5,9] and is essentially a detailed development of earlier papers by the present authors.[3,7] Holl[9] has particularly emphasized the importance of the defect concentration in the G.P. zones in determining the value of $d_c^{T_2}$.

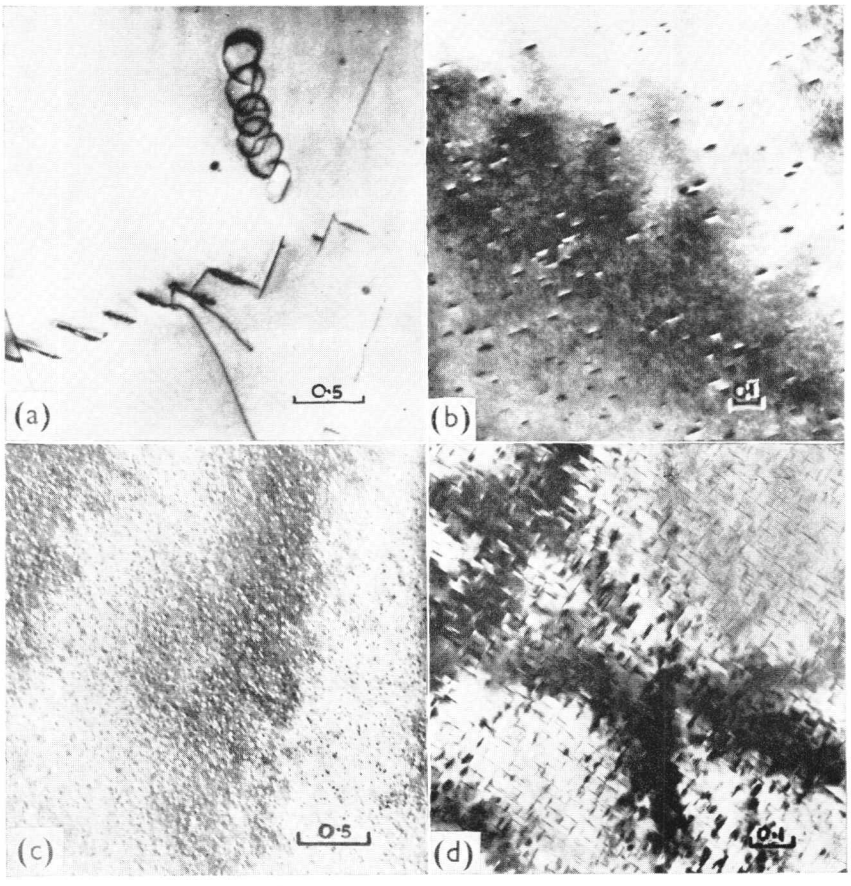

Fig. 8 Micrographs of Al–Cu specimens direct-quenched and aged at (a) 210, (b) 160, (c) 155, (d) 150° *C. Note heterogeneous precipitation of* θ′ *in* (a) *and increasing fineness of* θ″ *precipitate in* (b), (c), *and* (d).

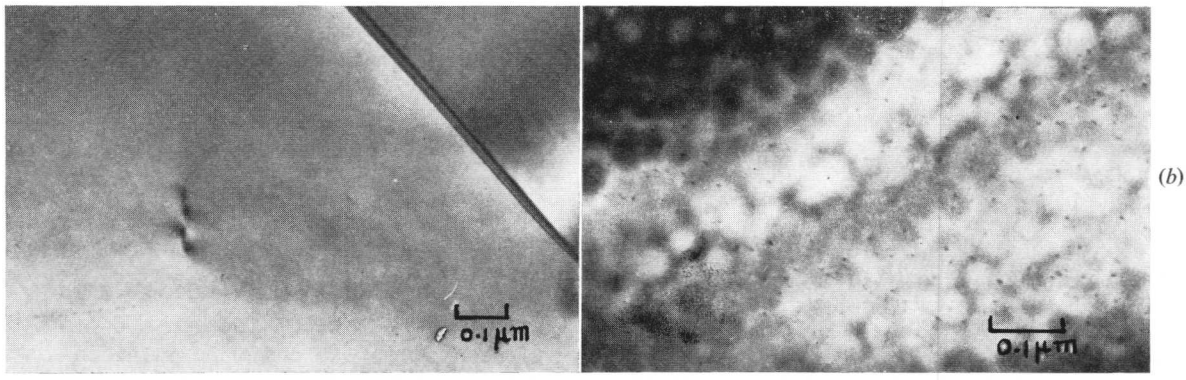

Fig. 9 *Micrographs illustrating the quench-rate-dependence of* $T'_{G.P.}$ *for Al–Ge.* (a) *Oil-quenched and aged at* 100° *C; no precipitates.* (b) *Water-quenched and aged at* 100° *C; precipitates visible.*

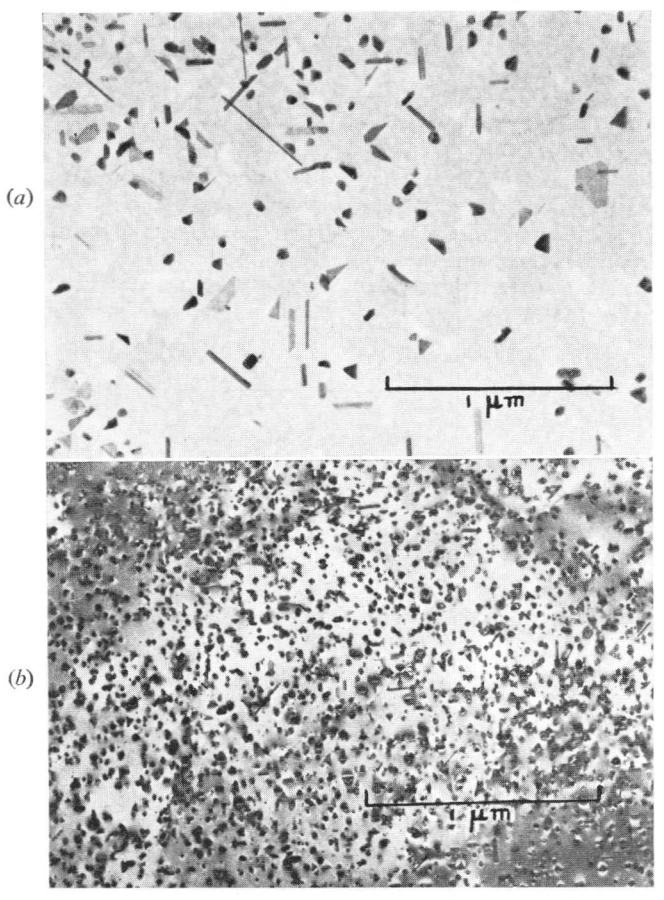

Fig. 10 *Micrographs illustrating the refinement of precipitate that can be achieved in Al–Ge by prolonged ageing below* $T_{G.P.}$ (a) *Water-quenched and aged immediately for* 5 *h at* 170° *C.* (b) *Water-quenched and aged for* 2 *h at* 50° *C followed by* 5 *h at* 170° *C.*

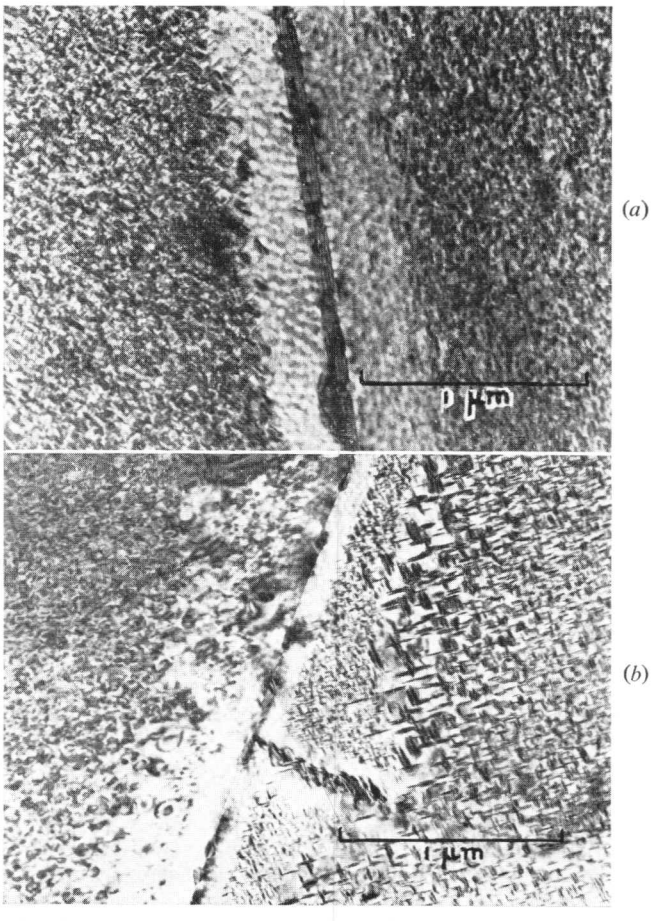

Fig. 11 *Micrographs illustrating the use of a second low-temperature ageing treatment to provide nuclei within a P.F.Z. in Al–Cu.* (a) *Water-quenched and aged immediately for* 5 *h at* 170° *C.* (b) *Water-quenched and aged successively for* 5 *h at* 170° *C and* 6 *h at* 140° *C.*

The only other theory that deals with the complexities arising from multiple heat-treatments is that of Pashley and his co-workers.[6,8] This theory has been described as " kinetic " by those authors, compared with the present " thermodynamic " theory. Such a distinction is artificial since any theory of precipitation must involve both thermodynamics and kinetics. Although the present theory starts from a similar thermodynamic basis to classical nucleation theory, the formation of particles is necessarily a kinetic process and equations (1)–(4) can equally well be written in terms of the atomic mechanism of precipitation, i.e. in terms of atoms leaving and joining the particles. In reality, the principal differences between Pashley's theory and the one presented in this paper are that, in the former, the critical temperature T_c is not identified with $T_{G.P.}$ and no transformation from G.P. zones to β is considered. Pashley *et al.*[8] have suggested that there are two facts explained by their theory which that of Lorimer and Nicholson[7] does not cover: the quench-rate sensitivity of $T_{G.P.}$ or T_c and the possibility of a coarsening of the normal precipitate distribution rather than a refinement for certain multiple heat-treatments. The present paper gives an explanation for the first point in terms of our theory and the second point can also be adequately explained, as will be described elsewhere. When two theories give adequate interpretations of such a large number of experimental facts, it is natural to enquire whether they are not different ways of expressing the same fundamental idea. We will now examine this possibility.

Both theories involve a special temperature. In our case it is the G.P. zone solvus temperature $T_{G.P.}$; in Pashley's case it is T_C, defined as " the temperature above which homogeneous self-nucleation of clusters does not occur ". However, G.P. zones can be identified as stable clusters of solute atoms and hence T_C is simply the highest temperature for homogeneous nucleation of G.P. zones, i.e. $T_C = T_{G.P.} - \Delta T_C = T'_{G.P.}$, where ΔT_C is the critical undercooling necessary to give homogeneous nucleation of G.P. zones. Thus, despite the remarks in the paper by Pashley *et al.*,[8] the two temperatures are equivalent, but the fundamental temperature is $T_{G.P.}$ and the higher the vacancy supersaturation the more nearly is this approached in direct-quenching experiments. T_C is simply equal to $T_{G.P.}$ less the critical undercooling for an atom mobility corresponding to the equilibrium vacancy concentration.

Turning to the interpretation of the results of double-ageing experiments, Pashley *et al.*[8] assume the Guinier model of G.P. zone formation (Fig. 4) at T_1 and suggest that clusters formed at T_1 will grow at T_2 if (using the present notation)

$$d \ln i > K_4 \qquad \ldots (6)$$

where K_4 is the coefficient of the Gibbs–Thomson equation, d is the cluster size at T_1, and i is the supersaturation at T_2. Equation (6) arises from requiring a sufficient supersaturation remaining at T_1 to overcome the Gibbs–Thomson effect when the alloy containing the small clusters is suddenly up-quenched to T_2. In this respect the theory is similar to the theory of reversion of Konobeevsky.[27] There is now ample evidence to prove that this theory is incorrect and that reversion can be readily interpreted in terms of metastable solvus lines.[15] In the same way, it seems likely that the effect considered by Pashley *et al.*[8] (equation (6)) is small compared with the temperature-dependence of i arising from the variation in solid solubility with temperature which is an exponential function of temperature.[28] Thus, on the arguments now presented G.P. zones become unstable simply when $i_{G.P.} < 1$ although $i_\beta > 1$ and hence transformation from G.P. zones to β is possible before the G.P. zones dissolve. In the case not discussed in the present paper when $T_2 < T_{G.P.}$ and hence $i_{G.P.} > 1$ at T_2, the behaviour of the alloy is still mainly determined by the temperature-dependence of the solid solubility in equilibrium with G.P. zones and the Gibbs–Thomson effect considered by Pashley *et al.* is of less significance. However, the effects would normally appear to be additive and this explains why the two theories so frequently give qualitatively the same result when applied to multiple-ageing treatments.

Conclusions

(1) A new theory of precipitate nucleation has been developed in which the basic feature is the ability of G.P. zones that are formed at low temperatures to act as nuclei for precipitates during ageing. The theory explains a number of important observations on the precipitation behaviour of alloys, e.g.

(*a*) the importance of the G.P. zone solvus temperature;
(*b*) the effect of excess vacancies on precipitate nucleation;
(*c*) the observation of precipitate-free zones at grain boundaries;
(*d*) the response of alloys to double-ageing treatments;
(*e*) the sensitivity of alloys to small changes in heat-treatment.

(2) The theory has been compared with the ideas suggested by Pashley *et al.*[6,8] and it has been shown that although the two theories make qualitatively similar predictions in many cases (accounting for the difficulty in performing critical experiments to test the two theories), the effects described in the present paper are likely to be more important in most practical cases.

References

1. J. W. Christian, " The Theory of Transformations in Metals and Alloys ". **1965:** Oxford, &c. (Pergamon Press).
2. I. S. Servi and D. Turnbull, *Acta Met.*, 1966, **14,** 161.
3. J. D. Embury and R. B. Nicholson, *ibid.*, 1965, **13,** 403.
4. J. L. Taylor, *J. Inst. Metals*, 1963–64, **92,** 301.
5. H. A. Holl, *ibid.*, 1964–65, **93,** 364.
6. D. W. Pashley, J. Rhodes, and A. Sendorek, *ibid.*, 1966, **94,** 41.
7. G. W. Lorimer and R. B. Nicholson, *Acta Met.*, 1966, **14,** 1009.
8. D. W. Pashley, M. H. Jacobs, and J. T. Vietz, *Phil. Mag.*, 1967, **16,** 51.
9. H. A. Holl, *Metal Sci. J.*, 1967, **1,** 111.
10. G. W. Lorimer, Ph.D. Thesis, Cambridge University, **1968.**
11. A. J. Ardell and R. B. Nicholson, *Acta Met.*, 1966, **14,** 1295.
12. G. Borelius, J. Andersson, and K. Gullberg, *Ing. Vetenkaps Akad. Handl.*, 1943, **10,** 169.
13. G. Borelius and L. E. Larsson, *Arkiv Fysik*, 1956, **11,** 137.
14. V. Gerold, *Aluminium*, 1961, **37,** 583.
15. A. Kelly and R. B. Nicholson, *Progress Mat. Sci.*, 1963, **10,** 151.
16. J. W. Cahn, *Acta Met.*, 1962, **10,** 907.
17. K. B. Rundman and J. E. Hilliard, *ibid.*, 1967, **15,** 1025.
18. V. Gerold and W. Schweizer, *Z. Metallkunde*, 1961, **52,** 76.
19. A. Guinier, *Solid State Physics*, 1959, **9,** 294.
20. H. K. Hardy, *J. Inst. Metals*, 1948–49, **75,** 707.
21. H. S. Rosenbaum and D. Turnbull, *Acta Met.*, 1959, **7,** 664.
22. D. Turnbull, *Solid State Physics*, 1956, **3,** 226.
23. C. Wagner, *Z. Elektrochem.*, 1961, **65,** 581.
24. M. L. V. Gayler, *J. Inst. Metals*, 1922, **28,** 213.
25. R. H. Beton and E. C. Rollason, *ibid.*, 1957–58, **86,** 77.
26. P. N. T. Unwin, G. W. Lorimer, and R. B. Nicholson, to be published.
27. S. T. Konobeevsky, *J. Inst. Metals*, 1943, **69,** 397.
28. W. Hume-Rothery, " Elements of Structural Metallurgy ". **1961:** London (Inst. Metals).

The Factors Controlling the Width of Precipitate-Free Zones at Grain Boundaries in Al–Zn

M. H. Jacobs and D. W. Pashley

Samples of Al–17·5 wt.-% Zn have been given a variety of heat-treatments which have involved either (1) direct quenching to the ageing temperature or (2) a two-step ageing treatment. Pronounced precipitate-free zones at grain boundaries were observed in samples, given either type of heat-treatment, when examined in an electron microscope. Two theoretical models are described, each based on the "kinetic" model, to account for the factors controlling the widths of the precipitate-free zones in both cases. There is excellent qualitative agreement between the predictions of the models and the experimental observations. The concept of a critical temperature for homogeneous nucleation is discussed and its interpretation, in terms of the "kinetic" model, contrasted with that of the, alternative, "thermodynamic" model.

The influence of two-step ageing treatments on the formation and distribution of precipitates in aluminium alloys has recently received much attention, and two models have been put forward to explain the observed behaviour. Nicholson and co-workers[1,2] have based their model on the concept that G.P. zones formed during an ageing treatment at T_1 will act as seeds for growth at a higher temperature T_2, even if T_2 is greater than the maximum temperature for self-nucleation of precipitates. This can occur provided the zones are above a certain critical size for spontaneous transformation to a more stable intermediate precipitate. According to this model, therefore, the thermodynamic stability of zones and intermediate precipitates is the main controlling influence. Pashley and co-workers,[3,4] on the other hand, have based an alternative model on the kinetic factors controlling the ability of clusters, nucleated at T_1, to grow at T_2.

For convenience, we will refer to these two models as the "thermodynamic" and "kinetic" models, respectively, although both models involve both thermodynamic and kinetic considerations. An important difference between the concepts involved in the two models concerns the interpretation of the critical temperature. According to the thermodynamic model,[2] G.P. zones fail to nucleate above a certain temperature, which is determined directly by the metastable G.P.-zone solvus.[5,6] According to the kinetic model,[4] self-nucleation of precipitates does not occur above a certain critical temperature T_c, because of inadequate solute supersaturation.

The original development of the kinetic model was based upon studies of the Al–1·2% Mg_2Si alloy. Similar studies have now been made with Al–17·5% Zn, and this paper shows how the kinetic model can be used to explain the results. In addition to dealing with the effect of two-step ageing on precipitation within the grains, the thermodynamic model has been used to explain the existence of precipitate-free zones (p.f.z's) at grain boundaries.[2] Pronounced p.f.z's are observed with the Al–17·5% Zn alloy, and we show how the kinetic model can be used to explain these, and their dependence on heat-treatment, both for two-step ageing treatments and for direct quenching to temperatures above or below T_c.

In some cases, we observe asymmetrical p.f.z's in Al–17·5% Zn, which have been interpreted[6] as the start of discontinuous precipitation. A few examples appear to be associated with the occurrence of grain-boundary migration during the precipitation process, but we have no detailed data and further work will be carried out before any account of these asymmetrical features is written.

Experimental Procedure

The Al–17·5 wt.-% Zn samples were in the form of rolled strip, ~ 0·004 in. thick. The heat-treatment of specimens and their subsequent preparation for electron microscopy was as described elsewhere.[4]

The Critical Temperature, T_c

The critical temperature, T_c, for homogeneous nucleation is defined, by the kinetic model, as the maximum temperature at which nucleation can occur when no excess vacancies are present at the ageing temperature.

The experimental technique used for determining T_c in this investigation was similar to that previously described[4] for an Al–Mg–Si alloy, i.e. after solution-treatment at a temperature T_s, the specimens were quenched to some intermediate temperature, T_I, and held there for a short time before the quench was continued to the ageing temperature T_A. If T_I is not too high above T_A, then an almost equilibrium concentration of vacancies will be present in the sample at the start of the ageing treatment at T_A.

Manuscript received 22 January 1968. M. H. Jacobs, B.Sc., Grad.Inst. P., and D. W. Pashley, B.Sc., A.R.C.S., Ph.D., F.Inst.P., are at Tube Investments Research Laboratories, Saffron Walden, Essex.

Fig. 1(*a*) illustrates the result obtained with a sample of Al–17·5 wt.-% Zn quenched from 560 to 180° C, held there for 1 min and then further quenched to 160° C, from which it is concluded that T_c is below 160° C since no precipitation is observed. Samples given a similar quench to 155° C exhibited copious precipitation so we conclude that T_c lies between 155 and 160° C for this alloy composition.

Similar experiments, carried out with an Al–10 wt.-% Zn alloy in which the quench was interrupted at 100° C for 5 min before continuing the quench to T_A, indicated that T_c lies between 60 and 70° C for this alloy.

It is important to emphasize that homogeneous nucleation is not restricted to temperatures below T_c and can occur above T_c, provided that sufficient excess vacancies are available during the nucleation process. Fig. 1(*b*) illustrates that this is so for a thin-foil sample of Al–17·5% Zn quenched directly from 560° C into an oil bath held at 160° C (cf. Fig. 1(*a*)).

Precipitate-Free Zones Produced by Direct Quenching to the Ageing Temperature

Theoretical Model

The concept of a critical temperature (T_c) is of fundamental importance in the interpretation of the factors controlling the width of p.f.z's produced by direct quenching. The following discussion will require a knowledge of the variation of T_c with solute concentration, which is shown schematically in Fig. 2. The important point is that a lower value of T_c is associated with a reduced solute concentration, as we have shown experimentally. Fig. 1(*b*) demonstrates that homogeneous nucleation can occur above T_c, provided that sufficient excess vacancies are present. We now postulate that nucleation is possible, with a given critical excess-vacancy concentration $(C_v)_{crit.}$, up to a maximum temperature, T_c'. The family of curves labelled T_c' in Fig. 2 then corresponds to increasing concentrations of excess vacancies. By direct application of the concepts summarized by this diagram, we can predict the width of p.f.z's at grain boundaries.

Case (1): *No Solute Depletion during the Quench*

We initially make the assumption that, immediately after the quench, the solute concentration is uniform throughout the grains and that no solute has segregated at the grain boundaries during the quench.

During, and for the transient period after, a quench from T_Q (the quenching temperature) to T_A an excess-vacancy profile will be established in the vicinity of a grain boundary, since although excess vacancies are retained well within a grain they are rapidly lost to a grain-boundary sink. This profile will be established irrespective of whether T_A is above or below T_c. However, in the absence of solute-depletion effects (discussed in case (2) below) nucleation will occur right up to the grain boundary if $T_A < T_c$ (this follows from the definition of T_c).

The shape of the excess-vacancy profile will depend upon the value of T_Q and the quenching rate between T_Q and T_A. Fig. 3 illustrates, schematically, the shape of the excess-vacancy profiles that would be expected for similar-sized specimens quenched into oil at T_A from a high, a medium, and a low quenching temperature (it is assumed that the grain boundary is the only vacancy sink operating and that no vacancies are lost owing to vacancy clustering and loop formation).

If we now confine the argument to the case where $T_A > T_c$, nucleation of solute clusters can only occur in regions of the specimen where the excess-vacancy concentration is greater than the critical value $(C_v)_{crit.}$ A–B in Fig. 3 thus defines the region within which precipitation will not occur in the sample quenched from the high T_Q and thus defines the p.f.z.; similarly C–D defines the p.f.z. in the sample quenched from the medium value of T_Q. Since the vacancy profile established on quenching from the low value of T_Q never exceeds $(C_v)_{crit.}$, nucleation is nowhere possible in this case.

Case (2): *Solute Depletion during the Quench*

We now consider the case where solute is lost from the vicinity of a grain boundary during the quench because either (1) heterogeneous precipitates are nucleated on the boundary during the cooling to T_A or (2) preferential segregation of solute occurs at the boundary during the cooling to T_A. In either case a solute-concentration profile will be established, as illustrated by Fig. 4(*a*). To decide whether or not nucleation can occur within the region of solute depletion, we refer to Fig. 2, from which it may be deduced that, with a certain excess-vacancy concentration present at T_A, there is a critical solute concentration, C_s (T_A), required for nucleation to occur. The critical solute concentrations for ageing at 120, 140, and 150° C (all of which are below T_c for an Al–17·5% Zn alloy) are indicated schematically in Fig. 4(*a*).

Consider the particular case of ageing at 140° C. Nucleation will not occur within the region defined by X–X, since the actual solute concentration is less than the critical value, C_s (140° C). X–X thus defines the p.f.z., whose width is clearly governed by the shape of the vacancy and solute-concentration profiles in the vicinity of the boundary.

If $T_A > T_c$ (where T_c is the critical temperature corresponding to the full solute concentration of the alloy), nucleation will not occur unless sufficient excess vacancies are present, as described in case (1) above; however, the additional effect of solute depletion must now be taken into account. From Fig. 2 it may be seen that, for a given T_A, a higher critical excess-vacancy concentration is required for nucleation to occur in a region of reduced solute concentration. Thus, if appreciable solute depletion occurs in the vicinity of a grain boundary the p.f.z. widths, as predicted in case (1) above, will be modified. Nevertheless, the following two points are to be noted:

(1) No p.f.z's would appear on ageing below T_c unless solute segregation effects are operative.

(2) No p.f.z's would appear on ageing above T_c unless vacancy effects are operative.

Experimental Results

The following results were obtained with specimens of Al–17·5% Zn.

$T_A > T_c$

The value of T_A was 160° C and all samples were quenched into an oil bath held at this temperature. The quenching temperature (T_Q) was 475, 370, or 300° C. Samples quenched from 475° C contained p.f.z's which were ~ 1 μm in width, whereas samples quenched from 370° C exhibited wider p.f.z's, ~ 3·5 μm in width. This result is consistent with Fig. 3, with 475 and 370° C corresponding to the high and medium values of T_Q. Samples quenched from 300° C exhibited no precipitation at all, which is the situation predicted in Fig. 3 for the vacancy profile corresponding to the low quenching temperature.

$T_A < T_c$

Narrower p.f.z's were observed in samples aged within a temperature range of ~ 35 degC below T_c, as illustrated by Figs. 4(*b*)–(*d*) for which T_A was 120, 140 and 150° C, respec-

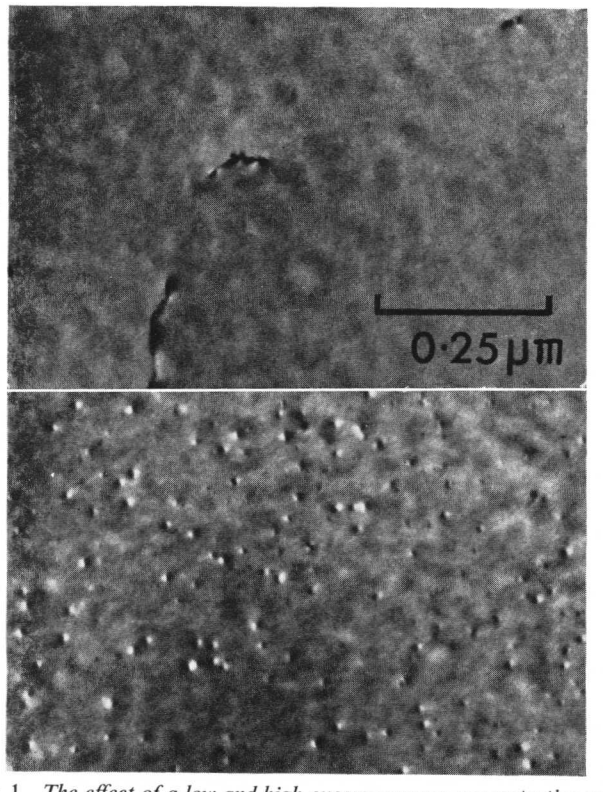

Fig. 1 The effect of a low and high excess-vacancy concentration on precipitation in Al–17·5 wt.-% Zn at 160° C. (a) *Interrupted quench at 180° C for 1 min before ageing at 160° C for 1 h;* (b) *direct quench to 160° C (oil bath) and aged for 1 h.*

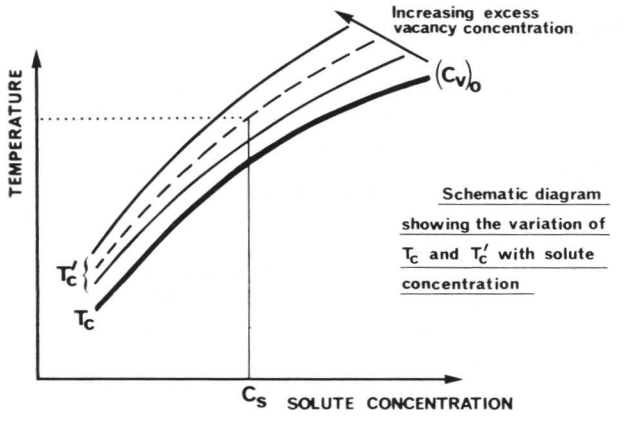

Fig. 2

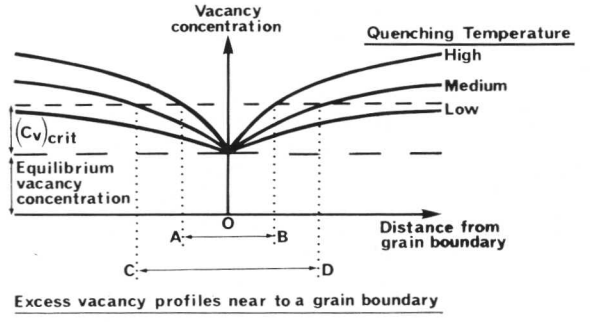

Fig. 3

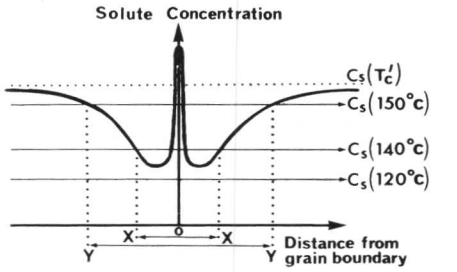

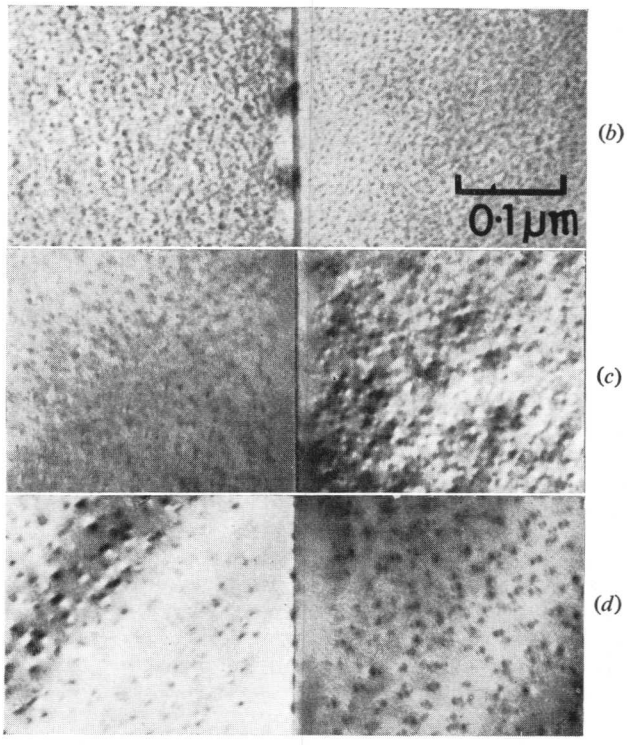

Fig. 4 The effect of solute depletion on precipitation in Al–17·5 wt.-% Zn in the vicinity of a grain boundary. (a) *Schematic diagram of the solute-concentration profile after direct quenching into oil;* (b) *direct quench to 120° C, aged for 2 h;* (c) *direct quench to 140° C, aged for 2 h;* (d) *direct quench to 150° C, aged for 1½ h.*

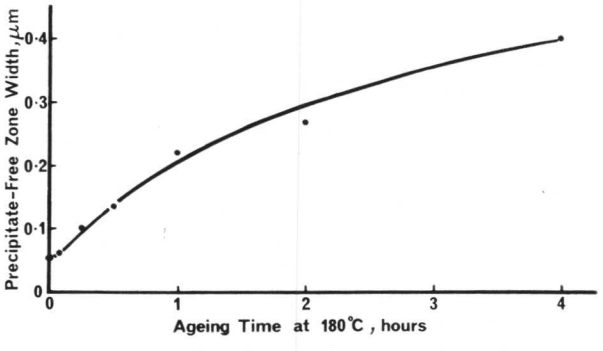

Fig. 5 The effect of pre-ageing time at 180° C on the width of precipitate-free zones established on subsequent ageing at 140° C for 2 h.

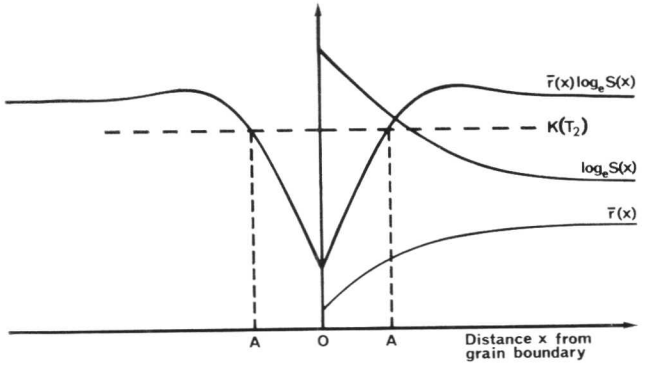

Fig. 6 The general form of the stability function $\bar{r}$ (x) log_e S(x) *(for a temperature* T_2*) in the vicinity of a grain boundary. A–A defines the region within which clusters, grown at* T_1*, will be unstable at* T_2.

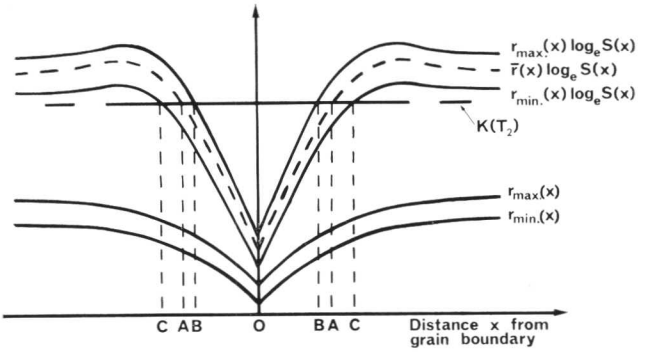

Fig. 7 The form of the stability function at T_2*, as for Fig. 6, when the sizes of clusters are distributed between* $r_{min.}$ *and* r_{max}.

tively. If we assume that a similar solute-concentration profile was established during the quench for all three samples, we may interpret the observed changes in p.f.z. width with the aid of Fig. 4(*a*), which predicts that the p.f.z. for ageing at 150° C (Y–Y) will be wider than that for ageing at 140° C (X–X). For ageing at 120° C however, precipitation will occur right up to the grain boundary, because the actual solute concentration never drops below the critical value.

Much wider p.f.z's have been obtained by means of a two-step treatment in which samples were given an extended pre-ageing treatment at 180° C before ageing at 140° C. Fig. 5 shows the variation of p.f.z. width as a function of ageing times at 180° C, obtained with a number of specimens. We explain these results by supposing that, with increasing ageing times at 180° C, a progressively wider region of solute depletion is established because of the rapid growth of grain-boundary precipitates and that this gives rise to a wider (solute-depleted) p.f.z. on ageing at 140° C. This is similar to the behaviour of an Al–Mg–Zn alloy reported by Cornish and Day,[7] who also explained their results in terms of solute depletion.

Precipitate-Free Zones Produced by Two-Step Ageing

Theoretical Model

Consider a two-step heat-treatment in which a sample is initially quenched to a temperature T_1 (below T_e), aged for a time t_1, and then subsequently aged at a higher temperature T_2 (either above or below T_e). Assume for the moment that no solute is segregated at grain boundaries during the heat-treatment.

Since $T_1 < T_e$, nucleation will occur at T_1 throughout the grains and right up to grain boundaries. If we consider the case where the quench establishes an excess-vacancy profile near to the grain boundaries, similar to one of those illustrated by Fig. 3, it is clear that, because of the dependence of the solute-diffusion rate on excess-vacancy concentration, clu sters nucleated near to a grain boundary will grow less quickly than those nucleated further away from the boundary. Thus, after an ageing time t_1 at T_1, the radius of the average-sized cluster, $\bar{r}$ (x), will vary with distance x away from a grain boundary, as illustrated schematically in Fig. 6.

If we assume that the cluster density, N, remains constant throughout the ageing times at T_1 that we are considering, we may determine[4] the volume fraction precipitated at a distance x from the grain boundary and so obtain the value of the remaining solute supersaturation, $S(x)$, if the temperature is now raised to T_2. To determine if the clusters are stable in their new supersaturation environment we invoke the stability condition of the kinetic model,[4] which may be written

$$\bar{r}\,(x)\,\log_e S(x) > K(T_2)$$

where $K(T_2)$ is a temperature-dependent constant. The general form of the function $\bar{r}\,(x)\,\log_e S(x)$ in the neighbourhood of a grain boundary is illustrated in Fig. 6 and we suppose the constant $K(T_2)$ is as indicated by the horizontal broken line. Clusters within the region defined by A–A will be unstable at T_2.

We now extend the model to include the situation where clusters at a distance x from a grain boundary have a size distribution, by letting $r_{max.}(x)$ and $r_{min.}(x)$ be the radius of the maximum- and minimum-sized clusters, which will vary as a function of x, after a given ageing time t_1 at T_1, as illustrated by Fig. 7. The functions $r_{max.}(x)\,\log_e S(x)$ and $r_{min.}(x)\,\log_e S(x)$ now determine the stability of the maximum- and minimum-sized clusters, respectively. Thus, the maximum-sized clusters are unstable at T_2 in the region defined by B–B in Fig. 7, whereas the minimum-sized clusters are unstable within the wider region defined by C–C. Between the two regions, B–C, either side of the grain boundary, there will be a gradation in the number of clusters stabilized from zero at B to N at C, and the width of B–C will depend on the size distribution of clusters.

Next, consider the situation after a longer period of ageing (t_2) at T_1. Growth of clusters will have continued in the vicinity of a grain boundary since more solute will have been available in this region compared with a region further from the grain boundary. The general forms of the $r_{max.}(x)\,\log_e S(x)$ curves, after ageing for t_1 and t_2, are illustrated in Fig. 8, from which we deduce that the region within which no stabilization occurs is reduced from B–B to B′–B′ for the increased period of ageing at T_1.

We now apply the ideas developed above to the formation of p.f.z's at T_2 and two cases may be distinguished.

Case (1): $T_2 > T_e$

Since $T_2 > T_e$, homogeneous precipitation will only be present at T_2 if clusters grown at T_1 remain stable when the temperature is raised. Thus B–B and B′–B′ of Fig. 8 will define the widths of the p.f.z's at T_2 after ageing times of t_1 and t_2 at T_1, respectively, from which we conclude that longer ageing times at T_1 will establish narrower p.f.z's at T_2. In practice, for long ageing times at T_1, the final reduction in p.f.z. width will be limited only by solute depletion to the grain boundary occurring during the quench and the treatment at T_1.

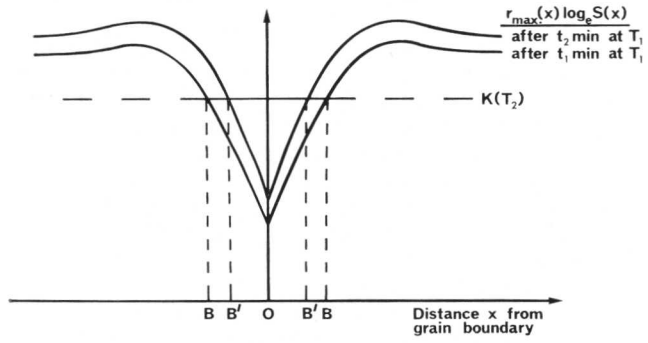

Fig. 8 Comparison of the stability curves at T_2, *for the maximum-sized clusters, after times* t_1 *and* t_2 ($t_1 < t_2$) *at* T_1.

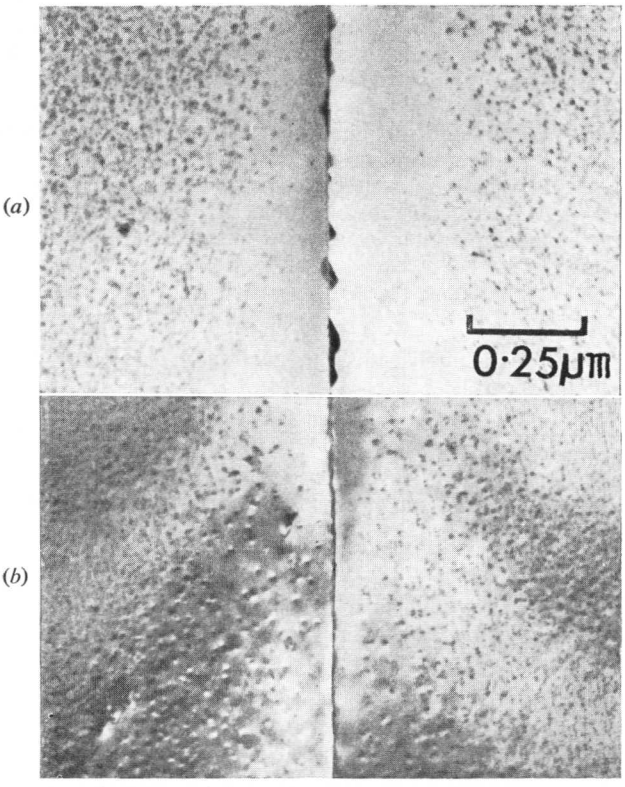

Fig. 9 The nature of the precipitation observed, in the vicinity of a grain boundary, in samples of Al–17·5 wt.-% Zn quenched into water at room temperature and aged for ½ *min before being subsequently aged at* (a) 160° C *for* 1 *h;* (b) 150° C *for* 1½ *h.*

Case (2): $T_2 < T_c$

If $T_2 < T_c$, B–B and B′–B′ of Fig. 8 still define regions within which no seeding of clusters occurs at T_2. On raising the temperature to T_2, clusters within these regions will immediately start to dissolve, but restabilization of some of the clusters will occur, as already described in detail.[4] Thus, within B–B or B′–B′, we would expect a lower density of clusters at T_2 compared with regions where clusters are seeded at T_1; there will be no true p.f.z. in this case. However, if local solute depletion has occurred, owing to grain-boundary precipitation, the effective critical temperature in a narrow region either side of the boundary may be reduced below T_2, so that in this region the situation will be as described in case (1) above, and a narrow p.f.z. will be formed.

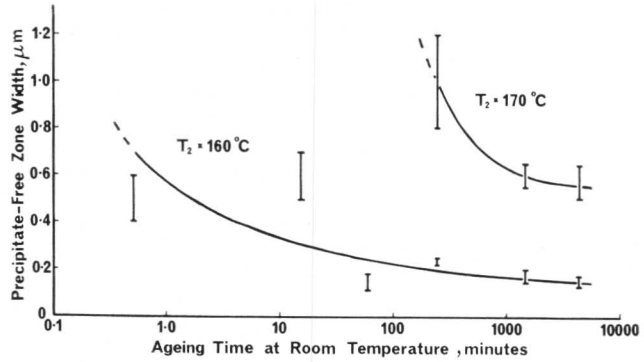

Fig. 10 The effect of pre-ageing time at room temperature on the width of precipitate-free zones established on subsequent ageing at either 160° C *for* 1 *h or* 170° C *for* 20 *min.*

Experimental Results

Two-step ageing studies have been carried out on samples of Al–17·5% Zn which were solution-treated at 560° C, quenched into water at room temperature, aged for times ranging between ½ min and 3 days, and subsequently aged with T_2 at either 150, 160, 170, or 180° C.

Case (1): $T_2 > T_c$

As predicted by the model, samples aged for short times at room temperature exhibited very wide p.f.z's on ageing at both 160 and 170° C, compared with samples aged for longer times at room temperature. Fig. 9(*a*) illustrates a typical p.f.z. obtained by ageing for ½ min at room temperature before ageing at 160° C. The slight change in cluster density at the p.f.z. boundary, as predicted by the model, is visible in this micrograph.

No precipitation was observed in samples pre-aged at room temperature for up to 1 h and subsequently aged at 170° C, whereas samples pre-aged for 4 h exhibited a very wide p.f.z. The observed variation of p.f.z. widths as a function of pre-ageing time at room temperature are plotted in Fig. 10 for T_2 at 160 and 170° C. No precipitation was observed in samples for which T_2 was 180° C, for pre-ageing times at room temperature of up to 3 days. The observed dependence of p.f.z. width on the magnitude of the temperature T_2 may be explained by the fact that the rate of decrease of $\log_e S(x)$ with increase in temperature T_2 is greater than that of $K(T_2)$. In other words, clusters must grow to a larger size before they are stable in the supersaturation associated with a higher value of T_2.

Case (2): $T_2 < T_c$

The p.f.z. shown in Fig. 9(*b*) is typical of those observed in a sample pre-aged at room temperature for ½ min before subsequently being aged at 150° C, which is below T_c. It illustrates the case, discussed above, where there is a region either side of the grain boundary where clusters are not seeded during the room-temperature treatment and where restabilization of clusters subsequently occurs at 150° C, producing a marked change in cluster density. We also note the narrow p.f.z. which, as discussed above, is believed to arise because of localized solute depletion near to the grain boundary.

Longer times of pre-ageing at room temperature caused the " seeding-free " zone to be progressively reduced in width, until further reduction was limited by solute depletion.

Discussion

We have now shown that the kinetic model developed in the earlier paper[4] is also capable of providing interpretation of the precipitation behaviour in Al–17·5% Zn. In particular, the results show that the kinetic model can be used to predict the occurrence of p.f.z's at grain boundaries, and the way in which the width of the p.f.z's depends upon the heat-treatment. This applies to the formation of p.f.z's by both conventional heat-treatments and by direct quenching to the ageing temperature. In general, the p.f.z's can arise from both solute and vacancy segregation on the grain boundaries, and the model provides a means of determining which of these two processes is effective for a given heat-treatment.

The excellent qualitative, or semi-quantitative, agreement between the numerous observations and the predictions of the kinetic model provides strong support for the validity of the kinetic model. In many cases the results were correctly predicted before the observations were carried out. However, the alternative thermodynamic model is also capable of providing an interpretation of many of our observations. For example, we believe that the predicted relative importance of solute and vacancy depletion in determining the width of the p.f.z's produced by direct quenching to the ageing temperature is identical for the two models. The important concepts, for this problem are:

(1) Direct quenching to temperatures below a certain critical temperature T will always lead to homogeneous precipitation unless solute depletion has occurred.

(2) Direct quenching to temperatures above T will not give rise to homogeneous precipitation unless excess vacancies are present to aid nucleation.

On the kinetic model, T is the critical temperature T_c as defined earlier.[4] On the thermodynamic model, T is slightly below the G.P.-zone solvus temperature, the amount below depending upon the undercooling necessary for a finite rate of nucleation to take place.[8] The required undercooling is reduced as the excess-vacancy concentration is increased.

Thus, although the two models predict similar behaviour, they differ in the significance attributed to the observed critical temperatures. Rapid direct quenching, which retains a high concentration of excess vacancies, increases the apparent critical temperature to a value T_c'. For Al–17·5% Zn, the maximum $(T_c' - T_c)$, observed with a salt-quench, is ~ 5 degC. For Al–1·2% Mg_2Si, $(T_c' - T_c)$ values of 30 degC are observed. It is possible that even faster quenches would give higher T_c' values. In terms of the thermodynamic model, therefore, T_c' is equal to, or slightly less than, the G.P.-zone solvus temperature.

It is not valid to attempt to distinguish the two models by comparing the observed values of T_c' with the G.P.-zone solvus temperatures determined from reversion experiments.[9] These determinations are usually carried out by quenching an alloy to room temperature, ageing it sufficiently at room temperature to produce detectable hardening, and then raising the temperature until softening occurs. As predicted by both models, precipitates nucleated at T_1 can act as seeds for growth at T_2, even when $T_2 > T_c'$. Thus, the observed reversion temperature is likely to be higher than T_c' (or the G.P.-zone solvus temperature). This fits with the value of T_c', as observed for the Al–17·5% Zn alloy (160° C), being less than the previously observed minimum reversion temperature (170° C). The only reliable means of determining T_c (or the G.P.-zone solvus temperature) is by direct-quenching methods such as used in this work.

Thus, we conclude that both models are capable of providing an interpretation of the effect of complex heat-treatments on precipitation both within grains and at grain boundaries, and that it is difficult to distinguish between the detailed predictions of the two models. This certainly applies in the case of qualitative, or semi-quantitative, aspects of the precipitation. Undoubtedly there will be some marked differences as regards more exact quantitative predictions, but neither model is sufficiently well developed to allow adequately quantitative predictions to be made. Attempts to make the kinetic model quantitative are being pursued.

Acknowledgement

This paper is published by permission of the Chairman of Tube Investments, Ltd.

References

1. J. D. Embury and R. B. Nicholson, *Acta Met.*, 1965, **13**, 403.
2. G. W. Lorimer and R. B. Nicholson, *ibid.*, 1966, **14**, 1009.
3. D. W. Pashley, J. Rhodes, and A. Sendorek, *J. Inst. Metals*, 1966, **94**, 41.
4. D. W. Pashley, M. H. Jacobs, and J. T. Vietz, *Phil. Mag.*, 1967, **16**, 51.
5. J. M. Silcock, T. J. Heal, and H. K. Hardy, *J. Inst. Metals*, 1953–4, **82**, 239.
6. A. Kelly and R. B. Nicholson, *Progress Materials Sci.*, 1963, **10**, 151.
7. A. J. Cornish and M. K. B. Day, Conference on Electron Microscopy in Metallurgy, Manchester, 1966.
8. G. W. Lorimer, *ibid.*, Swansea, 1967.
9. G. J. C. Carpenter and R. D. Garwood, *J. Inst. Metals*, 1966, **94**, 301.

The Effect of an Addition of 0·5 wt.-% Silver on the Ageing Characteristics of Certain Al–Cu–Mg Alloys

N. Sen and D. R. F. West

In Al–Cu–Mg alloys containing ~ 3 wt.-% Cu and 1·5 wt.-% Mg aged at 190° C, hardening results from G.P.B. zone formation and heterogeneous nucleation of *S* on dislocation loops and helices. When 0·5 wt.-% Ag is present only a small amount of *S* forms in the early stages of ageing, and the peak hardness is largely associated with the presence of metastable *T* phase; on overageing, *T* dissolves and matrix precipitation of *S* occurs. The degree of hardening is increased by the silver addition and *T* forms at temperatures up to 400° C. The effect of silver is considered to originate from an increased solute-atom/vacancy interaction which reduces the number of dislocation loops available for *S* nucleation. The G.P.B. zone reversion temperature is raised by the addition of silver.

The influence of minor alloy additions on the ageing behaviour of important aluminium alloy systems has been studied extensively, and some of the main aspects have been summarized by Brook.[1] In recent years the Al–Cu–Mg system has attracted attention in this connection, e.g. additions of Ag and Si have been studied.[2–4] Alloys with copper and magnesium in the weight ratio of 2·2 : 1 lie in a quasi-binary section in which the equilibrium precipitate is *S* phase, Al_2CuMg; hardening during ageing can occur by G.P.B. zone formation and by *S′* and *S* precipitation.[5,6] The difference in structure between *S′* and *S* is slight and in the present paper no distinction is made, the designation *S* being used.

Experimental Procedure

Alloys of the compositions shown in Table I were prepared by the British Aluminium Co., Ltd. from high-purity materials; the silicon and iron contents were each of the order of 0·005 wt.-%.

The alloys were semi-continuously cast as $2\frac{5}{8}$-in.-dia. billets, homogenized at 495° C, hot extruded, and cold rolled to 0·08-in.-thick strip for hardness measurements and 0·02-in.-thick strip for foil preparation. Specimens were solution-treated in a salt bath for 16 h at 500 ± 5° C for Alloys T and W and 495 ± 5° C for Alloys Q and X and were quenched into water at 20° C. The main ageing temperatures were room temperature and 190° C. Foils were prepared using an acetic/phosphoric/nitric acid–water solution at 0 ± 5° C.

TABLE I
Alloy Compositions

Alloy	Cu*		Mg*		Ag*		Al
	wt.-%	at.-%	wt.-%	at.-%	wt.-%	at.-%	
T	3·3	1·4	1·58	1·8	—	—	balance
Q	3·2	1·4	1·5	1·7	0·5	0·1	,,
W	2·7	1·2	1·3	1·5	—	—	,,
X	2·7	1·2	1·26	1·4	0·5	0·1	,,

* Analysed.

Reversion experiments were made on Alloys W and X to determine the G.P.B. zone solvus using the procedure of Beton and Rollason.[7] Specimens were aged for 7 days at room temperature to form G.P.B. zones and were then heated in a salt bath for 15–20 sec at various temperatures and quenched to 20° C. Plots of hardness vs. temperature of heating were made and the discontinuity was taken as the G.P.B. zone solvus temperature.

Results

Ageing Characteristics

At room temperature (Fig. 1) a hardness increase of ~ 40 HV occurred within ~ 1 day, while for times between 1 and 10 days little further hardening occurred. The addition of silver retarded the hardening, although the maximum hardness attained was increased slightly. Fig. 2 shows the effect on the ageing of Alloys T and Q of quenching to 100° C (boiling water) and to − 100° C (liquid nitrogen + petroleum ether). As the quenching rate increased with decreasing bath temperature the early hardening was accelerated, although only very slightly in Alloy Q; the maximum hardness was virtually unaffected.

On ageing Alloys T and Q at 130 and 190° C (Fig. 3) the curves were two-stage in type. The silver addition increased the first-stage hardening and accelerated the second stage. At 190° C the increment from as-quenched to peak condition was greater in Alloy Q, and a higher hardness was maintained during overageing.

Manuscript received 23 February 1968. N. Sen, Ph.D., and D. R. F. West, Ph.D., are in the Department of Metallurgy, Imperial College of Science and Technology, London.

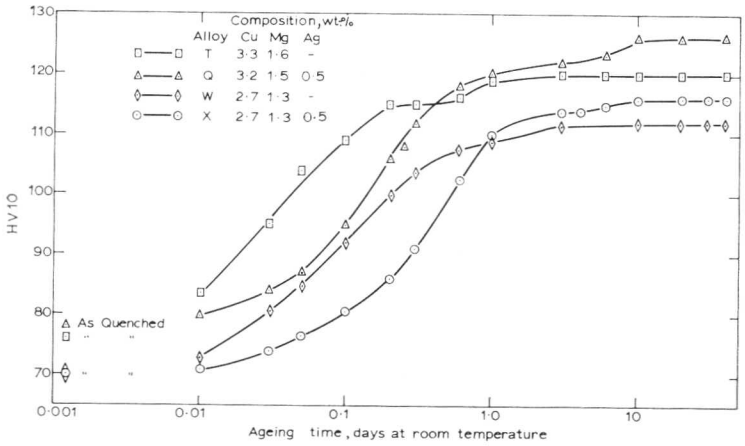

Fig. 1 *Room-temperature age-hardening behaviour of alloys quenched to* 20° *C after solution-treatment.*

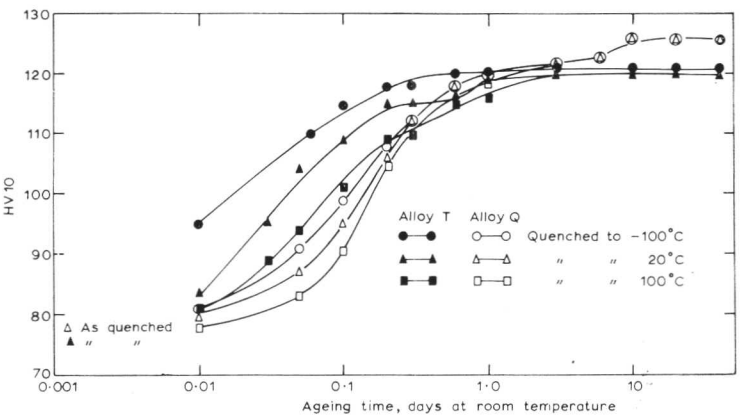

Fig. 2 *Effect of initial quenching conditions on room-temperature age-hardening of Alloy T and Alloy Q.*

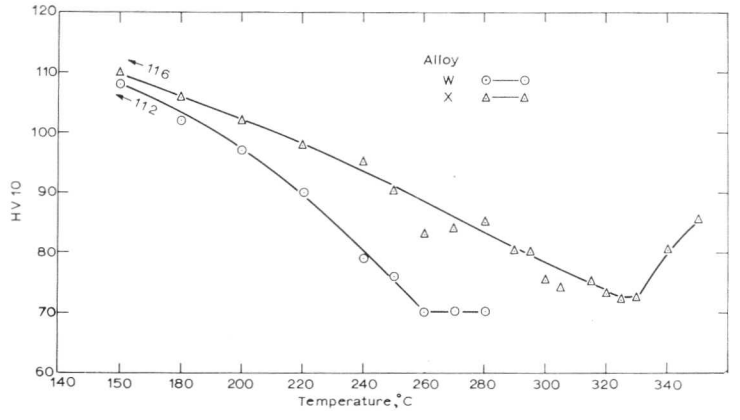

Fig. 4 *Reversion experiments: hardness vs. temperature of heating for Alloys W and X.*

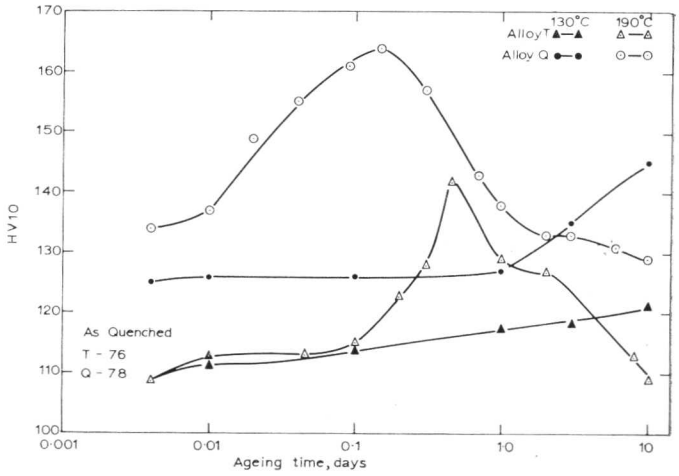

Fig. 3 *Age-hardening behaviour at* 130° *C and* 190° *C of Alloy T and Alloy Q.*

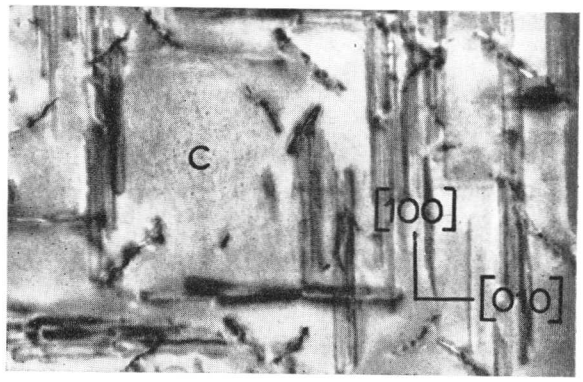

Fig. 5 *Alloy T aged to peak hardness* (11 *h*) *at* 190° *C.* S *laths along* $\langle 100 \rangle_{Al}$ *on dislocation loops, and G.P.B. zone structure* (*e.g. at C*); (001) *foil.* × 80,000.

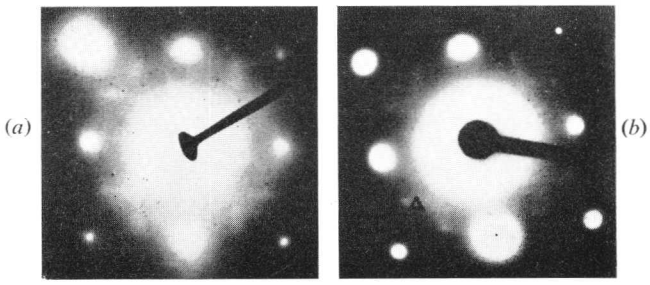

Fig. 6 *Alloy T.* (a) *Aged* 15 *min at* 190° *C. Electron-diffraction pattern showing diffuse streaks;* (001) *foil.* (b) *Aged* 30 *min at* 190° *C. Streaking showing intensity maxima, e.g. at A;* (001) *foil.*

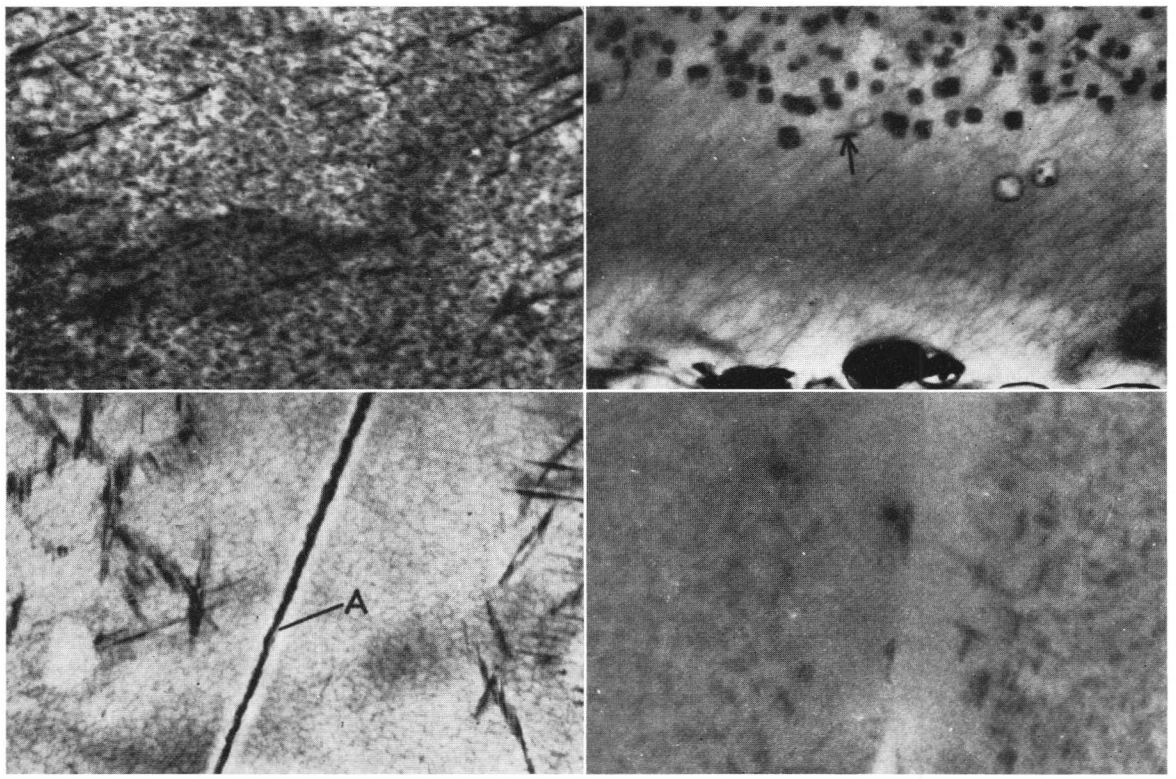

Fig. 7 Alloy Q, aged to peak hardness (3½ h) at 190° C, showing matrix precipitate of T *phase.* × 80,000.

Fig. 8 Alloy Q, aged 1 min at 350° C, showing P.F.Z. adjoining grain boundary and square plates of T *phase (arrow indicates plate-like shape; mottled background effect from foil preparation).* × 50,000.

Fig. 9 Alloy T, aged 0·2 day at 190° C, showing grain-boundary P.F.Z. including solute-depleted region (A). (Mottled background effect from foil preparation). × 40,000.

Fig. 10 Alloy Q, aged 0·1 day at 190° C after quenching to 100° C, showing P.F.Z. and T*-phase precipitate.* × 50,000.

The reversion temperature, taken as the G.P.B. zone solvus, was significantly higher in the silver-containing alloy, X, (325° C) as compared with that in the ternary alloy, W, (260° C) (Fig. 4). The latter temperature agreed well with previous work.[7]

Structural Changes during Ageing

Zone Formation

With room-temperature ageing of Alloy T for times up to ~ 7 days, zones were not detected although the hardening implies that they are present.[6] However, in the corresponding silver-containing alloy, Q, bright-field examination showed a fine matrix " precipitate " assumed to consist of G.P.B. zones. Although the shape of the particles was not clearly distinguishable it appeared to be roughly spherical. No associated electron-diffraction effects were observed. The fact that the zones were detected only in Alloy Q may be due to the presence of silver in the zones increasing the contrast.

On ageing for short times at 190° C (up to ~ 15 min for Alloy T, and up to ~ 3 min for Alloy Q) a similar matrix " precipitate " was detected in bright-field examination. During the second stage of ageing in Alloy T, including the peak-aged condition, zones co-existed with *S* phase. Fig. 5 shows a peak-aged structure in an (001) foil, with the zones appearing to be roughly spherical. As discussed later, these zones were not observed in the second stage ageing of Alloy Q.

Electron-diffraction streaking effects were observed from Alloy T aged at 190° C for times between ~ 15 min and 2 h, and from Alloy Q for times between ~ 3 and 10 min. In (001) foils diffuse streaking occurred through the {011} aluminium reciprocal lattice positions, parallel to [010] and [100] aluminium directions (Fig. 6(*a*)); after an initial period in these time ranges distinct intensity maxima were observed (Fig. 6 (*b*)). Dark-field observations using the maxima did not reveal any structure. However, bright-field examination showed an effect which, although not resolved very clearly, appeared to consist of needle-like particles.

S-Phase Precipitation

In the ternary alloy, T, aged at 190° C, *S* nucleation appeared to be entirely heterogeneous. *S* laths formed on dislocation loops and helices as previously reported,[8,9] throughout the second stage of ageing, and coarsening occurred on overageing. The structure at peak hardness is shown in Fig. 5.

In Alloy Q, *S* precipitation on dislocation helices and loops began to occur after the short plateau, but the amount of such precipitate was less than in Alloy T. A metastable phase then formed as described below, and at the hardness peak this phase predominated with relatively little *S* present (Fig. 7). However, beyond the peak, the metastable phase dissolved and increasing amounts of *S* precipitated. Much of this *S* formed in the matrix, and the nucleation may be

described as " homogeneous " in the sense that the nature of the nucleation sites was not identifiable.

Quantitative observations on samples overaged at 260° C showed that, for a given ageing time, the laths were slightly shorter in average length in Alloy Q (of the order of 10–20% difference), and were more numerous.[10]

T-Phase Precipitation

In Alloy Q, after ~ $3\frac{1}{2}$ h ageing at 190° C, a fine precipitate of size ~ 100 Å and density ~ 10^{16}/cm^3 formed throughout the matrix (Fig. 7). Zones were not detected in the presence of this phase. The phase formed early in the ageing sequence (after ~ 15 min ageing) but decreased in amount on over-ageing; after ~ 10 days ageing it had virtually disappeared. These observations agree with the results of Polmear *et al.*,[2] who reported the formation of metastable *T* phase in aged Al–Cu–Mg–Ag alloys.

In the present work diffraction examination of the aged structure at 190° C gave a pattern matching a cubic structure, but it was not conclusively identified. However, confirmation of the identity of the phase was obtained in a sample aged for 1 min at 350° C; coarse precipitate particles formed (Fig. 8), and an X-ray powder-diffraction pattern could be indexed to a b.c.c. cell of parameter 14·6 Å, which agrees reasonably with that of 14·28 Å reported for *T* phase, Al_6CuMg_4.[11] The particles in this sample appeared to be square plates (Fig. 8) of average size ~ 500 Å and density ~ 10^{14}/cm^3. Metastable *T* phase formed throughout the range 130–400° C, and the times of its complete disappearance ranged from ~ 40 days at 160° C to 1 min at 400° C. It was not detected on ageing for 1 min at 405° C. Plastic deformation before ageing completely suppressed *T*-phase formation[10].

Precipitate-Free Zones

In the study of Alloys T and Q a precipitate-free zone (P.F.Z.) was observed adjacent to grain boundaries after ageing. The zone width tended to be greater with the slower cooling rate obtained by quenching to 100° C.

Fig. 9 shows the structure of Alloy T after 0·2 days ageing at 190° C. Because of vacancy depletion and the consequent scarcity of dislocation loops, a zone ~ 0·6 μm wide on each side of the boundary is virtually free of *S* phase. Within this zone there is a region ~ 500 Å wide (marked A), on each side of the boundary, attributed to solute depletion from boundary precipitation of globular *S* particles. With increasing ageing times the *S* laths tend to grow into the vacancy-depleted zone, so that eventually the P.F.Z. is effectively eliminated.

In Alloy Q, the P.F.Z. is smaller than that in the ternary alloy; for a given ageing time the zone width increased with ageing temperature (e.g. Figs. 8 and 10). These zones were still solute-supersaturated as indicated by the tendency for *T*-phase particles near the zone edge to grow larger than those in the grain interior (Figs. 8 and 10). Where *S* phase had nucleated on dislocation helices, the adjoining regions were depleted in *T* phase.

Discussion

The behaviour of vacancies during initial quenching and the early stages of ageing can significantly affect zone formation and the type and number of sites available for precipitation. Electron-microscope studies[12] have shown important differences between the ternary and silver-containing alloys. Thus, in the silver-free alloy T, the as-quenched structure contains numerous dislocation loops and also some dislocation helices formed by vacancy condensation. In Alloy Q, containing 0·5 wt.-% Ag, the total number of dislocations is much less, and those present are mainly helices. It appears that there is a lower vacancy mobility and a stronger solute-atom/vacancy interaction in the silver-containing alloy. These observations are used as a basis for the following discussion.

Zone Formation

The details of zone formation in Al–Cu–Mg alloys are not fully understood. Silcock[6] has studied an Al–3·2% Cu–1·5% Mg alloy and has shown that G.P.B. zones give rise to room-temperature hardening, to the first-stage hardening at 190° C, and that they also contribute to peak hardness at 190° C. However, while Silcock proposed a needle-like form, Gerold and Haberkorn[13] considered the zones to be spherical.

The study of the morphology of the zones is made difficult by the small particle size and small contrast; also, in the present work, there was a tendency for a mottled foil surface to develop during electrothinning. A significant point arises from the work of Weatherly on Al–Cu–Mg and Al–Cu–Mg–Si alloys;[14] he observed a needle-like morphology, and found that in (001) foils the particles lying with their long axis parallel to the electron beam were more readily detected than those particles in other orientations. This fact may provide the explanation for the apparently spherical shape observed in the present work with some ageing conditions (e.g. Fig. 5).

Electron-diffraction streaking effects have been observed in previous work.[3,14] Silcock,[6] in an X-ray study, reported an effect designated " G.P.B. + streak " and suggested that this might represent the first manifestation of *S* phase. The data obtained in the present work are insufficient to provide any definite interpretation. It appears possible that the streaking may be associated with the early stages of *S* precipitation on dislocations. However, further work involving the study of a range of foil orientations is required to determine the origin and nature of the diffraction streaking effects.

With regard to the kinetics of G.P.B. zone formation, there are several features that can be interpreted in terms of vacancy effects. The slower initial rate of room-temperature hardening in Alloy Q as compared with Alloy T (Fig. 1), and the implied slower rate of zone formation, are attributable to the stronger solute-atom/vacancy interaction. It is possible that complex clusters of vacancies with magnesium, copper, and silver may form. This vacancy binding could retard the early stages of zone formation, but the clusters may be mobile[15] and combine with one another, leading to more rapid hardening at a later stage; vacancies may remain incorporated in the zones. In the ternary alloy, when copper and magnesium atoms migrate with vacancies to form clusters, a reduction in strain energy should result when these atoms occupy adjacent positions, since the lattice expansion due to the atomic size of magnesium is counteracted by a contraction of similar magnitude due to copper. Thus, vacancies could be released from their solute-atom binding and become available to assist diffusion of further solute atoms. In the ternary alloy an increase in initial quenching rate gives an increase in the retained vacancy concentration,[12] which accelerates zone formation sufficiently to increase noticeably the initial hardening rate at room temperature (Fig. 2). When silver is present with the stronger solute/vacancy interaction, the quenched-in vacancy concentration varies less with quenching rate and the rate of hardening is less affected (Fig. 2). The lower initial hardening rate in Alloy W as compared with T, and in X as compared with Q (Fig. 1), may be attributed

not only to the lower solute supersaturation, but also to lower vacancy supersaturation.

In terms of a metastable G.P. zone solvus, the higher reversion temperature in the presence of silver (Fig. 4) implies that the zones have a lower free energy relative to the matrix than do the zones in the ternary alloy. For a given copper and magnesium content and a given ageing temperature, the addition of silver thus increases the degree of supersaturation with respect to the metastable solvus and also increases the volume fraction of zones formed. Considered in kinetic terms[16] it may be suggested that the critical size for the stability of a zone is reduced by the silver; this could simply be a consequence of a greater free-energy difference between zones and matrix but may also derive from the incorporation of vacancies into the zones. Thus, on heating to a given temperature smaller silver-containing zones could remain undissolved as compared with the zones in the ternary alloy.

The extent of the hardening produced by zone formation is greater in the silver-containing alloy, e.g. as shown by the maximum room-temperature hardness and by the plateau hardnesses in Alloys T and Q on ageing at 130° C and 190° C (Figs. 1 and 3). This could be due both to an increased chemical-hardening effect resulting from the presence of silver in the zones and to a greater volume fraction of zones in Alloy Q. The slightly greater room-temperature hardening with increasing alloy supersaturation may also result from a greater volume fraction of zones.

S- and *T*-Phase Precipitation

In Alloy T, the pattern of *S* precipitation is determined by heterogeneous nucleation of *S* laths on dislocation loops and helices. In Alloy Q the extent of heterogeneous *S* nucleation is much less because of the smaller number of dislocations present; a higher supersaturation of the solid solution is thereby maintained during the early stages of ageing. Under these conditions of supersaturation, it appears that *T* phase forms in the matrix as a metastable phase in preference to homogeneous nucleation of *S* phase, implying a smaller activation energy for nucleation of the cubic *T*-phase structure. It is suggested that there may be a general effect in which trace additions that lead to strong vacancy binding, with a consequent lowering in the density of quenched-in dislocation loops and helices, can retard *S* precipitation and thus favour *T*-phase formation. In this connection the results of Wilson *et al.*[3] on an Al–Cu–Mg–Si alloy are of interest; the dislocation density was relatively low and square-shaped precipitate particles formed during ageing which may possibly be *T* phase.

That vacancies play a role in *T*-phase nucleation is indicated by the greater atomic volume of the *T*-phase structure as compared with that of the matrix structure and by the formation of a P.F.Z. The increasing width of the P.F.Z. with increasing ageing temperature and the narrower zone in the silver-containing alloy can be interpreted in terms of vacancy and solute supersaturations on the basis of Embury and Nicholson's work on Al–Mg–Zn alloys.[17] *T* phase forms below the G.P.B. zone solvus of the Al–Cu–Mg–Ag system and it is possible that it nucleates from G.P.B. zones, which may themselves contain vacancies.

The suppression of *T* phase in specimens plastically deformed before ageing can also be explained in terms of vacancy and solute supersaturation. The dislocations introduced by plastic deformation favour heterogeneous nucleation of *S* so that the requisite degree of solute supersaturation for *T*-phase nucleation is not maintained. They also provide additional vacancy sinks and thereby reduce the vacancy supersaturation.

In Alloy Q aged without deformation, the particles of *T* phase grow with increasing ageing time for a period, but ultimately dissolve in favour of *S* precipitation. In the absence of substantial numbers of dislocation loops, the *S* nucleates in the matrix at unidentified sites. The necessary degree of solute and vacancy supersaturation is presumably achieved by solution of *T* phase. That solution of *T* phase may release vacancies is suggested by the presence of small dislocation loops that are seen in overaged samples but not in peak-aged samples. The incorporation of vacancies into *S* nuclei may be significant in reducing the critical nucleus size for the matrix precipitation of *S*.

The observation made on samples aged at 260° C, that the average *S* lath size is smaller in Alloy Q than in Alloy T for a given ageing time, can be explained by the bulk of the *S* in Alloy Q forming at a relatively late stage in the ageing sequence. The greater number of laths per unit volume in Alloy Q suggests that the rate of nucleation is greater under the conditions of solute and vacancy supersaturation when *T* phase is redissolving than it is in Alloy T where *S* forms heterogeneously on dislocation loops in a matrix already containing G.P.B. zones.

Conclusions

The stability of G.P.B. zones and the strengthening contribution are increased by the presence of silver.

In an Al–3·3% Cu–1·6% Mg alloy aged at 190° C, *S* precipitation occurs heterogeneously on dislocation loops and helices. When silver is added the stronger solute-atom/vacancy interaction markedly reduces the number of quenched-in dislocations. Heterogeneous nucleation of *S* is thus restricted and metastable *T* phase forms; eventually *T* phase dissolves and matrix precipitation of *S* occurs.

There is evidence that vacancies are involved in the nucleation of *S* and *T* phases in the silver-containing alloy.

Acknowledgements

Acknowledgements are made to Professor J. G. Ball for the provision of research facilities, to the Ministry of Technology for support of the work, to the British Aluminium Co., Ltd. for the supply of alloys, and to Professor R. B. Nicholson and Dr. P. R. Swann for helpful discussions. The investigation formed part of work approved for the award of the Ph.D. degree of London University to one of the authors (N.S.).

References

1. G. B. Brook, *Fulmer Research Inst. Special Rep.* (**No. 3**).
2. J. T. Vietz and I. J. Polmear, *J. Inst. Metals*, 1966, **94**, 410. J. H. Auld, J. T. Vietz, and I. J. Polmear, *Nature*, 1966, **56**, 568.
3. R. N. Wilson, D. M. Moore, and P. J. E. Forsyth, *J. Inst. Metals*, 1967, **95**, 177.
4. G. C. Weatherly and R. B. Nicholson, to be published.
5. H. K. Hardy, *J. Inst. Metals*, 1954–55, **83**, 17.
6. J. M. Silcock, *ibid.*, 1960–1961, **89**, 203.
7. R. H. Beton and E. C. Rollason, *ibid.*, 1957–58, **86**, 79.
8. D. Vaughan, unpublished work.
9. R. N. Wilson and P. G. Partridge, *Acta Met.*, 1965, **13**, 1321.
10. N. Sen, Ph.D. Thesis, Univ. London, **1967.**
11. G. Phragmén. *J. Inst. Metals*, 1950, **77**, 489.
12. N. Sen and D. R. F. West, *J. Mat. Sci.*, 1968, **3**, 266.
13. V. Gerold and H. Haberkorn, *Z. Metallkunde*, 1959, **56**, 568.
14. G. C. Weatherly, Ph.D. Thesis, Univ. Cambridge, **1966**.
15. E. W. Hart, *Acta Met.*, 1958, **6**, 553.
16. D. W. Pashley, J. W. Rhodes, and A. Sendorek, *J. Inst. Metals*, 1966, **94**, 48.
17. J. D. Embury and R. B. Nicholson, *Acta Met.*, 1965, **13**, 403.

Effect of Plastic Deformation on the $\theta'' \rightarrow \theta'$ Transformation during the Ageing of an Al – 4% Cu Alloy at 160° C

J. D. Cook and J. Nutting

By cold working an Al–4% Cu alloy before ageing, the transformations are considerably modified. The rate of hardening is found to increase logarithmically with the amount of prior deformation, while electron-metallographic examination reveals that with increasing amounts of strain the θ′ phase is nucleated at shorter ageing times. The total amount of θ′ present after a given ageing time is also increased until, after some 15–20% cold work, no evidence for the presence of the θ″ phase is obtained. This suggests that the formation of θ″ is hindered by straining but the mechanism by which this occurs is uncertain. It is well known that the θ′ phase can be nucleated directly on dislocations but only two of the possible three θ′ orientations occur on a dislocation of given Burgers vector. However, during plastic deformation of a polycrystalline mass, dislocations of varying Burgers vectors are introduced, and as a consequence the dislocation-nucleated θ′ shows no preferential orientation distribution. This precludes any attempt to prove directly that the θ′ is totally dislocation-nucleated, although evidence is put forward which supports this view. With increasing dislocation density and hence the increasing number of nucleating sites, θ′ particle density increases with plastic strain and thus the particle size decreases. It is also found that the spread of size about the mean is decreased, and this can be shown to be a consequence of the initial nucleation-site density being large. Examination of material which has been given a room-temperature ageing treatment before deformation shows the same characteristics, but the θ′ particles in this case were even smaller after deformation. The results obtained are discussed in relation to the Lifshitz–Wagner equation relating particle growth to time of ageing during Ostwald ripening.

Ageing a solution-treated and quenched Al–4% Cu alloy results in a breakdown of the supersaturated solid solution:

$$\text{Supersaturated } \alpha \rightarrow \text{G.P. zones} \rightarrow \theta'' \rightarrow \theta' \rightarrow \theta$$

G.P. zones form at low temperatures when copper atoms segregate to the $\{100\}_{Al}$ planes and produce small clusters which grow to give discs of copper ~ 3 Å thick and some 15 Å in dia. Further ageing results in the formation of the θ′ phase by a process which is not clearly understood, but from size considerations[1] it is likely that the zones dissolve as θ″ is formed. It is also possible for θ″ to nucleate directly from the matrix without the need for prior zone formation.[2] The mechanism of the further change $\theta'' \rightarrow \theta'$ has not been studied extensively but again the θ′ phase can be nucleated directly from the matrix. The formation of θ, the equilibrium precipitate, requires long ageing times at relatively high temperatures (300 days at 190° C produces 5% θ.)[3] However θ does nucleate in regions of distortion at low temperatures and is commonly observed on grain boundaries. The sequence of the metastable phases is influenced considerably by the ageing temperature.

The free-energy change associated with precipitation can be written as follows:

$$\Delta F = \Delta F_{\text{Volume}} + \Delta F_{\text{Surface}} + \Delta F_{\text{Strain}}$$

In this expression the volume term is normally negative and the surface and strain terms positive. However, it has been shown[4] that the presence of a dislocation so reduces the strain term that its sign may change, increasing the probability of precipitate nucleation at the dislocation.

The deliberate introduction of dislocations into the quenched material should therefore make precipitation very much easier. The present work attempts to prove this in the case of Al–4% Cu and to relate the subsequent mechanical and metallurgical properties to the influence of strain upon the θ′ precipitate morphology.

Experimental Method

An alloy containing 4·0% Cu, 0·003% Si, and 0·0015% Fe was used. After hot and cold rolling to strip, the material was solution-treated at 540° C and quenched. Varying amounts of plastic strain were introduced by cold rolling immediately after quenching and the specimens were then aged at 160° C. The strip specimens were used for preparing mechanical-test specimens and thin foils for transmission electron metallography. The temperature of 160° C was chosen so that the ageing sequence in the absence of strain was:

$$\text{Supersaturated } \alpha \rightarrow \theta'' \rightarrow \theta'$$

The θ phase was only formed on grain boundaries at 160° C. As this temperature is just above the zone solvus, few if any G.P. zones are formed.

Manuscript received 12 February 1968. Professor J. Nutting, M.A., Sc.D., Ph.D., is Head of the Metallurgy Department, Houldsworth School of Applied Science, University of Leeds, where the work was carried out. J. D. Cook, B.Sc., Ph.D., A.I.M., L.R.I.C., is now in the Metallurgy Division, A.E.R.E., Harwell, Berks.

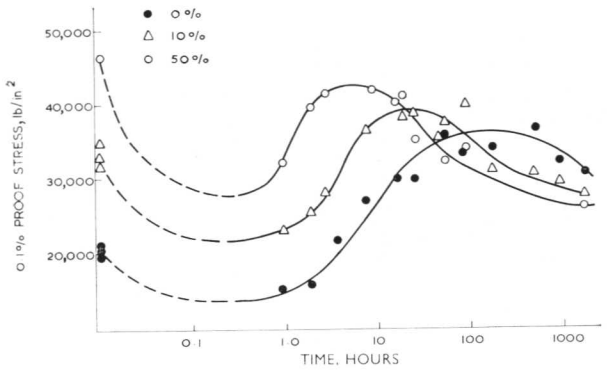

Fig. 1 *The influence of ageing time at* 160° *C and prior strain (reduction in thickness by rolling) upon the* 0·1% *PS.*

Results

The Effect of Prior Strain

The influence of ageing upon the 0·1% PS after differing amounts of prior strain is shown in Fig. 1. The shapes of these curves were almost identical when Vickers hardness measurements were used.

The deformed material attained maximum strength much sooner than undeformed material and, as the amount of initial strain was increased, so the time needed to reach peak strength was decreased. This relationship between the amount of prior strain and the time to reach peak strength was found to be logarithmic in agreement with previous work.[5] The reduction in strength on overageing was quicker as prior deformation was increased, so that effectively the influence of strain was to move the whole curve to the left on the time scale.

To investigate the metallographic changes accompanying the increase in ageing rate, the technique of transmission electron microscopy was used. Fig. 2(*a*) shows a micrograph of an undeformed specimen and Fig. 2(*b*) one of a specimen rolled 5%. The difference in the density of dislocations can easily be seen. Precipitates were not observed in either specimen. Ageing at 160° C for 4 h resulted in the precipitation of θ′ being well advanced in the strained material, whereas only θ″ was seen in the unstrained specimen (Figs. 3(*a*) and (*b*)).

This early formation of the θ′ phase in lightly worked material was the major difference in metallographic structure, but in heavily worked materials there was also evidence of some dislocation rearrangement, probably indicating the start of recovery.

The formation of the θ′ phase at such an early stage may be due either to an increase in the kinetics of the supersaturated solid solution → θ″ and θ″ → θ′ reactions, or to direct nucleation of θ′ from the supersaturated matrix.

For the latter process to be preferred, either nucleation of θ′ must be so much more favourable than the formation of θ″ that very little θ″ is formed, or the introduction of strain must interfere with the nucleation of θ″. The θ″ phase was difficult to detect in material also containing θ′ as streaking in $\langle 100 \rangle_{Al}$ directions on diffraction patterns, from which the presence of θ″ could be inferred, was also given by small θ′ particles. However other workers using X-ray methods have found[2,3] that at strains > ~ 15% no θ″ was formed, and this conclusion was confirmed by the present investigation. Graf and Guinier[6] suggested that the reason for this was that θ″ could only nucleate on $\{100\}_{Al}$ planes and these were so distorted that nucleation could not take place, i.e. nuclea-

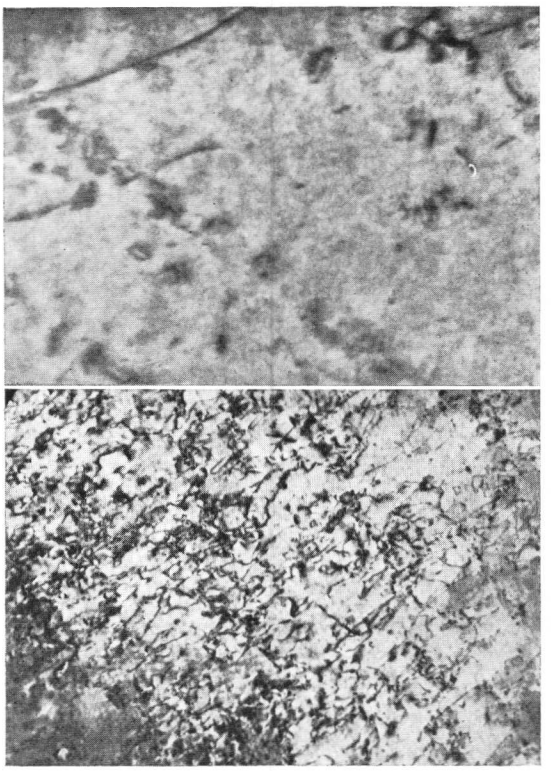

Fig. 2 (a) *Al–4% Cu alloy solution-treated and quenched.* (b) *As* (a) *but plastically deformed to give* 5% *reduction in thickness. Thin-foil transmission electron micrographs.* × 40,000.

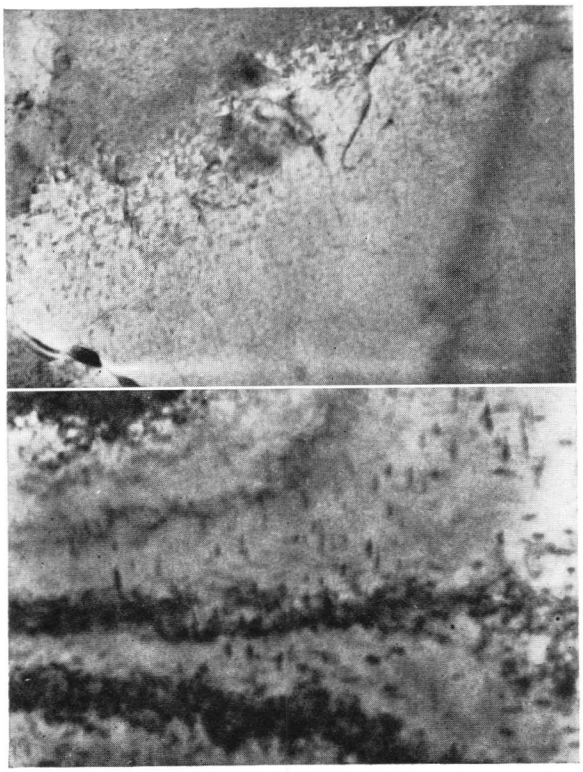

Fig. 3 (a) *Al–4% Cu alloy solution-treated, quenched, and aged at* 160° *C for* 4 *h.* (b) *As* (a) *but plastically deformed to give* 5% *reduction in thickness before ageing at* 160° *C for* 4 *h. Thin-foil transmission electron micrographs.* × 40,000.

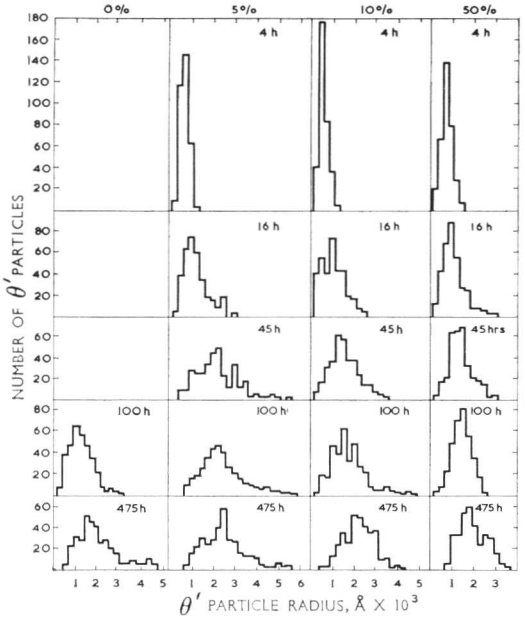

Fig. 4 Histograms showing the influence of prior strain and ageing time at 160° C upon the θ′ particle radii.

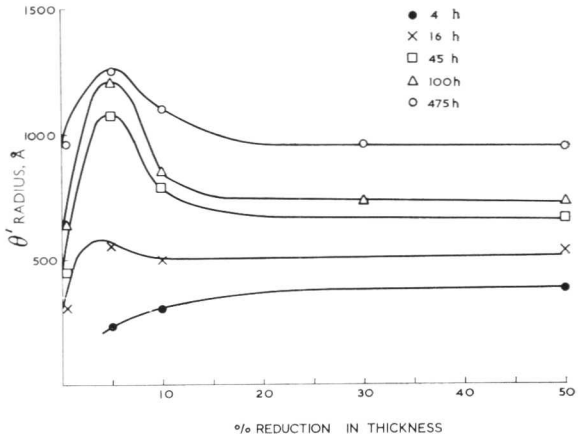

Fig. 5 The influence of plastic strain upon the mean θ′ particle radius after different ageing times at 160° C.

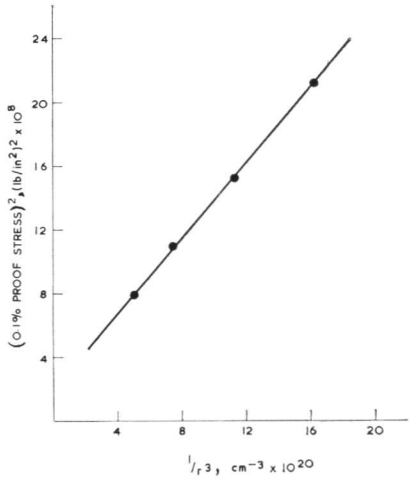

Fig. 6 The relationship between θ′ particle radius after ageing at 160° C for 475 h and the 0·1% PS determined directly after cold rolling.

TABLE I

% Reduction in Thickness	Radii of θ′ Particles, Å		
	Time of Ageing at 160° C		
	4 h	16 h	45 h
0	—	300	450
5	225	550	1075
10	300	500	788
50	388	538	663

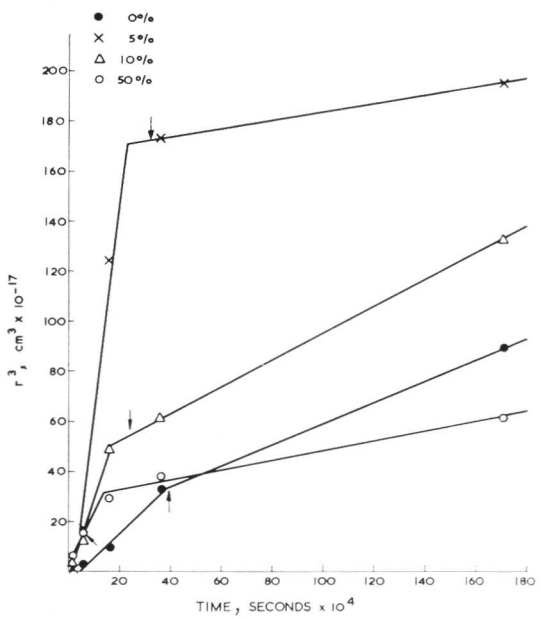

Fig. 7 The relationship between the time of ageing at 160° C and the mean θ′ particle radius after different amounts of cold rolling. The arrows denote the times at which maximum strength is attained.

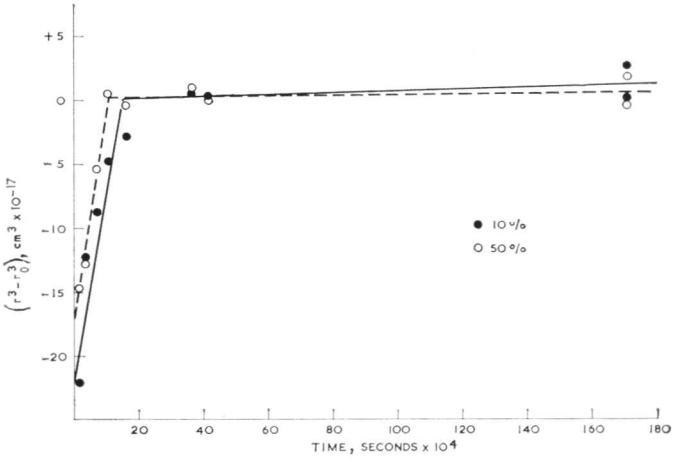

Fig. 8 The influence of ageing time at 160° C upon the growth of θ′ particles by Ostwald ripening after different amounts of plastic deformation.

tion on dislocations is not favoured because the θ″ phase is coherent. Consequently when the density of dislocations and their associated strain fields becomes high, θ″ can no longer be nucleated.

Thus, as no θ″ was present after ~ 15% deformation, the increase in the amount of θ′ cannot be due to an increase in the kinetics of the sequential changes and must be caused by direct nucleation of θ′ from the supersaturated solid solution.

The θ′ phase has been shown to nucleate preferentially on edge dislocations,[7] but it is not known whether it is only nucleated on such defects, or whether it can be nucleated in a defect-free matrix. If only two of the possible three orientations of θ′ were found within a grain, this would confirm that the θ′ was totally nucleated on dislocations of a single Burgers vector. Unfortunately, as the specimens were polycrystalline, at least five slip systems were operative in any one grain, giving a wide spread of dislocation Burgers vectors with a statistical spread of θ′ orientations. However, Silcock[8] using single crystals found that the majority of the θ′ particles formed were in only two orientations. On the other hand, Von Heimendahl[9] claims that the matrix of a very highly deformed material has to be " cleaned " of dislocations before θ′ can nucleate, but it is not clear whether by this he means that θ′ cannot nucleate on dislocations. In the present work θ′ was seen to nucleate in areas of very high dislocation density produced by heavy deformations (70%).

In an attempt to resolve the uncertainty as to the modes of θ′ nucleation, it was thought that a detailed study of θ′ morphology as a function of prior strain would clarify some of the issues. Accordingly, particle-size distributions of θ′ were determined from measurements of particle diameters as observed on electron micrographs. While errors may be introduced by this simple procedure, they should make little difference to comparative results.

The particle-size distributions as a function of ageing time and prior strain are shown in Fig. 4. These histograms show that, except at low ageing times, not only did particle size decrease as the strain was increased but the range of sizes also decreased. These facts seem to indicate that the θ′ was nucleated on dislocations, because the presence of large numbers of dislocations would give many nuclei which would result in a small θ′ particle size with only small deviations about a mean. Fig. 5 illustrates the effect of deformation on the mean θ′ particle size.

At ageing times < 16 h the particle size increased with deformation; thereafter it decreased but nowhere did it decrease to below the mean size in undeformed material. It must be emphasized here that mean sizes were plotted and, as Fig. 4 shows, the spread at low deformations was quite wide.

The peaks shown in Fig. 5, which occur at ~ 5% strain, are thought to result from the fact that at strains < ~ 15% θ″ particles were present with the θ′. Under these conditions θ′ particles could grow at the expense of the θ″ and without hindrance from other θ′ particles. While this situation prevails, the increasing rate of diffusion of copper through the matrix with increasing plastic strain will result in faster growth of the θ′ particles.

Increasing the strain increases the number of θ′ nuclei and decreases the amount of θ″; consequently the copper available for precipitation has to be shared between a greater number of θ′ particles and their growth is retarded. Thus, the mean particle size will decrease with increasing strain.

With strains in excess of 20%, the dislocation density does not increase rapidly with strain, and so the mean particle size is only slowly decreased with further strain.

If it is assumed that the θ′ precipitate density is directly related to the dislocation density, then for a fixed volume fraction of precipitate there should be a relationship of the form

$$\rho \propto 1/r^3$$

where ρ is the dislocation density and r the mean precipitate radius. It was difficult to determine high dislocation densities directly from electron micrographs, but it may be assumed that the initial dislocation density is related to the square of the 0·1% PS of the as-rolled specimens.

A relationship of the type expected from the above arguments was in fact observed, for as Fig. 6 shows, there is a linear relationship between the square of the 0·1% PS of the as-rolled material and the reciprocal of the cube of the mean θ′ particle radius after ageing for 475 h at 160° C.

If substantial diffusion rates can be influenced by dislocation density,[1,10] then it is easy to explain the effect of prior deformation on the initial growth rates of θ′.

The results given in Table I and Fig. 7 show that with short ageing times the growth rate is very sensitive to prior cold work. However at longer ageing times, when the equilibrium volume fraction of θ′ is approached, growth can take place only by the selective coarsening process termed Ostwald ripening. These changes in growth mechanism are illustrated in Fig. 7 where it can be seen that after an initial rapid growth of θ′ the growth rate becomes much slower.

The time-dependence of growth by Ostwald ripening can be expressed by the Liftshitz–Wagner equation[11,12]

$$r^3 - r_0^3 = \frac{8 \cdot \gamma_F \cdot D \cdot C_e \cdot V_m^2}{9 \cdot R \cdot T} \cdot (t - t_0) \qquad \ldots (1)$$

where r is the mean particle radius at time t, r_0 the mean particle radius at the onset of ripening (time t_0), D the diffusion coefficient, V_m the molar volume, C_e the equilibrium concentration of solute, γ_F the interfacial free energy of the precipitate, R the gas constant, and T the absolute temperature.

Boyd,[13] when studying the precipitation of θ′ from undeformed Al–4% Cu alloys, found a linear relationship between the logarithms of the mean radius and time which initially had a slope of $\frac{1}{3}$ in agreement with the requirement of equation (1). However, his attempt to calculate the value of the θ′/matrix interfacial energy (γ_F) from these results gave a value greatly in excess of that found by other methods.

In the present work r^3 was plotted vs. time for differing amounts of prior strain as shown in Fig. 7. It is now assumed that the region showing slower growth rates is that associated with Ostwald ripening and this assumption enabled an estimate of r_0, the mean size of the particles at the beginning of ripening, to be determined from the point of intersection of the lines of rapid and slow growth rates. As can be seen from Fig. 7 the ageing times corresponding to the points of intersection are close to the ageing times for maximum strength. It was now possible to obtain values for $(r^3 - r_0^3)$ and a linear relationship was found between the positive values of this parameter and the ageing time. The data were not very extensive but did indicate that with greater strains the slopes were lower. Assuming a value of $D = 10^{-16}$ cm/sec, the values of γ_F calculated from the present

results were high at low prior strains but were reduced to ~ 10,000 ergs/cm^2 with strains > 50%. While this value is high, it is only an order of magnitude greater than the expected value of 500–1000 ergs/cm^2. These results could indicate that it is only in the absence of other phases that true Ostwald ripening occurs.

The Effect of Pre-Ageing at Low Temperatures

In a further series of experiments, specimens were aged at room temperature for various times after solution-treatment, then plastically deformed as before, and finally aged at 160° C for differing times.

Electron metallographic examination revealed that not only were the θ′ particles smaller but their size range was narrower and they formed sooner than those obtained without prior ageing. This type of behaviour was found over the whole range of room-temperature ageing times investigated (0·75–28 days) and no appreciable differences were detected that could be attributed to variations in the pre-ageing time.

These results suggested that nucleation was enhanced even further by the prior ageing treatment. The reason for this may be that the presence of G.P. zones formed during the room-temperature ageing treatment modify the dislocation distribution on subsequent deformation, so that there are more effective nucleation sites associated with the dislocations. Also, as the dislocations will be held up by the zones, this is equivalent to a pre-existing segregation of copper to the dislocation.

The initial growth of the θ′ phase was more rapid with prior ageing, but then it quickly slowed down indicating an earlier start of Ostwald ripening.

The procedure already described for estimating r_0 was used, and the resulting graphs of $(r^3 - r_0^3)$ as a function of ageing time at 160° C are given in Fig. 8. From the slopes of these lines it was possible to calculate γ_F and values of ~ 750 and 2500 ergs/cm^2 were obtained for the 50 and 10% cold-worked material, respectively. The errors inherent in this calculation are very large but, allowing for these, this estimate of γ_F, particularly that found for the more highly deformed material, is reasonably close to the expected value.

This result is in agreement with the previous conclusion that for true Ostwald ripening the θ′ phase must be the only phase present, and it must be stable at the temperature and over the time range being studied.

Ageing without prior strain does not appear to fulfil these requirements as either θ″ is present with θ′ or the latter becomes unstable as θ is formed.

Conclusions

(1) Plastic deformation increases the ageing rate according to a logarithmic relationship.

(2) Plastic deformation suppresses θ″ formation and very much favours θ′ nucleation at 160° C.

(3) The dislocations introduced by plastic deformation provide favourable nucleation sites, and it is likely that in a deformed alloy the θ′ phase is totally dislocation-nucleated.

(4) In undeformed alloys there is no evidence to suggest that θ′ can be nucleated other than at the dislocations already present within the material.

(5) The Lifshitz–Wagner equation describing Ostwald ripening of θ′ may only be followed after treatments which ensure that neither θ″ nor θ is present within the grains, a condition unlikely to prevail in directly aged material.

Acknowledgements

The authors would like to thank the Ministry of Technology for a research grant enabling this investigation to be undertaken. They are also grateful to Dr. G. C. Weatherley for many stimulating discussions.

References

1. J. W. Christian, " The Theory of Transformations in Metals and Alloys ". **1965:** Oxford (Pergamon Press).
2. J. M. Silcock, T. J. Heal, and H. K. Hardy, *J. Inst. Metals*, 1953–54, **82,** 239.
3. R. Graf, *Publ. Sci. Tech. Ministère Air France*, 1956, No. **(315).**
4. J. W. Cahn, *Acta Met.*, 1957, **5,** 169.
5. M. L. V. Gayler, *J. Inst. Metals*, 1946, **72,** 543.
6. R. Graf and A. Guinier, *Compt. Rend.*, 1954, **238,** 2175.
7. G. Thomas and J. Nutting, " The Mechanism of Phase Transformations in Metals", p. 57. **1956:** London (Inst. Metals).
8. J. M. Silcock, *Acta Met.*, 1960, **8,** 589.
9. M. Von Heimendahl, *ibid.*, 1967, **15,** 417.
10. E. W. Hart, *ibid.*, 1957, **5,** 597.
11. I. M. Liftshitz and V. V. Slyozov, *J. Physics Chem. Solids*, 1961, **19,** 35.
12. C. Wagner, *Z. Elektrochem.*, 1961, **65,** 581.
13. J. D. Boyd, Ph.D. Thesis, Univ. Cambridge, **1966.**

Precipitation of NaCl-Type Carbides in Austenite and Their Behaviour in the Neighbourhood of Grain Boundaries

J. M. Silcock and A. W. Denham

Observations on the nucleation and growth of MC carbides in alloys containing Nb, Ta, V, and Zr are described. Normal $\frac{a}{2}$ [110] dislocations climb in several ways during precipitation in order to provide vacancies for growth of the carbide. Factors affecting the width of grain-boundary zones denuded in Frank partial precipitation (F.P.P.) and matrix dot precipitation (M.D.P.) are described.

This paper is a summary of observations at C.E.R.L. and full experimental details will be published elsewhere. Five classes of precipitate are known. One of these, large grain-boundary particles, will not be discussed in detail; generally $Cr_{23}C_6$ is formed in preference to the NaCl-type carbide unless the carbon supersaturation is low. The formation of these large carbides causes solute depletion in the neighbourhood of grain boundaries, giving narrow ($\sim 0{\cdot}1$ μm) precipitate-denuded zones.

The remaining classes are intragranular and can be regarded as two major types, one dislocation-nucleated and the other nucleated on a very fine scale. The latter has been variously termed " matrix "[1] or " random dot "[2] precipitation. Since there are several forms that can be regarded as precipitation within the matrix, and since there are probably nucleating sites although the dots appear random, this will be termed " matrix dot " precipitation (M.D.P.).

The factors affecting the prevalence of each class and their behaviour at grain boundaries will be described. Differences in the latter compared with the behaviour of Al-base alloys[3–5] will be emphasized although vacancy concentration is important in both cases.

One feature that must be remembered throughout is that the metal atoms in the precipitate are arranged on an f.c.c. lattice as in the matrix, and hence only a simple expansion of the lattice is required. This expansion is large; the precipitate is depleted in carbon (generally approximating to the composition M_4C_3) but even so the linear expansions for V, Ti, Ta, Nb, and Zr carbides are 15, 20, 23, 24, and 31%, respectively. One vacancy collapsing on the surface of a carbide particle will accommodate the expansion due to 2, 1·1, and 0·8 M atoms transferring from matrix to carbide in the case of V, Nb, and Zr carbides, respectively. If a concentration of 10^{-4} vacancies were retained on quenching an alloy containing 0·4 at.-% NbC in solution (the solubility at 1300° C), this would only accommodate 3% of the precipitate. It is not surprising, therefore, that precipitation is generally connected with a mechanism of creating vacancies, and that strain contrast is observed around carbide particles although the interfaces contain dislocations.

Manuscript received 30 January 1968. Miss J. M. Silcock, B.Sc., and A. W. Denham, M.Sc., are in the Central Electricity Research Laboratories, Leatherhead, Surrey.

Normal Nucleation on Quenched-In Whole Dislocations

Dislocations aid nucleation[6] owing to segregation of solute atoms, a reduction in the strain associated with precipitation, and the provision of interface dislocations. Since the M solute atom is large the binding energy to dislocations may be as high as 0·2–0·3 eV. The concentration at a dislocation is then 10–40 times greater than that in solution at 700° C.

For NbC a dislocation reduces the strain to zero in one direction for a 15-Å particle. Clear " Ashby–Brown "-type contrast[7] is observed at particles of 40–100 Å dia. on dislocations after a few hours ageing at 700° C. The strain is about half that calculated from the known misfit and it is clear that the dislocation only partially relieves the strain. Such particles are of a similar size to the separation of the partial dislocations (calculated from the low stacking-fault energy of the matrix) and yet the dislocation between the particles climbs to provide vacancies for further strain relief. Fresh nucleation occurs in the new position of the dislocation.

Edge dislocations appear to climb more readily than screws although nucleation does occur on screw dislocations. Presumably the screw dislocations easily form edge sections in the presence of the large solute atoms. The dislocations sometimes climb to produce areas of small closely spaced particles on {110} planes, particularly at high ageing temperatures after slow quenching rates. This involves climb of the whole edge dislocation in a direction perpendicular to the Burgers vector. These are rarely strictly planar arrays and the dislocations more frequently have a tangled appearance.[8] After ageing at 700° C the loops in the tangle are not all of the same Burgers vector and it appears that some punching-out of dislocation loops must occur. At still higher ageing temperatures, e.g. 800°C, the particles grow more rapidly and punching of loops is more frequent.

Nucleation on Frank Partial Dislocations (F.P.P.)

This mechanism of precipitation is now well known.[8,9] Dislocations which have climbed on to a {111} plane with its normal 35° to the Burgers vector may split into Frank and Shockley partials and the former climbs[10] to give an extrinsic stacking fault providing vacancies for growth of the thin carbide particles nucleated. The Frank partial cannot split and the nuclei do not thicken quickly in the direction of the Burgers vector as in the case of a whole dislocation. A large number of particles of uniform thickness are nucleated and are quickly isolated from the Frank dislocation by its climb. The rate of climb is controlled by the diffusion of the *M* solute atoms to the dislocation. Growth of the particles occurs and this involves movement of further Frank partials[2] or movement of the Shockley close behind the Frank.[13]

A dislocation can nucleate two orientations of Frank partial and generally only two orientations of F.P.P. are observed from one dislocation. Climb loops are therefore preferred nucleation sites to punched-out loops although isolated particles initiate F.P.P. growth, presumably from a punched-out dislocation.[2] Most of the F.P.P. nuclei form during the early stages of ageing when the concentration of *M* atoms is high but after sufficient precipitation to lower the vacancy concentration. Nucleation of F.P.P. appears to be complete when about one-eighth of the total NbC has formed in a 0·25 at.-% Nb, 0·23 at.-% C alloy aged at 700° C, and in agreement with this an alloy containing 0·18 at.-% C solution-treated at 1200° C (~0·22 at.-% Nb in solution) formed only a few F.P.P. The number of nuclei increase as the dislocation density increases to $\sim 6 \times 10^9$ cm/cm^3 (depending on the initial supersaturation) and then decrease as the proportion of precipitate forming initially on dislocations reduces the solute concentration below that required for nucleation.

Growth of F.P.P. continues at very low solute supersaturation and in a 0·35 at.-% Nb, 0·31 at.-% C alloy growth may continue until over half of the total precipitate has formed. Further growth in thickness of the F.P.P. particles may result in as much as 0·8 of the matrix precipitate being F.P.P.

Region Denuded in F.P.P. at Grain Boundaries

The following experimental facts obtained from NbC-forming steels[11] require explanation:

(1) A fairly wide denuded zone occurs (normally ~ 2 μm) which decreases only slightly with decreasing ageing temperature within the limited range available.

(2) The width is particularly sensitive to cooling rate but the increase at slow cooling rates can be reduced by subsequent deformation before ageing. Also if an undissolved particle gives accelerated ageing near a grain boundary in a slow-cooled specimen the denuded region is again reduced.

(3) The zone width is slightly increased by increasing the stacking-fault energy of the matrix, and also by additions of manganese which apparently do not increase the stacking-fault energy.

(4) The zone width increases with decreasing Nb content but is unaffected by changes in carbon content at a constant Nb concentration.

(5) Dislocations near grain boundaries show fewer climb loops during decoration than dislocations well away from grain boundaries (Fig. 1).

Statement (1) shows that the process responsible must have a low activation energy and statement (4) shows that one of the most feasible processes—denudation of carbon by grain-boundary carbide precipitation—is not responsible. Counts of

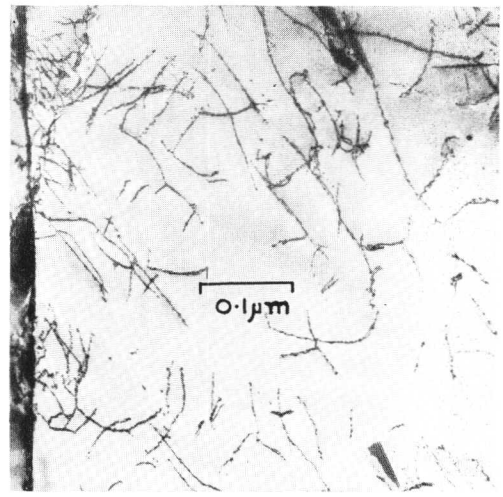

Fig. 1 Climb loops become more prominent away from the grain boundary (i.e. towards the right-hand side). Alloy 16% Ni, 16% Cr, 0·4% Nb, 0·3% C, slow-quenched from 1300° C, elongated 2%, and aged for 8 h at 700° C.

the numbers of nuclei within a grain do not show a dependence on stacking-fault energy, nor is there a clear sign of a change of growth rate with stacking-fault energy and yet there is an effect on denuded zone width. This can be explained if nucleation and growth are controlled by *M*-atom concentration and diffusion when the vacancy concentration is low but also the critical vacancy concentration at which a Frank partial may climb is higher when the stacking-fault energy is lower. Then if the grain boundary behaves as a vacancy source maintaining an equilibrium vacancy concentration, the distance from a boundary at which a Frank partial can climb is controlled by the vacancy-concentration gradient. Within the grain the growth of NbC maintains a low vacancy concentration. Slower-quenched specimens have a low dislocation density and age more slowly, so that the vacancy-concentration gradient at the boundary will be shallow compared with rapidly quenched specimens. When the dislocation density in these specimens is increased, ageing is faster and the vacancy-concentration gradient at the boundary is steeper, allowing nucleation and growth of stacking faults closer to the boundary. One fact which appears to contradict this conclusion is that M.D.P. forms within the zone denuded in F.P.P. However, when both types of precipitate form, M.D.P. are sparse and are still very small when F.P.P. have ceased growing.

Matrix Dot Precipitation (M.D.P.)

Matrix dot precipitation occurs at low temperatures and is prolific in the vanadium-containing alloys. The maximum densities observed are given in Table I. The densities are lower for higher ageing temperatures and slower quenching rates. As the dot carbides grow they punch out dislocations which may develop into F.P.P. or, with high-carbon vanadium steels, into {100} planar aggregates. When M.D.P. and F.P.P. form concurrently there is generally no sharp upper temperature for formation of M.D.P. and M.D.P. may form at higher temperatures than F.P.P. In the more concentrated alloy the replacement of M.D.P. by dislocation decoration and planar growths occurs in a more restricted temperature range (Fig. 2) and the upper limiting temperature T_u is higher for higher supersaturations. The disappearance of M.D.P. is accompanied by a sharp drop in the hardness increase on ageing.

TABLE I

M.D.P. Densities

Alloy, at.-%	Maximum Densities of M.D.P. Observed (particles/cm^3)	Appearance of an Upper Temperature Limit	Hardness Increase (HV) on Ageing at (°C): 650	700	750
1·5 V, 0·5 C	$\sim 10^{15}$	No	55	44	37
2·2 V, 1·0 C	5×10^{16}	Yes	200	120	110
3·0 V, 1·0 C	2×10^{17}	Yes	260	230	130
0·4 Ta, 0·4 C	2×10^{15}	No	—	110	(87 at 800° C)
0·15 Zr, 0·15 C	10^{16}	Yes	50	17	13

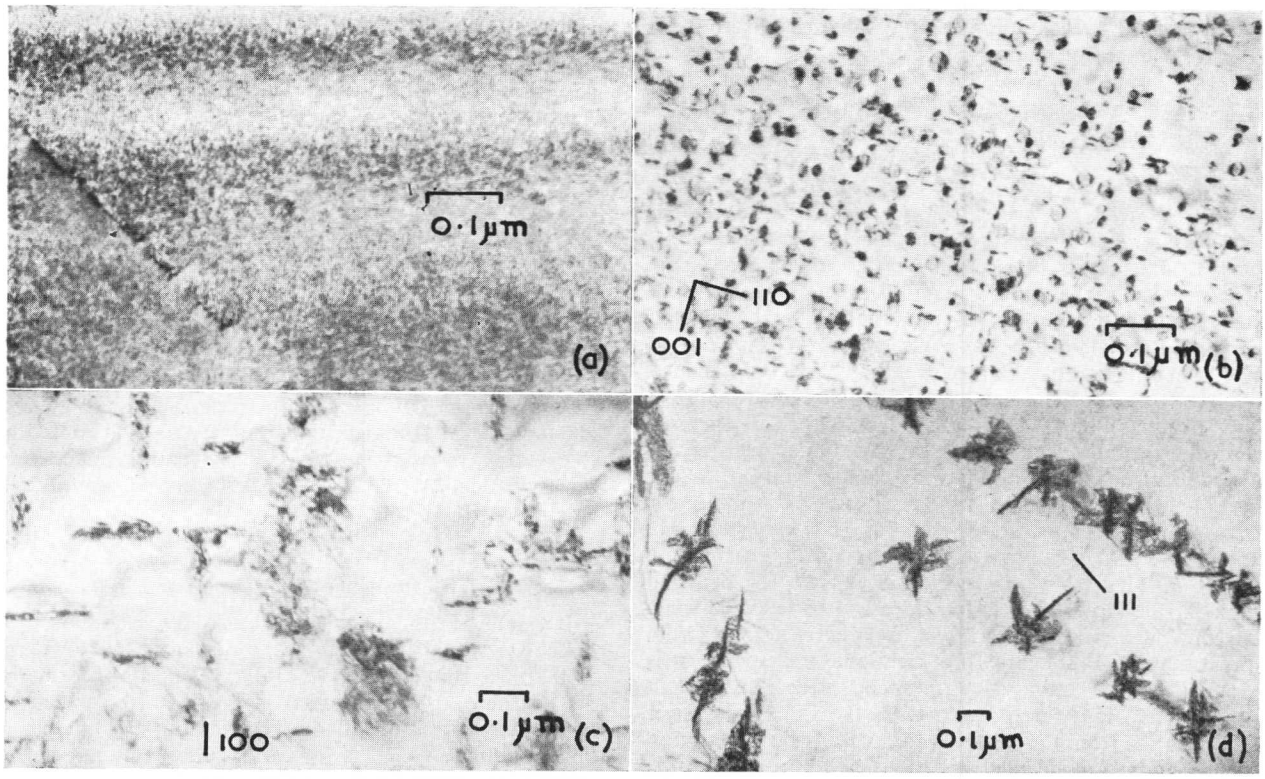

Fig. 2 *M.D.P. at low ageing temperatures changing to dislocation decoration at high ageing temperatures. Alloy* 16% *Ni*, 16% *Cr*, 3% *V*, 1·0% *C, water-quenched after* 1 *h at* 1275° *C, and aged for:*
(*a*) 20 *h at* 600° *C;* $\sim 10^{17}$ *M.D.P./cm*^{3}. (*b*) 20 *h at* 680° *C; small* {100} *planar growths developed from M.D.P.*
(*c*) 20 *h at* 730° *C; foil plane is* (012). (*d*) 2 *h at* 750° *C; dislocation decoration and planar growths only; foil plane is* (112).

In 16% Cr, 16% Ni-base alloys with a constant vanadium content there is a critical carbon content below which M.D.P. does not form. This carbon content is a little higher for higher vanadium contents but is of the order of 0·5 at.-% C, which is a much higher C content than can be obtained in solution in most of the other alloys. Fewer Ta alloys have been examined but the critical carbon content is of the order of 0·2 at.-% and for Zr alloys it must be much lower. M.D.P. has only been observed in a few Nb-containing alloys with low Nb concentration or high nickel content and is more readily observed in slowly cooled specimens.

It is difficult to examine the effect of solution-treatment temperature since most alloys are close to the solidus and many contain undissolved carbides at 1300° C. In the 1·5 at.-% V, 0·05 at.-% C alloy there is no difference between 1250 and 1300° C but 1150° C gives only dislocation decoration. This may be due to a decrease in supersaturation since flakes of $Cr_{23}C_6$ were detected in the 1150° C specimens. Direct transfer of the encapsulated specimens from solution-treatment to the ageing temperature in air decreased the density of M.D.P. to $\sim 10^{14}$ particles/cm^3 for 0·4 at.-% Ta, 0·4 at.-% C. The effect is similar to a slower cooling rate. The M.D.P. is completely suppressed only if changes in solute concentration occur or in some cases when ageing just below T_u. A prior ageing treatment below T_u only affected the subsequent ageing above T_u if detectable carbides formed during the first treatment. A prior ageing for a short time above T_u (so far limited to 800° C) did not prevent or seriously reduce the density of M.D.P. forming below T_u.

Nucleation occurs at short ageing times and the number of

TABLE II

Approximate Width of Denuded Zones for M.D.P. in the Ta-Containing Alloy

Alloy Treatment	Width, μm
Water-quenched from 1340° C, aged at 700° C	0·2–0·3
,, ,, ,, 1300° C, ,, ,, ,,	0·4–0·5
,, ,, ,, 1340° C, aged at 800° C	0·5–0·6
Air-cooled from 1300° C, aged at 700 or 800° C	1·2–1·5
Direct quench to 700° C (in air)	1·0–1·3
,, ,, ,, 700°C (in salt)	0·5–0·7

particles generally reaches a maximum value before a quarter of the total quantity of precipitate has formed. Since it is difficult to see the very small particles, counts at earlier times may err on the low side and nucleation is probably over before one-tenth of the precipitate forms. The small dots show strain contrast which in the early stages have a line of no contrast perpendicular to the operating reflection (i.e. spherical symmetry[7]). However, the larger particles tend to have a line of no contrast in a constant direction or give peculiar contrast effects.[12] Extraction replicas show that the particles are platelets and when large (~200 Å) they can be seen to be platelets in thin foils. In the Ta-containing alloys the platelets are mainly on {111} planes but some are on {100} planes. In the V-containing alloys they are mainly on {100} planes, probably because of the low elastic modulus of austenite in <100> directions.[14] It is impossible to obtain accurate strain values without a detailed knowledge of particle size and shape. Using the relationships given by Ashby and Brown[7] for spherical particles, the strain is never as great as would be expected from the misfit except perhaps for a few very small-dia. particles (~25 Å). The image width remains approximately constant with increasing size, which gives a lower calculated strain. At the larger sizes dislocations can be detected when using low-index reflections and yet apparently normal strain contrast may be obtained with a high-index reflection. It is obvious that the strain values may be misleading but it appears certain that for most particles the values are lower than calculated from the misfit so that vacancy condensation or the formation of misfit dislocations occurs at very small particle sizes. This is consistent with previous suggestions that the particles form on collapsed vacancy loops[1,2] or segregates involving vacancies.[12,13] Growth occurs by punching out dislocation loops.

No definite evidence has yet been obtained of a forerunner of the carbide. There is only a small increase in resistivity on ageing which is of similar magnitude to that detected in Fe–Cr–Ni alloys.[15] A few electron-diffraction patterns show diffuse streaks through matrix spots but this is attributed to small carbides since carbide particles are definitely present in these specimens.

The effect of variations in heat-treatment on the width of the region at grain boundaries denuded in M.D.P. is given in Table II. It is obvious that the cooling rate is the most important variable. Similar results were obtained for the low-V alloy.

Since the solute atoms are large there is probably a high binding energy with vacancies and it seems likely that complexes form rather than collapsed loops. Nucleation on loops and dislocations would be expected to occur at similar temperatures and vacancy loops have not been observed in any stainless steels. The complexes must be unable to grow into large segregates since no diffraction evidence has yet been obtained. If they form at a relatively high temperature (say 900° C) most of the features observed can be explained. The formation of M.D.P. is governed by the ability of these complexes to nucleate the *M*C carbide as compared with dislocation nucleation and the complexes will become less efficient as the critical nucleus size increases. Vacancies will be lost near grain boundaries during quenching so that fewer complexes form in this region. The rate of cooling at high temperatures will then be the most critical factor controlling the supersaturation of vacancies available for forming complexes.

In the concentrated V-containing alloys *preferential* precipitation occurs within ~0·3 μm of the grain boundaries (Fig. 3). This is always preceded or accompanied by the formation of large $Cr_{23}C_6$ particles at the grain boundary. There must therefore be a region adjacent to the grain boundary denuded in chromium. It seems unlikely that depletion of chromium would increase the supersaturation of V_4C_3 which would then give enhanced nucleation. Depletion of chromium reduces the stability of the austenite but the ageing temperature is high for this to create defects to nucleate the V_4C_3. A third possibility is that the diffusion rate of chromium is higher than that of iron or nickel so that vacancies are formed during migration of chromium to the grain boundaries. If this is the explanation, nucleation of all *M*C-type carbides should accompany $M_{23}C_6$ formation, but only in V-containing alloys can the initial carbon content be sufficiently high.

It may be possible to explain the enhancement by assuming that the grain boundary again acts as a vacancy source, allowing the M.D.P. near the boundary to grow more rapidly than elsewhere. In the presence of high carbon concentrations there is no depletion in nuclei near the boundary and only the enhanced growth rate is observed.

Growth Involving {100} Planes or Directions

It would be thought that climb on {100} planes or in ⟨100⟩ directions would not occur in f.c.c. materials. However, the {100} plane is involved in several mechanisms of formation of *M*C carbide. As mentioned above, a factor which might favour the formation of thin platelets on {100} planes is the bulk modulus, which is low in ⟨100⟩ directions so that the strain is accommodated at a lower stress.

Rosettes form on {100} planes in slowly cooled Nb-containing alloys and in the F.P.P.-denuded zones the carbide platelets are quite coarse with straight segments parallel to ⟨100⟩ directions (Fig. 4). There is generally a large platelet in the centre. The dislocations associated with this structure always appear to have a normal $\frac{a}{2}$ [110] Burgers vector which is not in the plane of growth. However, the particles and dislocations are so closely situated that it is not always possible to determine the Burgers vectors clearly.

Aggregates of platelets on {100} planes are more common in the V-containing alloys. The particles are very small (~50–100 Å) and not connected as described above. Again it is difficult to be certain of the Burgers vector but it seems to be the normal $\frac{a}{2}$ [110] type. The {100} planes of particles are not so well defined as the F.P.P. {111} planes (Fig 2) because *the dislocations can glide whereas the Frank partials cannot.* It is easier for dislocations to climb in close-packed directions. If a dislocation on a {111} plane with a Burgers

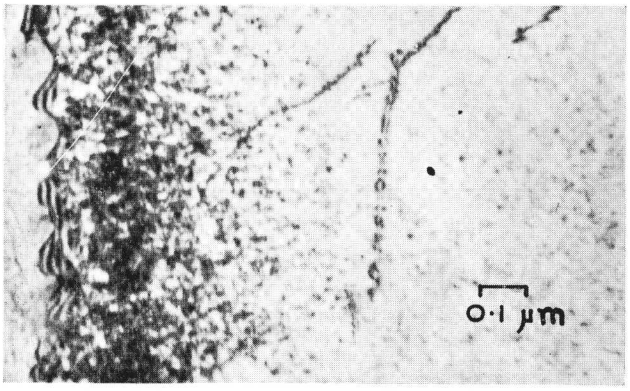

Fig. 3 Enhanced precipitation at grain boundary. Alloy as Fig. 2 but aged for 1 h at 700° C.

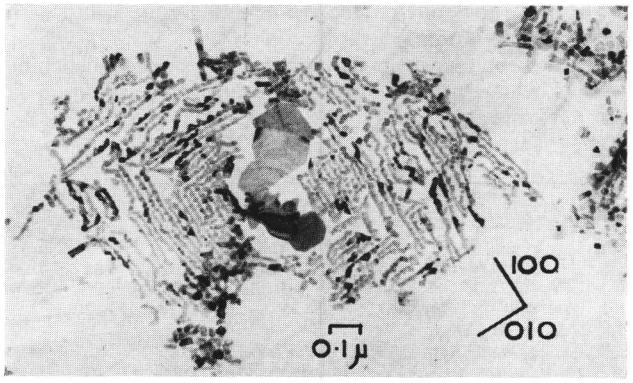

Fig. 4 Extracted {100} aggregate of NbC from a grain-boundary region denuded in F.P.P.

vector $\frac{a}{2}$ [$\bar{1}$10] lies in the [0$\bar{1}$1] direction and if instead of climbing normal to the slip plane it climbs in an [011] direction, it will then climb on a (100) plane. This is possibly the geometry of the dislocation movement.

An even more fascinating climb process occurs in the Ta-containing alloys. Long dipoles are observed in ⟨100⟩ directions (Fig. 5). These have a $\frac{a}{2}$ [110] Burgers vector perpendicular to the direction of the dipole. The dipole is decorated with very small carbide particles and at the head of the dipole a large spot of strong contrast is always observed. This appears to be a particle in some cases but may only be strong dislocation contrast. It appears that a $\frac{a}{2}$ [110] dislocation may climb in an [001] direction leaving a sessile dipole in its trail. Nucleation along the dipole, requiring further vacancies for strain relief, may perhaps be the driving force. However, these particles remain small and there may be an additional factor at the head of the dipole.

Conclusions

It is clear that there are many details requiring clarification but the main conclusions are:

(1) The normal $\frac{a}{2}$ [110] dislocations can climb in a variety of ways to produce vacancies to relieve the strain of MC carbide formation. Planar aggregates of particles on ⟨110⟩ or {100} planes or strings of particles in ⟨100⟩ directions may result, besides the tangled arrays frequently observed.

(2) F.P.P. results from the splitting of normal dislocations and their nucleation frequency is controlled mainly by the dislocation density before ageing and the supersaturation of the M atoms. The width of the denuded zone at grain boundaries is governed by the time available for re-establishing the normal equilibrium vacancy concentration, which is continually depleted by precipitation within the grain.

(3) M.D.P. formation is related to excess quenched-in vacancies but these are bound into complexes at fairly high temperatures. Owing to the strong dependence on carbon content it is considered that M–C–vacancy complexes are involved. The temperature at which complexes form is apparently above that of the observed transition to mainly dislocation-nucleated carbide, T_u, so that the complexes are not destroyed by short times above the transition temperature T_u as are the zones in aluminium alloys. The complexes do not grow at temperatures below T_u and prior ageing at low

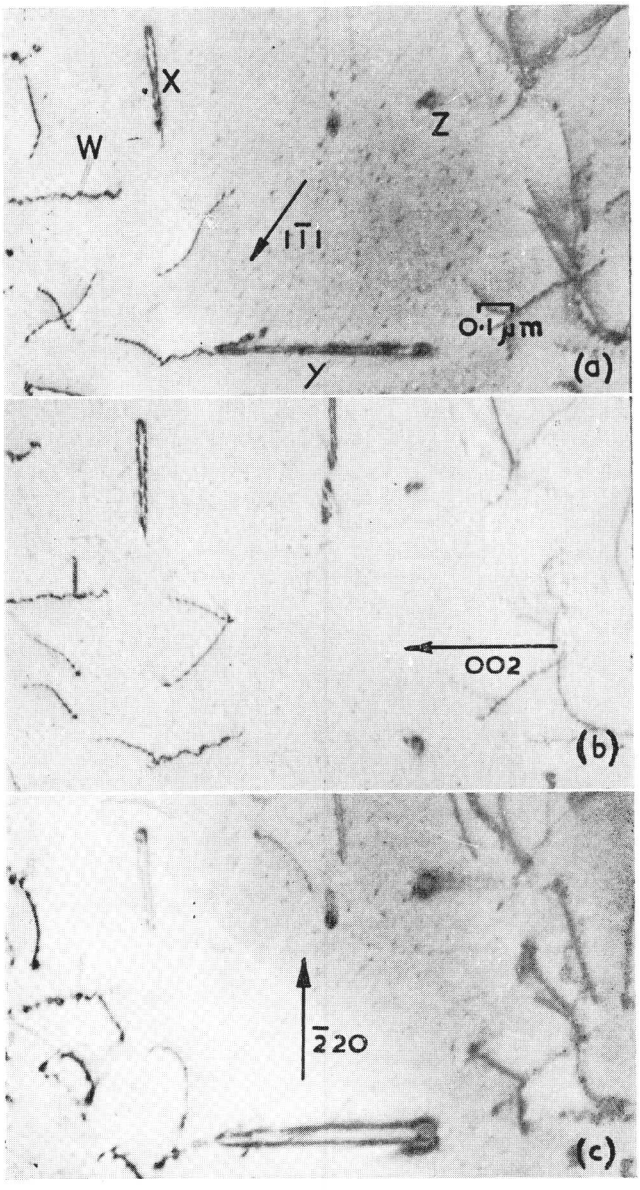

Fig. 5 W, X, Y, and Z are (100) dipoles. Alloy 16% Ni, 17·4% C, 0·3% Ta, 0·3% C, solution-treated at 1340° C, water-quenched, and aged for 1 h at 700° C. (110) foil; the arrow marks the operating reflection.

temperatures does not reduce the denuded zone width as it does in aluminium-based alloys.

(4) Grain boundaries act as vacancy sinks during quenching but may behave as vacancy sources during precipitation of the *M*C carbides.

Acknowledgements

The authors would like to thank many of their colleagues at C.E.R.L. for help with the experimental work and discussions. Thanks are also due to the Central Electricity Generating Board for permission to publish.

References

1. F. H. Froes, D. H. Warrington, and R. W. K. Honeycombe, "Proceedings of Sixth International Congress for Electron Microscopy" (Kyoto, 1966), Vol. 1, p. 431. **1967:** Tokyo (Maruzen Co.).
2. J. M. Silcock, *Acta Met.*, 1966, **14,** 687.
3. J. D. Embury and R. B. Nicholson, *ibid.*, 1965, **13,** 403.
4. G. W. Lorimer and R. B. Nicholson, *ibid.*, 1966, **14,** 1009.
5. D. W. Pashley, M. H. Jacobs, and J. T. Veitz, *Phil. Mag.*, 1967, **16,** 51.
6. D. Turnbull, "Impurities and Imperfections", p. 121. **1955:** Metals Park, Ohio (Amer. Soc. Metals).
7. M. F. Ashby and L. M. Brown, *Phil. Mag.*, 1963, **8,** 1083.
8. J. M. Silcock, *J. Iron Steel Inst.*, 1963, **201,** 409.
9. J. S. T. Van Aswegen and R. W. K. Honeycombe, *Acta Met.*, 1962, **10,** 262.
10. J. M. Silcock and W. J. Tunstall, *Phil. Mag.*, 1964, **10,** 361.
11. J. M. Silcock and K. W. Sidding, to be published.
12. J. M. Silcock, "Proceedings of Sixth International Congress for Electron Microscopy" (Kyoto, 1966), Vol. 1, p. 407. **1967:** Tokyo (Maruzen Co.).
13. J. J. Irani and R. T. Weiner, *Nature*, 1965, **205,** 975; *J. Iron Steel Inst.*, 1965, **203,** 913.
14. K. Salmutter and F. Stangler, *Z. Metallkunde*, 1960, **51,** 544, C. E. Trans. 2066.
15. J. Barford, M. J. Knight, and J. M. Silcock, *J. Iron Steel Inst.*, 1966, **204,** 122.

Carbide Transformations in Ferritic Steel

J. M. Darbyshire and J. Barford

The tempering of ternary and quaternary martensites and bainites of composition (Fe + 0·1–0·2 wt.-% C + Cr, Mo, V) has been studied by means of dilatometry, resistometry, and electron microscopy. A continuous-heating technique was employed to examine the tempering process over the range from room temperature to 700° C. The transformation of cementite to alloy carbide above 500° C is characterized by a resistivity decrease and a volume change. The presence of carbide-forming elements retards the growth and modifies the morphology of cementite during tempering up to 500° C. Differences in the nucleation modes and growth rates of VC and Mo_2C were observed and the probable contributory factors are discussed.

During the past ten years there have been many metallographic investigations of the tempering process in alloy steels.[e.g.1–3] However, much of the earlier work was performed on complex commercial alloys containing several strong carbide-formers and only recently has more emphasis been placed on simple alloys in an effort to understand more thoroughly the mechanisms involved.

An alternative approach is to study the kinetics of the process, since a knowledge of the time- and temperature-dependence of the fourth stage of tempering should provide quantitative data on the mode of nucleation, shape, and distribution as well as growth characteristics of alloy carbides. There have been many investigations of the kinetics of the first and third stages of tempering in Fe–C alloys, but few investigations of alloy-carbide precipitation kinetics have been reported.[4–7] Recently, Barford[8] has shown that the volume changes accompanying NbC formation in an austenitic steel may be used as an accurate measure of alloy-carbide kinetics. Thus, this technique may be suitable for the study of alloy-carbide formation in ferritic steels. Changes in electrical resistivity are also commonly observed to occur during precipitation reactions, but the method has not been used extensively to follow alloy-carbide formation in ferritic steels.[7,9,10] Precipitation kinetics cannot be defined with accuracy simply from hardness variations. The present work correlates volume and resistance changes with hardness variations and structural observations during alloy-carbide precipitation in ferritic steels, and considers some aspects of the kinetics of the isothermal transformation from cementite to VC and Mo_2C.

Manuscript received 12 February 1968. J. M. Darbyshire, B.Sc., A.R.S.M., and J. Barford, Ph.D., A.I.M., are in the Central Electricity Research Laboratories, Leatherhead, Surrey.

TABLE I

Alloy	Wt.-% C	Wt.-% Alloying Element
P 14	0·14	
V 1205	0·12	0·5 V
Mo 1213	0·12	1·3 Mo
Mo 2040	0·2	4·0 Mo
Cr–V 1505	0·13	1·5 Cr; 0·5 V

Experimental Methods

Materials

The alloys used were vacuum-melted by B.I.S.R.A. from pure Swedish iron and pure alloying elements to the compositions shown in Table I.

Dilatometry

Strip specimens, 4 cm × 1 cm × 0·5 mm, were heat-treated to give complete solution of alloy carbides and quenched at two different rates to give martensitic and bainitic structures ($\sim 10^4$ and 10^2 degC.sec^{-1}, respectively).

As-quenched specimens were then heated, at a steady rate of 90 degC.h^{-1}, from room temperature to 700° C in a differential dilatometer[11] employing a fully tempered specimen of the same alloy as a standard. A plot of relative length change vs. temperature was continuously recorded. Specimens intended for metallographic examination and hardness measurements were tempered in a salt bath heated at the same rate.

The time–temperature-dependence of the $Fe_3C \rightarrow VC$ and $Fe_3C \rightarrow Mo_2C$ transformations in Alloys V 1205 and Mo 1213 was studied isothermally by a dilatometric technique. After solution-treatment and quenching, specimens were aged for 2 h at 350° C to precipitate all carbon as Fe_3C, followed by further ageing in the temperature range of alloy-carbide formation. During the latter treatment the specimen length was continuously monitored. The treatment at 350° C is essential, otherwise both cementite and alloy carbide would form concurrently during the early stages of reaction at the higher temperature, and unambiguous data on alloy carbide kinetics could not be obtained.

Electrical-Resistance Measurements

The specimens for electrical-resistance measurements consisted of parallel-sided strips cut from 0·2-mm-thick sheet which were solution-treated under the same conditions as the dilatometer specimens. Two 0·002-in.-dia. Pt/Pt–Rh thermocouples were spot-welded on to the specimen to con-

trol and monitor the temperature and 0·002-in.-dia. Pt wires were used as potential leads. The sample was resistance-heated at 90 degC.h^{-1} to the desired temperature and then allowed to cool to room temperature for resistance measurements. The measured resistance was corrected for variations in room temperature.

Results and Discussion

Dilatometric Changes

After quenching to martensite all the alloys show a contraction of nearly constant magnitude on heating up to 500° C. This effect is well established and is due to the precipitation of iron carbides.

In the plain carbon steel (Fig. 1) precipitation begins when the temperature is $> \sim 50°$ C and proceeds continuously up to a temperature of 500° C, above which no further length changes are observed. However, in the V and Mo steels a marked expansion occurs on heating above 500° C (Figs. 2 and 3).

Volume changes after the slower quench, giving a bainitic structure, show that 90% of the carbon present has precipitated as cementite during the quench. However, the subsequent expansions on further heating are exactly the same as in rapidly quenched specimens, indicating that no alloy carbides have formed during the quench.

Correlation of Measured and Calculated Dilations

The plain carbon steel shows only the well-established shrinkage due to iron-carbide formation on tempering to 500° C. There can be little doubt that the expansions on tempering between 500 and 700° C shown by the V and Mo steels are due to alloy-carbide formation since secondary hardening occurs in the same temperature range and VC and Mo_2C were identified by electron diffraction from carbon extraction replicas.

The magnitudes of the linear dilations to be expected for both cementite and alloy-carbide formation have been calculated on the assumption that all available alloying element reacts with carbon to give the stoichiometric carbide and any remaining carbon persists as cementite. The structural data were obtained from Pearson[12] and the calculated dilations are compared with the experimental values in Table II.

No lattice-parameter data are available for 0·1% C martensites, thus the c and a values for high-carbon martensites were extrapolated back to 0·1% C. Since it is generally accepted that low-alloy martensites containing only 0·1% C are cubic,[13] a mean lattice parameter A_0, calculated from the values of c and a, was used to calculate the martensite unit-cell volume.

Because of the high M_s temperatures of the low-alloy steels used ($\sim 450°$ C) it is difficult to obtain a martensite without significant autotempering. Thus the magnitude of the dilation due to cementite precipitation is very sensitive to quench rate. Fig. 2 shows the limits of the variation in dilation due to cementite formation in specimens of Alloy V 1205 judged visually to have been rapidly quenched. The dotted line shows the minimum dilation, while the full line shows the maximum and indicates that at least 20% of the available carbon may be precipitated during an ostensibly rapid quench. However, the maximum dilation observed is in good agreement with the calculated value.

The dilations due to alloy-carbide formation showed less scatter and the measured expansions due to the transformation of cementite to VC and Mo_2C are in good agreement with the calculated values for Alloys V 1205, Cr–V 1505, and Mo 2040. The correlation between calculated and experimental dilations is not as good for Mo 1213. This is simply because complete transformation of cementite to Mo_2C is not obtained at this low Mo content.

Resistance Changes

Fig. 1 shows the normalized resistance and dilatometric changes for Alloy P14 (the total changes were $\Delta R/R = 10{\cdot}5\%$ and $\Delta l/l = 0{\cdot}035\%$, respectively). The derivative curves included in this figure show two clear peaks for the dilatometric data. The resistance derivative shows three peaks, the first two corresponding to those of the dilatometric data. The first two resistivity peaks at ~ 100 and 250° C are clearly due to ε-carbide and cementite precipitation, respectively,[14] but the third resistivity peak is not associated with any inflection in the length-change curve. It occurs over the range 350–500° C which is associated with the dissolution of the intra-martensitic cementite particles and the formation of coarser particles at inter-martensitic boundaries. Since this process is not associated with any significant decrease in carbon concentration it would not be expected to affect the density of the material. However the electrical resistance of a material is sensitive to the degree of dispersion of a precipitated phase and is therefore likely to be affected by the redistribution of cementite. There is no measurable change in room-temperature resistance on heating above 625° C within the α-Fe range.

Fig. 2 shows the normalized resistance and dilatometric changes for Alloy V 1205 (the total room-temperature resistance change was 17·6%). The derivative curves are included and both show peaks at ~ 100 and 250° C as did the Fe–C alloy. The dilatometric-derivative curve clearly shows the onset of VC precipitation to begin at 500° C, reaching a maximum rate at 620° C. The resistance-derivative curve shows more complex behaviour, giving a small peak at 475° C and a larger one at 580° C. Comparison with the normalized resistance curve shows the 475° C peak to be due to a sharp resistance decrease between 450 and 500° C which we attribute to cementite coarsening (at a higher temperature than in Alloy P 14) before VC precipitation. This is followed by a further 50 degC range with no resistance change.

It is commonly observed that anomalous resistance changes occur in the early stages of precipitation processes, usually in the form of a resistance increase. This is commonly ascribed either to very small and closely spaced precipitates or to coherency strain fields. It is unlikely that these effects will make a significant contribution to density and therefore we expect the dilatometric method to give a more definitive description of the onset of VC formation. This anomalous resistance effect occurs in the present system and the beginning of the resistance plateau corresponds exactly with the change in sign of the length change; that is, with the beginning of VC precipitation.

The resistance-derivative peak for VC precipitation occurs about 40 degC lower than the dilatometric peak. This is due to the existence of the resistance plateau and is caused by two conflicting effects: one is a tendency for the resistance to decrease due to removal of both substitutional and interstital atoms from solution and to the dissolution of cementite; the other effect is a resistance increase due to fresh precipitation. Once the latter effect has decreased (under conditions of continuous heating this may be due to re-solution of small

TABLE II

Alloy	At.-% C	At.-% *M*	A_0 Martensite, kX	Vol. 100 Atoms Martensite, kX^3	Vol. 100 Atoms Fe + Fe_3C, kX^3	Linear Dilation, %	
						Calculated	Experimental
P 14	0·66		2·864	1166·75	1165·5	−0·036	−0·038
			A_0 (Fe*M*), kX	Vol. 100 Atoms Fe*M* + Fe_3C	Vol 100 Atoms Fe + *MC*		
V 1205	0·464	0·5466	2·8610	1167·062	1168·420	+0·039	+0·035
Mo 1213	0·525	0·7597	2·8627	1168·153	1169·857	+0·035	+0·012
Mo 2040	0·9423	2·3566	2·8672	1170·471	1172·168	+0·048	+0·053
Cr–V 1505						+0·039	+0·030

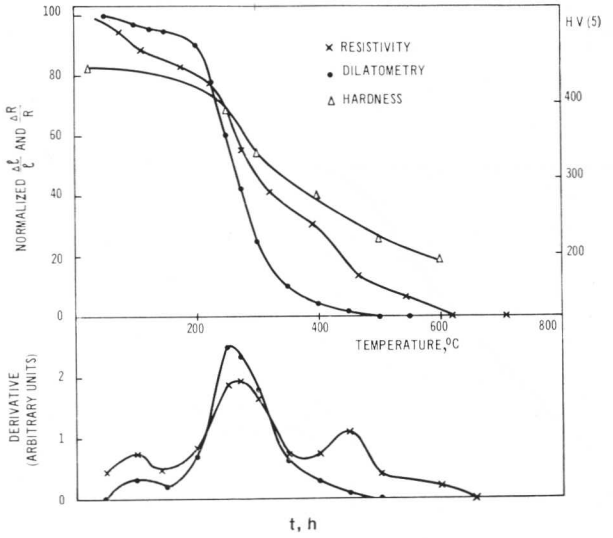

Fig. 1 *Alloy P* 14. *Normalized resistivity, length, and hardness changes on continuous heating.*

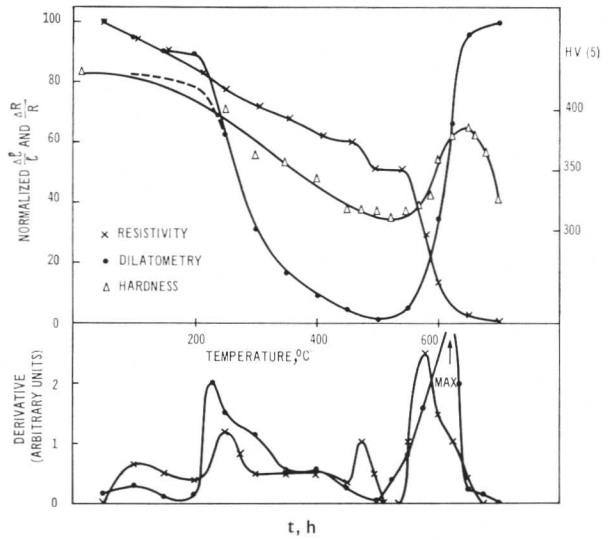

Fig. 2 *Alloy V* 1205. *Normalized resistivity, length, and hardness changes on continuous heating.*

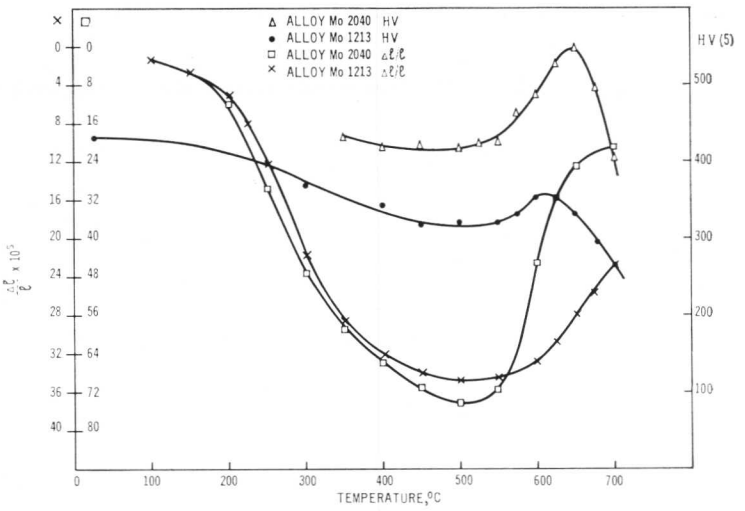

Fig. 3 *Alloys Mo* 1213 *and Mo* 2040. *Length and hardness changes on continuous heating.*

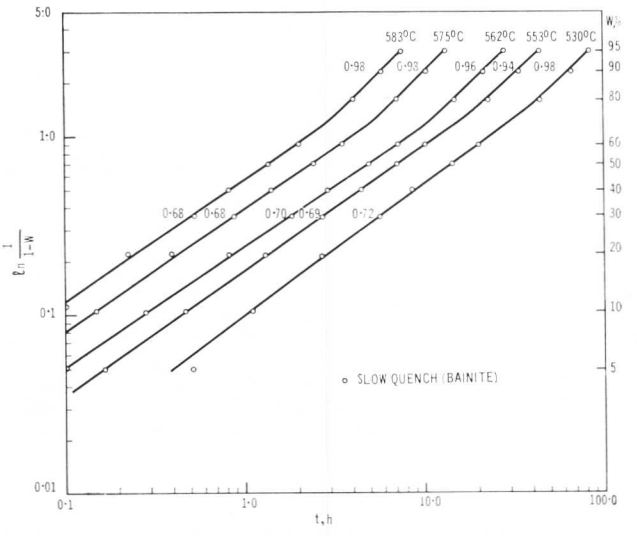

Fig. 4 *Alloy V* 1205. *Isothermal precipitation of VC (bainite).*

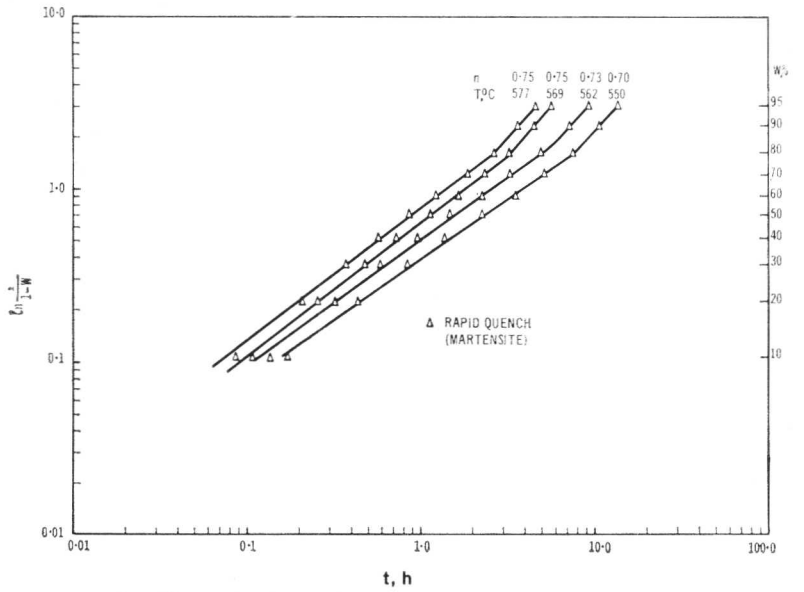

Fig. 5 Alloy V 1205. *Isothermal precipitation of VC (martensite).*

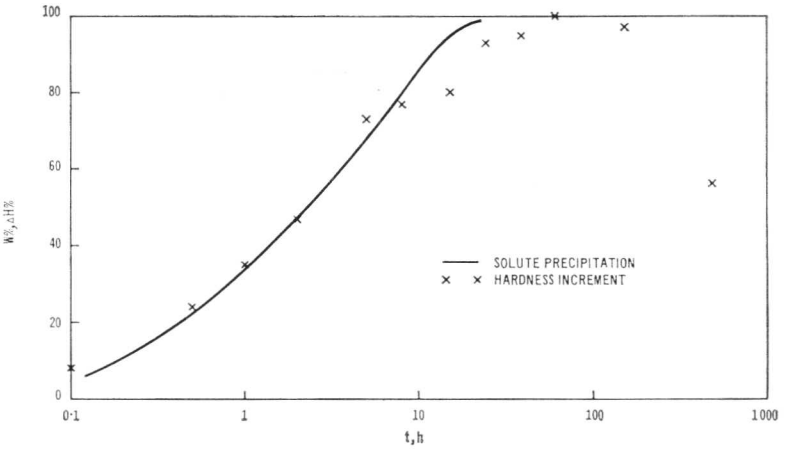

Fig. 6 Alloy V 1205. *Comparison of time-dependence of solute precipitation and normalized hardness increment. Aged at* 550° *C.*

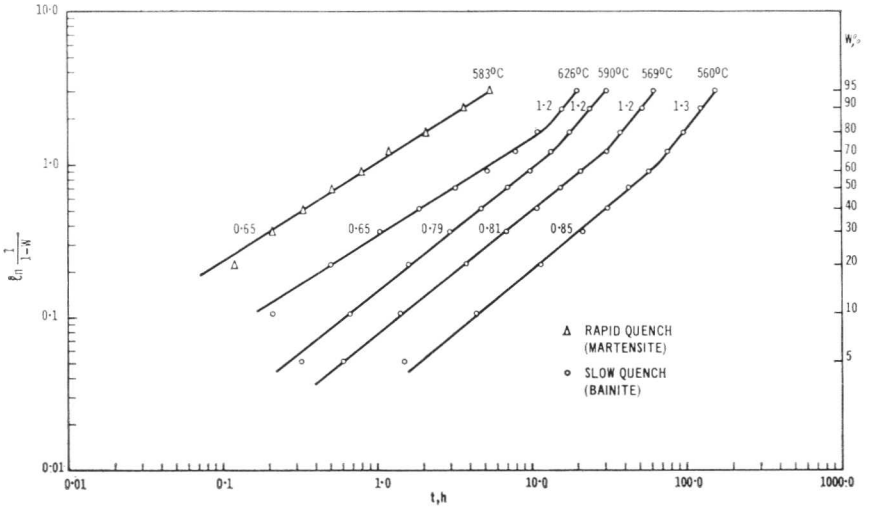

Fig. 7 Alloy Mo 1213. *Isothermal precipitation of* Mo_2C.

unstable nuclei or to coherency breakdown) the resistance will drop sharply to a value dictated by the current supersaturation and the derivative curve will show a peak, although the actual rate of precipitation may not be a maximum at that temperature. These anomalous resistance changes make isothermal data difficult to interpret, and illustrate the difficulty of using resistance changes alone to follow precipitation reactions.

Alloy-Carbide Formation

The information that can be derived from continuous heating experiments is essentially qualitative. However, it provides some useful clues to the general precipitation behaviour which may then be examined in greater detail by isothermal experiments. Because of the presence of an effect giving a resistivity rise in these materials[7] and the resulting difficulty in interpreting resistivity changes in terms of fraction of solute precipitated, dilatometry has been used to study isothermal precipitation.

On continuous heating, peak hardness corresponds to VC precipitated fractions of 0·95 in the simple V alloy and 0·8 in the Cr–V alloy. This effect could be explained in terms of continuous nucleation of VC during tempering between 500 and 650° C. Alternatively the effect could be due to a high density of VC nucleation on dislocations. Electron microscopy of extraction replicas indicates that VC forms as a random-dot precipitate by a " fresh site " nucleation process. However, different investigators working on similar steels disagree as to the nucleation site.[15,16]

The situation is clarified when the isothermal data are considered. These data have been analysed by means of the generalized Johnson–Mehl equation

$$W = 1 - \exp[-(t/\tau)^n]$$

where W is the fraction of solute (expressed in terms of fractional length change) precipitated in time t, and n and τ are constants. Recent treatments by Ham[17,18] of diffusion-controlled precipitation have shown that this equation should closely approximate the true time-dependence of precipitation for a considerable fraction of the reaction time for a number of precipitate modes. The value of the time exponent n may provide information regarding the nucleation and growth mechanisms involved. Figs. 4 and 5 show the time–temperature-dependence of the $Fe_3C \rightarrow VC$ transformation in bainitic and martensitic matrices over the range 530–580° C. In both structures the value of n is $\sim 0{\cdot}7$ for $W < 0{\cdot}70$. This is very close to the value of $\frac{2}{3}$ proposed by Harper[19] in a semi-empirical extension of the Cottrell–Bilby approach to the precipitation of interstitial solute on dislocations by a strain-ageing mechanism. Although the experimental data of a number of workers all provide a good fit with the Harper equation the theoretical arguments of Ham[18] and Bullough and Newman[20] indicate that the equation should be valid only in the very early stages of precipitation. Despite the uncertainty regarding the exact mechanism of strain-ageing and its kinetics, the results obtained here may be taken to show that precipitation of VC occurs predominantly on dislocation sites. The possibility of continuous nucleation is eliminated since this would be characterized by a value of n of at least 2·0.

The occurrence of peak hardness near the end of the precipitation process may be explained on the grounds that nucleation on dislocations in a material of high dislocation density will give rise to small diffusion paths and rapid particle growth. Since the density of nucleation is high, the particles are not big enough to have maximum dislocation-pinning effect at room temperature until solute precipitation is virtually complete.

The rate of isothermal precipitation and the corresponding variation in hardness for Alloy V 1205 aged at 550° C are shown in Fig. 6. Up to $W = 0{\cdot}75$ the hardness increases in direct proportion to the fraction of solute precipitated. But above this value the hardness increment lags and peak hardness is not reached until 60 h, whereas solute precipitation is complete in 25 h. Thus, some degree of coarsening of VC particles is necessary for peak room-temperature hardness and, under conditions of continuous heating, this may occur before the end of the precipitation process proper.

When the fraction of VC precipitated is $> 0{\cdot}7$ there is an abrupt change in kinetics, the value of n changing from 0·7 to $\sim 1{\cdot}0$. This is interpreted in terms of a recovery process when precipitate particles pinning the dislocations attain some critical size.[21]

In contrast to the precipitation of VC, Mo_2C precipitates relatively slowly in Alloy Mo 1213 (Fig. 3). The isothermal data of Figs. 4 and 7 show this effect to be most marked in the bainitic structures where the difference in VC and Mo_2C precipitation rates is approximately an order of magnitude. In addition, peak hardness occurs after only 30% Mo_2C precipitation in Alloy Mo 1213 (Fig. 3). The value of the time exponent n for precipitation of Mo_2C in the martensitic matrix is 0·65, but in the bainitic structure the value of n progressively increases from 0·65 on ageing at 626° C to 0·85 on ageing at 560° C. Thus it is reasonable to infer that Mo_2C also precipitates predominantly on dislocations when the dislocation density is high. However because of the large misfit between the lattices of Mo_2C and α-Fe it is possible that dislocation nucleation may be more difficult than for VC and that only certain dislocation sites, such as jogs or intersections, are preferred. Other regions of higher lattice disturbance will then become of greater importance as nucleation centres. Thus in the bainitic structure with a lower dislocation density, the number of particles nucleated on sites other than dislocations will be relatively great. This effect will be accentuated at lower ageing temperatures when the number of thermodynamically stable nuclei is increased.

Raynor *et al.*[22] observed Mo_2C precipitates to form envelopes around existing Fe_3C particles. It is probable that these nucleate on dislocations at the interface between the cementite and the matrix, but in view of the isolated nature of each " envelope " it is reasonable to treat individual " envelopes " as single particles of finite initial size growing under diffusion-controlled conditions. From the work of Ham[17] we expect that the growth of such envelopes will affect the overall kinetics, and in particular increase the value of n. Precipitation on interfaces such as martensite needle boundaries will also tend to increase n.

Examination of extraction replicas shows that the distribution of precipitate particles is much less dense in the Mo steel than in the V steel and supports the view that Mo_2C is more difficult to nucleate than VC (Figs. 8 and 9).

A lower nucleation density in the Mo steel would account for differences in the rates of Mo_2C and VC precipitation, and this is at present under investigation. Another contributory factor may be that V diffusion is more rapid than Mo diffusion but at present no data are available to substantiate this. Differences in solute supersaturation also favour faster VC precipitation.

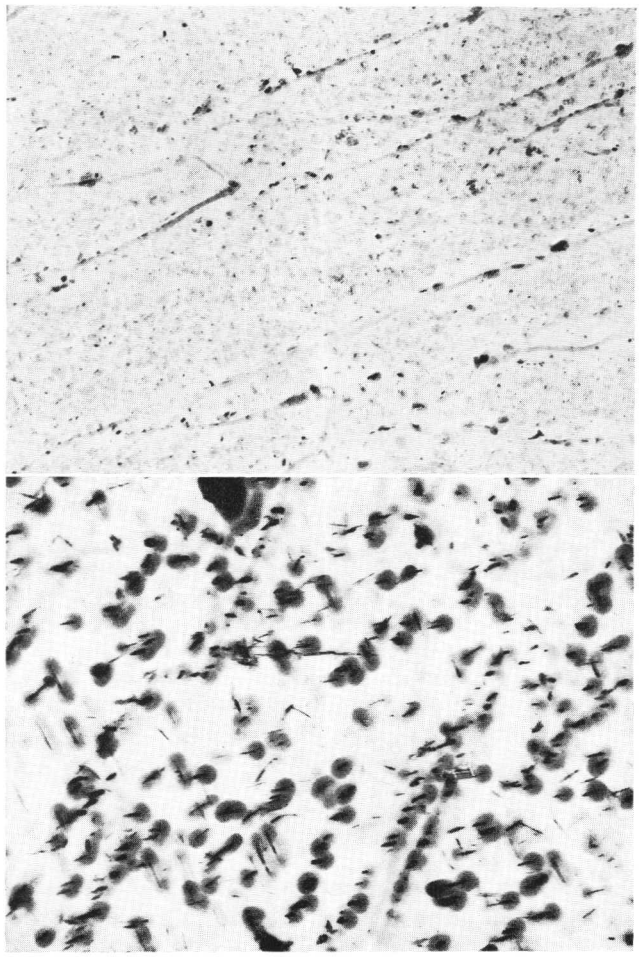

Fig. 8 *Alloy V* 1205. *Aged* 1 *h at* 700° *C* (*martensitic matrix*). × 24,000.

Fig. 9 *Alloy Mo* 1213. *Aged* 1 *h at* 700° *C* (*martensitic matrix*). × 24,000.

In addition to an effect on the rate of carbide precipitation, variation in the nucleation density would modify the relation between peak hardness and the fraction of solute precipitated. If the number of Mo_2C nuclei is less than the number of VC nuclei then, after precipitation of a given fraction of solute, the size of individual Mo_2C particles would be increased relative to VC. Dislocation recovery may then begin before the matrix is fully depleted of solute and peak hardness would be attained during the early stages of precipitation. This would also be true of any hardening contribution due to interaction between dislocations and coherency strain fields around Mo_2C precipitates, since early break-down of coherency may be expected on account of the marked mismatch between the lattices of the carbide and the matrix.

It may be noted that Alloy Mo 2040 behaves in a similar manner to V 1205 insofar as precipitation rate and peak hardness are concerned (Fig. 3). The higher solute supersaturation of Mo 2040 will greatly increase the driving force for nucleation, resulting in an increased density of Mo_2C particles compared with Mo 1213 and a corresponding increase in precipitation rate.

The only other attempt to measure isothermal precipitation rates of VC and Mo_2C is described in a recent publication by Wilkes.[7] We note that although the steels are of similar composition to those used in the present work, there is apparently little similarity in behaviour. For example, the total resistance change for V 1205 for the first, third, and fourth stages of tempering is 17·6% whereas in an alloy of rather higher V content Wilkes finds only ~ 6% decrease. The rates of precipitation also differ significantly. However, the major difference lies in the form of the derived rate curves and the value of the time exponent. The reasons for these discrepancies are not clear but a likely cause is the different experimental methods and starting conditions of the materials. We indicated earlier some of the difficulties associated with the use of electrical-resistance changes to follow precipitation rates when an initial increase in resistance is followed by a decrease. In general, under these conditions it is not possible to define precisely the time-dependence of the decay of supersaturation, although this may be possible in some cases.[23] Finally, Wilkes' resistivity data refer to the tempering of an ostensibly virgin martensite whereas ours refer solely to alloy-carbide precipitation, the metastable precipitate, cementite, having been completely formed at 350° C before isothermal measurements were made in the alloy-carbide temperature range. Thus the short-time resistivity data must contain a contribution due to cementite formation which will merge into the alloy-carbide reaction at longer times. The cementite distribution will also be different and we have found this factor to have a significant effect on alloy-carbide formation.[24]

In view of the effect of solute supersaturation on precipitation rate we would have expected VC precipitation in Wilkes' alloy (1% V, 0·1% C) to have proceeded more rapidly than in V 1205. However, on ageing at 550° C, our dilatometric measurements indicate precipitation to be complete after ~ 25 h whereas Wilkes' data indicate a continuing resistivity decrease up to 4000 h. Hardness measurements on V 1205 show overageing to begin after 60 h at 550° C and the hardness has dropped to 50% of its peak value after 400 h. We would therefore suggest that the slow precipitation rate implied by the resistivity measurements is partly attributable to overageing.

Conclusions

(1) The precipitation of iron carbide during tempering of a ferritic martensite is accompanied by a volume contraction and a decrease in electrical resistivity.

(2) The transformations of cementite to VC and Mo_2C are accompanied by volume expansions and corresponding decreases in electrical resistivity.

(3) Since conflicting resistivity increases due to coherency strain, and resistivity decreases due to solute depletion, occur in the early stages of alloy-carbide precipitation, a more definitive description of the cementite to alloy-carbide transformation may be obtained from dilatometric data.

(4) Differences in both the observed rates of VC and Mo_2C precipitation and the precipitate fractions corresponding to peak hardness can be largely attributed to differences in the number of sites suitable for VC and Mo_2C nucleation.

Acknowledgement

The authors wish to thank the Central Electricity Generating Board for permission to publish this paper.

References

1. E. Smith and J. Nutting, *J. Iron Steel Inst.*, 1957, **187,** 314.
2. A. K. Seal and R. W. K. Honeycombe, *ibid.*, 1958, **188,** 9.
3. F. B. Pickering, "Precipitation Processes in Steels", (Special Rep. No. 64), p. 23. **1958:** London (Iron Steel Inst.).
4. R. W. Balluffi, M. Cohen, and B. L. Averbach, *Trans. Amer. Soc. Metals*, 1951, **43,** 497.
5. P. Payson, *ibid.*, 1959, **51,** 60.
6. T. Sato, H. Kaneko, and T. Nishizawa, *J. Australian Inst. Metals*, 1960, **5,** 123.
7. P. Wilkes, *Metal Sci. J.*, 1968, **2,** 8.
8. J. Barford, *J. Iron Steel Inst.*, 1966, **204,** 134.
9. T. M. F. Ronald and C. Bodsworth, *ibid.*, 1965, **203,** 252.
10. P. Wilkes and H. J. Bray, *Iron and Steel*, 1966, **39,** 308.
11. J. Barford, *J. Sci. Instruments*, 1963, **40,** 444.
12. W. B. Pearson, " Lattice Spacings and Structures of Metals and Alloys ". **1958:** London (Pergamon Press).
13. W. S. Owen, E. A. Wilson, and T. Bell, 2nd Internat. Materials Symposium, Univ. California, 1964.
14. J. F. Butler, *J. Iron Steel Inst.*, 1966, **204,** 127.
15. E. Tekin and P. M. Kelly, *ibid.*, 1965, **203,** 715.
16. E. Smith, *Acta Met.*, 1966, **14,** 583.
17. F. S. Ham, *J. Phys. Chem. Solids*, 1958, **6,** 335.
18. F. S. Ham, *J. Appl. Physics*, 1959, **30,** 915.
19. S. Harper, *Phys. Rev.*, 1951, **83,** 709.
20. R. Bullough and R. C. Newman, *Proc. Roy. Soc.*, 1962, [A], **266,** 209.
21. J. M. Darbyshire and J. Barford, *Acta Met.*, 1967, **15,** 671.
22. D. Raynor, J. A. Whiteman, and R. W. K. Honeycombe, *J. Iron Steel Inst.*, 1966, **204,** 1114.
23. J. Barford, M. J. Knight, and J. M. Silcock, *ibid.*, 1966, **204,** 122.
24. J. M. Darbyshire and J. Barford, unpublished work.

Iron Carbides in Tempered Steels

S. Murphy, J. A. Whiteman, and J. H. Woodhead

The anomalous 250° C Curie point found in quenched and tempered iron–carbon alloys has been investigated. Magnetic analysis showed that this Curie point was present in both high- and low-carbon alloys on tempering below 500° C and the reason for this Curie point was investigated by thin-foil electron microscopy and electron diffraction. The 250° C Curie point was associated with the presence of cementite with modified lattice parameters, which probably resulted from a relationship with the matrix in which it formed. The nature and extent of the modification are described in detail. In the early stages of tempering the modification to the cementite is large and the Curie point is higher than 250° C. After tempering at 400° C there is little modification and the Curie point is ~ 245° C. The modified cementite dissolved when normal cementite formed in the needle and lath boundaries. There is little evidence for the formation of ε-carbide during tempering.

When steels are quenched and then tempered, the high-carbon supersaturation in the martensite is relieved by the formation of iron carbides. There are a number of these, but only two have been identified in tempered steels. At low tempering temperatures an h.c.p. carbide is formed[1,2] known as ε-carbide. After tempering at higher temperatures this disappears and is replaced by cementite, θ, which is stable for long periods at the highest tempering temperatures.

At intermediate tempering temperatures, the temper carbide has certain physical properties that distinguish it from both ε and θ iron carbides. It has a Curie point near 250° C,[3–5] and the X-ray and electron-diffraction patterns have anomalous features.[6–8] Some investigators have suggested that another iron carbide is formed intermediate between ε and θ;[3,7,9,10] others maintain that the effects are due to the shape and size of the cementite particles when they first appear.[8,11] Those who favour the formation of a different iron carbide usually claim that it is " rhombic ", though some say that it is χ-carbide, otherwise known as Hägg carbide or iron percarbide, with a monoclinic structure very similar to cementite in its atomic arrangement.[12,13]

χ-carbide has a Curie point at or near 250° C.[14] It has been identified in carburized-iron catalyst powders[14] and in thin films of carburized iron.[15] Certain diffraction patterns from tempered steels have been attributed to its presence.

Manuscript received 6 March 1968. S. Murphy, M.Met., Ph.D., J. A. Whiteman, B.Sc., M.Met., Ph.D., and J. H. Woodhead, B.Met., are in the Department of Metallurgy, University of Sheffield.

The magnetic evidence shows that the high-Curie-point carbide is present in steels in large amounts at low tempering temperatures; thus it is remarkable that so few positive identifications of χ-carbides have been made. It is difficult to see how coherency stresses, or shape and size of the particles, could raise the Curie point of cementite.[16,17]

The investigation outlined here was an attempt to resolve this long-standing problem. Detailed magnetic data were obtained using a sensitive high-field Sucksmith balance, and a direct examination of the structures produced by tempering was made by electron microscopy of thin foils. Most of the work was done on vacuum-melted and refined iron–carbon alloys containing 0·81 and 0·16% C, but supplementary data were obtained from a plain carbon 0·39% C Kaldo steel and an Fe–19% Ni–0·5% C alloy. Specimens for examination were austenitized at appropriate temperatures according to the composition, and quenched to produce martensite. Magnet specimens were gradually tempered in the balance and foil specimens were heat-treated in fluidized beds or lead baths at temperatures up to 550° C.

Results of the Magnetic Investigation

The magnet specimens were progressively tempered in the Sucksmith balance and the magnetic moment measured at different temperatures during the heating and cooling cycles. Curves of magnetic moment vs. temperature were constructed from these data. The thermomagnetic curves reflect the magnetic properties of the ferromagnetic phases present, from a temperature slightly below a previous maximum temperature. A point of inflection in such a curve represents the Curie point of a constituent phase. This was easier to detect if the slopes of the thermomagnetic curves were plotted vs. temperature; the Curie point then appeared as a peak in the resulting curve. Curves obtained for the 0·81% C and 0·16% C steels are shown in Figs. 1 and 2.

Fig. 1 shows that no Curie peak was visible after tempering at 260° C; therefore it must have been at a temperature of 250° C or higher. Tempering up to ~ 350° C gave a broad hump in the curve between 200 and 250° C and at 400° C this was resolved into two distinct peaks. The peak at 215° C is due to cementite, and that at 245° C is due to the unknown carbide. The hump between 200 and 250° C is due to two or more overlapping peaks. Austenitizing and transforming to pearlite gave a sharp cementite Curie point at 208° C. The height of the peaks gave an approximate measure of the relative amounts of the carbides. At 260° C there is virtually no cementite, from 300 to 350° C there are approximately

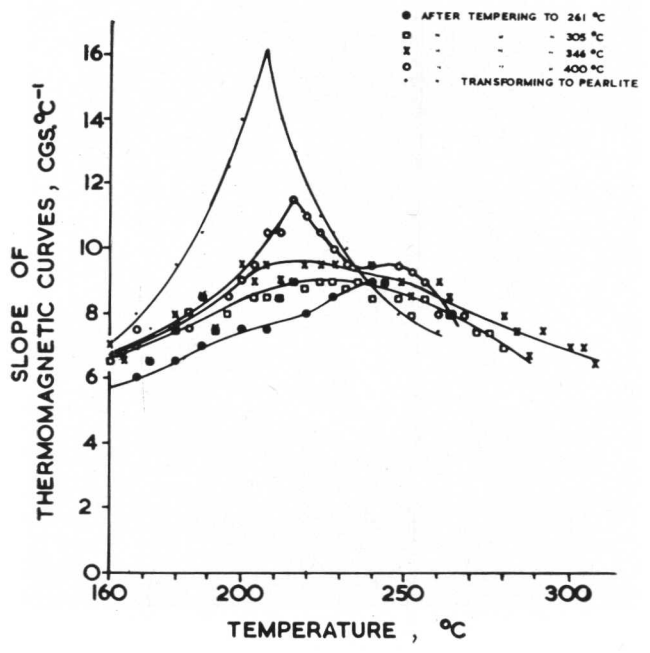

Fig. 1 *Curie-point peaks from data for high-carbon steel.*

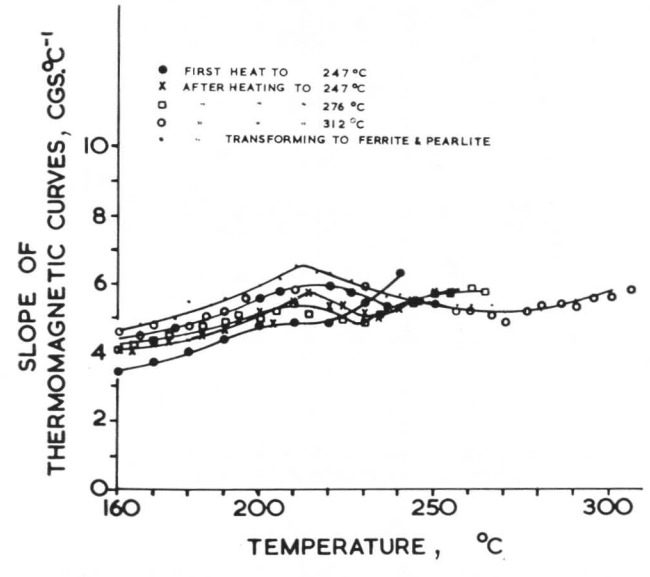

Fig. 2 *Curie-point peaks from data for low-carbon steel.*

equal amounts of each carbide, and at 400° C there is more cementite than the high-Curie-point carbide.

The curves of Fig. 2 are similar to Fig. 1 except that the magnitudes of the peaks are very much smaller owing to the lower carbon content of the steel. In addition the two peaks at 200 and 250° C are resolved at lower temperatures. Tempering up to ~ 280° C produced very little change in the amounts of carbide but above 310° C the amount of cementite increased and after austenitizing and transforming to pearlite only the cementite Curie peak remained.

This suggests that in both high- and low-carbon steels, tempering at low temperatures gives rise to a carbide with a high Curie point. Below 300° C this is the major carbide constituent but at 400° C there is more cementite present. The Curie point of the early carbide may be above 350° C initially, but it gradually approached 250° C. It is probable that the high-Curie-point carbide has a composition rather different from that of cementite, and that its replacement by cementite is a discrete process rather than one of gradual change.

An increase in magnetic moment in the 0·16% C steel specimens on low-temperature tempering was observed, though the effect varied greatly from one specimen to another. The only reasonable explanation for such an effect is carbon-enrichment of the autotemper carbide, a process that could have liberated free iron by solution of some of the pre-existing carbide. Calculation of the composition of the carbide gave the stoichiometric formula $Fe_{4\cdot6}C$. This may be the same carbide as that with a Curie point near 250° C.

Electron Microscopy and Diffraction Results

High-Carbon Steel

In the as-quenched condition this steel contained a small amount of autotemper carbide which was identified as cementite. Tempering at 125° C, where a distinct first-stage tempering reaction was indicated by the magnetic results, increased the amount of carbide considerably. This appeared as laths within the grains and as very thin patchy precipitates on twin planes of the matrix. In nearly every case this carbide was identified as cementite, though some diffraction patterns were obtained that could be indexed as ε-carbide. The situation hardly changed until tempering temperatures in the region of 300° C were reached. Then the intragranular carbide increased considerably in size and grain-boundary cementite films were more frequent. Tempering at 400° C produced a slight reduction in the amount of intragranular precipitate and growth of the boundary carbide. The matrix diffraction spots were sharper at this stage. After tempering at 550° C all the carbide was in the grain boundaries as spheroidized particles and the matrix had recovered to a large extent.

While no new type of carbide could be identified at the early stages, it became clear that the first cementite to form differed in interplanar spacings and angles from normal cementite. Shifts of the *d*-spacings of the axial planes from the values of normal cementite were computed and are plotted vs. tempering temperature in Fig. 3. There is a great deal of scatter, but in general the $(100)_\theta$ and $(001)_\theta$ spacings are greater than normal and the $(010)_\theta$ spacings are low. Above 250–300° C the discrepancies decrease, but it was principally by solution of the intragranular carbide and reprecipitation on grain-boundary cementite that the normal structure was finally attained.

Low-Carbon Steel

This steel contained large bundles of lath martensite but occasional patches of twinned martensite were found. About the same amount of autotemper carbide was found as in the high-carbon steel, but as the total carbon content was only one-fifth of that of the latter the degree of autotempering was high. The carbide was formed in several distinct sites. Most of it appeared as needles growing in several directions within a grain, but it was also observed as diffuse patches associated with dislocations and as a fine precipitate on the twin planes of internally twinned regions, an example of which is shown in the dark-field micrograph of Fig. 4. The carbide on the twin planes was identified as cementite but the other intragranular precipitate could not be identified. Tempering the steel caused the intragranular precipitate to grow; at the same

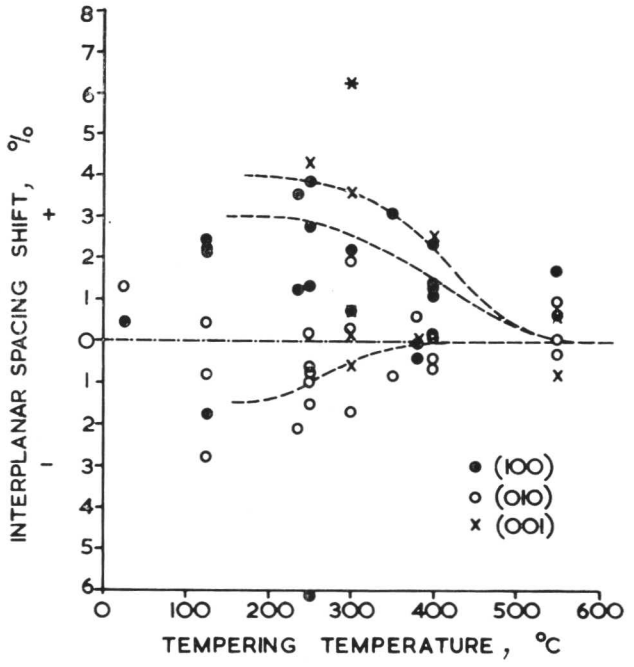

Fig. 3 Variation of shifts in axial plane spacings from the normal cementite values.

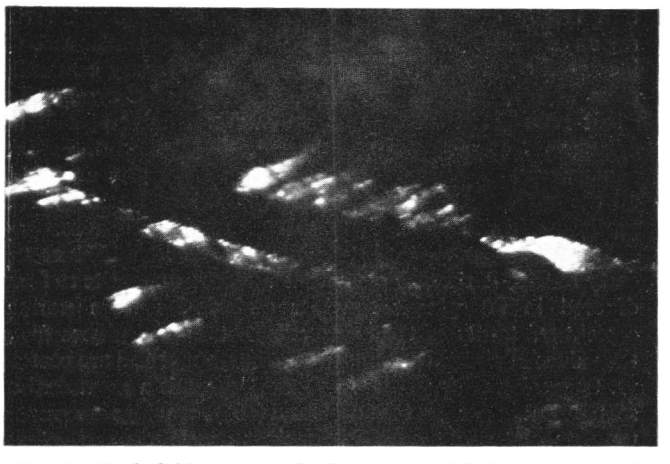

Fig. 4 Dark-field micrograph showing precipitation of cementite on twin planes in 0·16% C steel, as quenched. × ~ 61,000.

time the needle-boundary cementite films appeared and eventually became the dominant morphology.

After tempering at 350° C, some definite cementite diffraction patterns were obtained from the intragranular precipitate but, even when reasonably complete patterns were obtained, some defied interpretation.

Again the cementite formed at low temperatures was found to be modified, but two types of modification were observed. Only where the orientation relationship was the same as that in the 0·81% C steel (see below) were the modifications similar to those found in that steel.

After tempering at 550° C the appearance of the temper products was similar in every way to that in the 0·81% C steel.

Orientation Relationships

Several orientation relationships between cementite and the matrix were found. All of them have the common feature

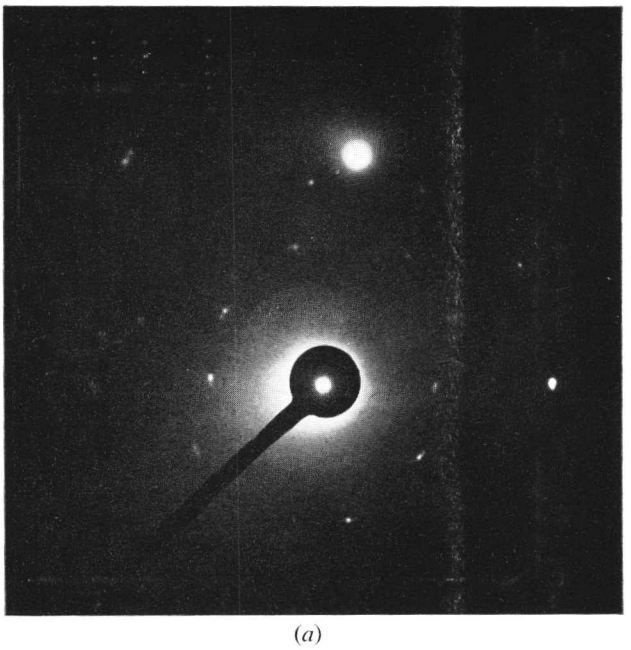

(*a*)

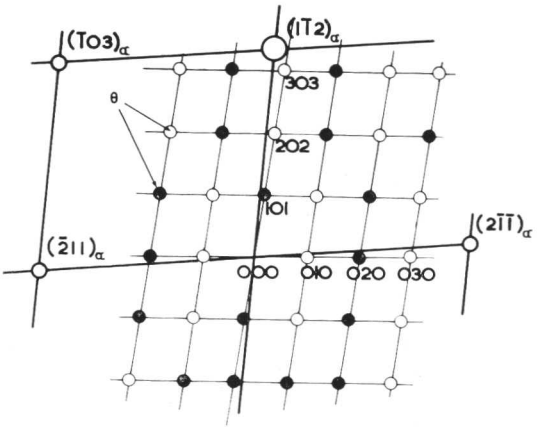

(*b*)

Fig. 5 Possible modified cementite diffraction pattern $[\bar{1}01]_\theta$. *0·16% C steel tempered 15 min at 352° C.*

$$\{103\}_\theta \parallel \{101\}_{\alpha'}$$

By far the most common relationship was that proposed by Isaichev,[6] where

$$(103)_\theta \parallel (101)_{\alpha'}$$
$$(010)_\theta \parallel (1\bar{1}\bar{1})_{\alpha'}$$

This is near to that proposed by Bagaryatsky:[14]

$$(001)_\theta \parallel (211)_{\alpha'}$$
$$(010)_\theta \parallel (1\bar{1}\bar{1})_{\alpha'}$$
$$(100)_\theta \parallel (0\bar{1}1)_{\alpha'}$$

In many cases it was impossible to distinguish between the two as they differ only by a rotation of $3\frac{1}{2}^\circ$ about $[010]_\theta$. Where possible, account was taken of the tetragonality of the matrix, and it was found in over three-quarters of the diffraction patterns from unambiguous matrix zones that the following planes were nearly parallel:

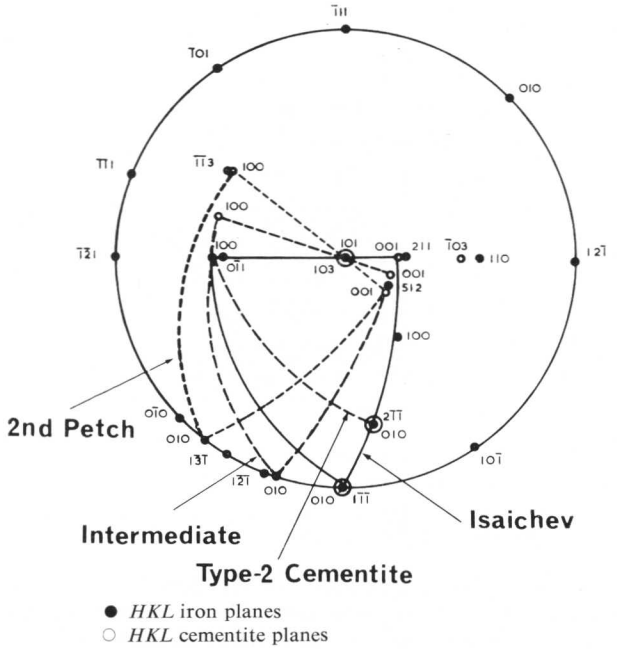

Fig. 6 Stereogram showing relationship between the observed orientation relations of cementite with martensite.

$$(001)_\theta \text{ near } (211)_{\alpha'}$$
$$(100)_\theta \text{ near } (0\bar{1}1)_{\alpha'}$$

as against, for example:

$$(001)_\theta \text{ near } (112)_{\alpha'}$$
$$(100)_\theta \text{ near } (1\bar{1}0)_{\alpha'}$$

In one specimen from the high-carbon steel, ferrite had formed during the quench in an austenite-grain boundary. The cementite in the ferrite had the second orientation relationship put forward by Petch:[19]

$$(001)_\theta \parallel (2\bar{1}5)_\alpha$$
$$[100]_\theta \parallel [31\bar{1}]_\alpha$$

This orientation relationship was also found once in the low-carbon steel after tempering at 352° C.

From the same low-carbon steel foil another diffraction pattern was obtained that could not be identified at first (Fig. 5). Eventually it was realized that this could be a $[\bar{1}01]_\theta$ zone with very extensive modifications. If this is indeed so, the orientation relationship is similar to that of Isaichev, except that the $(010)_\theta$ planes are approximately parallel to $(2\bar{1}\bar{1})_{\alpha'}$ planes.

Finally, a diffraction pattern from a specimen of the 0·39% C Kaldo steel tempered for 12 days at 300° C yielded an orientation relationship that lay between that of Isaichev and that of Petch.

The relationship between these orientation relationships is shown in Fig. 6.

Discussion

Modifications of the Early Cementite

The position of the diffraction spots in patterns obtained from thin foils can be altered in several ways unconnected with actual changes in the diffracting phase. A phenomenon that could produce the observed effects is extremely small thickness of the diffracting carbide in one or more directions. This causes streaking of the reciprocal lattice points in the direction of the small dimension and can result in substantial effects on single-crystal diffraction patterns.

Cementite diffraction patterns from tempered steels do show streaking up to ~ 400° C, at which temperature it can be very intense. The usual thin plane of the particle is $(001)_\theta$, but occasionally definite evidence for a small dimension normal to one of the $\{101\}_\theta$ planes was obtained. However, a careful analysis of results from certain zones ruled out these geometrical diffraction effects as the primary cause of the *d*-spacing shifts, though in some cases they have had a modifying effect on the measured spacings.

To establish the reason for the real interplanar spacing shifts, the implications of the orientation relationships were examined.

Bagaryatsky showed that a twinned α-iron structure has a very similar arrangement of iron atoms to that in cementite.[18] Andrews[20] showed that an untwinned α-iron lattice can also be regarded as a " transition-cell " of cementite. The volume changes involved in the transformation of a " transition-cell " of iron into a unit cell of cementite depend upon the exact orientation of the cell with respect to the tetragonal matrix. For a 1% C martensite the shifts in cementite interplanar spacings necessary to fit the carbide to the matrix are shown below.

	Orientation Relationship		*HKL*	% Shift
(1)	$(100)_\theta$	$(110)_{\alpha'}$	100	− 8·84
	$(010)_\theta$	$(1\bar{1}\bar{1})_{\alpha'}$	010	− 1·45
	$(001)_\theta$	$(211)_{\alpha'}$	001	+ 4·42
(2)	$(100)_\theta$	$(110)_{\alpha'}$	100	− 10·79
	$(010)_\theta$	$(1\bar{1}\bar{1})_{\alpha'}$	010	− 1·45
	$(001)_\theta$	$(1\bar{1}2)_{\alpha'}$	001	+ 6·74

Because of the low mobility of iron atoms at the very low temperatures at which cementite is first formed, volume changes would be expected to be important in deciding the orientation adopted. In fact, relationship (1) was most commonly encountered and gives the minimum volume change. Apart from $(100)_\theta$ planes, which always showed a moderate expansion in *d*-spacing rather than a large contraction, the measured *d*-spacings of the early cementite were similar to those predicted by relationship (1). Accommodation of the large $(100)_\theta$ spacings is probably fairly easily done by movement of edge dislocations on the $(211)_\alpha$ planes. In Fig. 3, the points taken from diffraction patterns where relationship (2) holds are marked *. These are clearly much higher than is the case for points where relationship (1) holds and are close to the values predicted by (2).

From this it seems that cementite forms from a " transition-cell " in martensite according to the orientation relationship giving minimum volume change during transformation, and that the cell dimensions of the cementite thus formed are influenced by the dimensions of the transition cell giving rise to it. The modified cell dimensions are not caused by coherency stresses between the carbide and the matrix, at least at higher tempering temperatures, but, as with the anomalous $(100)_\theta$ expansion, are an intrinsic property of the carbide. However, the effect of a tetragonal matrix on the carbide contained within it did influence the interaxial angles of the cementite. It was frequently observed that the carbide cell was not exactly orthogonal, and it was found that the angular displacement varied linearly with the carbon content of the associated martensite. Only in the case of ferrite are $(211)_\alpha$,

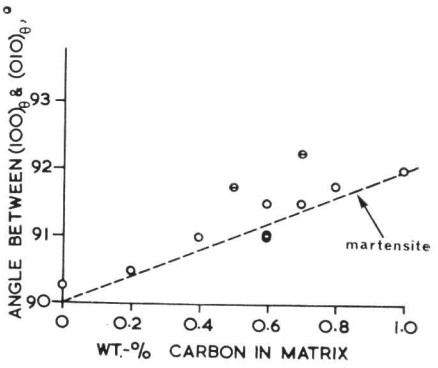

Fig. 7 Angle between cementite planes as a function of the matrix carbon content.

$(0\bar{1}1)_\alpha$, and $(1\bar{1}\bar{1})_\alpha$ planes mutually perpendicular. Some $[001]_\theta$ zones in relationship (1) were chosen to illustrate this point as a sufficient number of examples was available. The result is shown in Fig. 7. The anomalously high values at 0·7% C and 0·5% C were from diffraction patterns showing low $(100)_\theta$ spacings and were affected by $(101)_\theta$ streaking. Apart from these, the correspondence with the line representing the angle between the $(0\bar{1}1)_{\alpha'}$ and $(1\bar{1}\bar{1})_{\alpha'}$ is excellent.

Orientation Relationships

The figures for the alteration in cementite spacings and angles were obtained by assuming that the Bagaryatsky orientation relationship holds. At the transition-cell stage the Isaichev and Bagaryatsky relationships are identical, but in all observed cases the carbide differed in the *a* parameter from the true transition-cell. The reason why the Isaichev orientation is adopted by the precipitated cementite is related to the fact that the matrix is tetragonal. In the transition-cell case, $(103)_\theta$ is parallel to a $(101)_{\alpha'}$ plane and $(\bar{1}03)_\theta$ parallel to $(110)_{\alpha'}$. In the case of a 1% C steel these matrix planes have spacings of 2·062 and 2·017 Å, respectively. The parameters of the early cementite were calculated from Fig. 3 as $a \simeq 4{\cdot}66$ Å, $c \simeq 7{\cdot}00$ Å; hence the $\{103\}_\theta$ has a spacing of 2·08 Å. On development of a nucleus of early cementite there is thus a preferential fit between the $(103)_\theta$ and the $(101)_{\alpha'}$ planes and the non-orthogonality of the early cementite cell further improves this. As the carbide grows, the coherency stresses between the planes rotate the carbide into the Isaichev relationship, and this is maintained as tempering reduces both the matrix tetragonality and the carbide $\{103\}_\theta$ spacings. The coherency between $(001)_\theta$ and $(211)_{\alpha'}$, for example, is destroyed once the Isaichev orientation is adopted, but $(103)_\theta$ and $(101)_{\alpha'}$ are the most closely packed planes in the two structures and this has an overriding effect.

Indeed the presence of the other orientation relationships, for example the second Petch relationship in cubic ferrite, might indicate that a preferential alignment of one of the $\{103\}_\theta$ planes and a $\{101\}_\alpha$ might come about without the aid of matrix tetragonality, but there is insufficient evidence to demonstrate this point.

Low-Carbon Steels

At this point the problem of the carbide formed in low-carbon steels can be reconsidered. It can be stated that cementite formed in high-carbon steels has certain modifications, which we shall call Type 1. In low-carbon steels the cementite formed in martensite needle boundaries and in twinned regions has similar modifications. The majority of

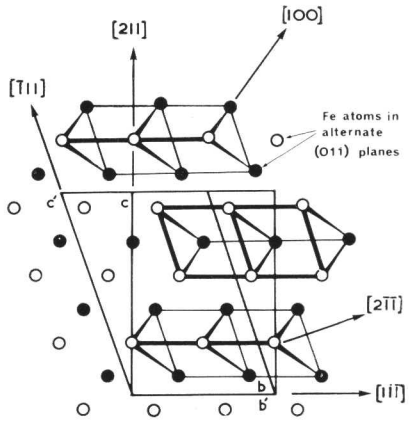

bc Andrews transition cell
b'c' Type-2 transition cell

Fig. 8 Relationship between Andrews transition-cell and cell corresponding to Type-2 distortion of carbide.

the early carbide in this steel was not identified, and if it is also cementite, was certainly not subject to Type-1 modifications. While one single crystal pattern cannot be considered as adequate identification for a crystal structure, the pattern mentioned earlier as a possible $[\bar{1}01]_\theta$ zone does suggest a particularly elegant solution to this problem. Again the transition-cell concept is used, but the cell adopted is slightly different from that chosen by Andrews.[20] In Fig. 8 the new version and the usual Andrews cell are shown on a $[0\bar{1}1]_\alpha$ projection of α-iron. This new cell would be monoclinic in ferrite. Production of a cementite nucleus from this could occur principally by an invariant plane strain followed by shuffling of the iron atoms into the appropriate positions.

The orientation relationship, interplanar angles, and spacings predicted by this mechanism are very close to those shown by the anomalous $[\bar{1}01]_\theta$ zone, but are shifted towards the cementite values. If this hypothetical cementite structure is termed Type 2, the question arises as to why Type 1 is found predominantly in high-carbon steels and Type 2 in low-carbon steels.

The answer is probably that put forward originally by Bagaryatsky.[14] He showed that an α-iron structure twinned across every third $(211)_\alpha$ plane gave an arrangement of iron atoms very close to that of cementite, with large prismatic interstices on the twin planes into which carbon could readily migrate. The dimensions of such a cell are near to those of the Andrews cell. Even a single twin plane could cause nucleation of cementite. Hence a twinned martensite would produce Type-1 distortions and lath martensite, Type 2.

Obviously much more work is needed before Type-2 distortions can be fully understood

Correlation of the Results of the Magnetic and Electron-Microscope Investigations

In the 0·16% C steel, the results of the magnetic investigation and the electron-microscope study agree as to the initial heavy autotempering of the material. The carbide formed is probable iron-rich. In the 0·81% C steel autotempering is slight and the cementite has normal cell dimensions (Fig. 3).

Tempering the high-carbon steel at 125° C gave a considerable magnetic effect corresponding to the first stage of tempering. The electron-diffraction evidence showed that thin patchy films of cementite were formed on the twin planes of the martensite. These were sometimes thick enough to

yield a good diffraction pattern. In the 0·16% C steel the twinned regions showed a similar effect, but their total volume was so small that a discernible magnetic effect would not have been expected and none was observed. The electron-diffraction work has shown that in the high-carbon steel the cementite formed at low temperatures was heavily modified. It is a major constituent up to 300° C and exists in substantial quantities at 400° C. The magnetic evidence showed that a phase with Curie point varying from above 250 to 245° C exists in similar proportions in the same temperature range, and it is reasonable to conclude that the modified cementite is the phase with that Curie point. The fact that the Curie point does not vary very much once it has arrived at ~ 250° C indicates that the composition has attained a steady value. The metallographic evidence that the final formation of cementite occurs by solution and reprecipitation is in agreement with this.

The magnetic investigation suggests that the carbide in the autotempered low-carbon steel and that produced by tempering the high-carbon steel are the same. This is not supported by the electron-diffraction evidence. However, it may be that if both types of carbide are modifications of cementite then, despite the differences in cell shape and size, the carbon contents and atomic arrangement may be similar, and hence the Curie points are very near to each other.

Summary

The cause of the anomalous 250° C Curie point in tempered steels has been established. It is due to the presence of a form of cementite modified by its mode of formation from the parent martensite. The nature and extent of these modifications have been described, though differences hypothesized for low-carbon steels cannot be considered proved.

At the earliest stages of tempering the modifications are large and the Curie point is > 250° C. After tempering up to 400° C the modifications are considerably less and the Curie point falls to ~ 245° C. The modified cementite is finally removed by re-solution due to competitive growth of grain-boundary cementite. Little evidence was obtained for the formation of ε-carbide.

References

1. Ya. S. Umansky, *Trudy Moskov. Inst. Stali.*, 1949, **28**.
2. K. H. Jack, *Acta Cryst.*, 1950, **3**, 392.
3. J. Crangle and W. Sucksmith, *J. Iron Steel Inst.*, 1951, **168**, 141.
4. J. Pomey and R. Coudray, *Compt. Rend.*, 1953, **237**, 62.
5. Ya. I. Kagan and I. Ya. Sidorenko, *Fizika Metallov i Metallovedenie*, 1962, **13**, 842.
6. I. V. Isaichev, *Zhur. Tekhn. Fiziki*, 1947, **17**, 835.
7. N. V. Gudkova, E. I. Levina, and V. A. Tolomasov, *Fizika Metallov i Metallovedenie*, 1957, **4**, 500.
8. K. H. Jack, *J. Iron Steel Inst.*, 1951, **169**, 26.
9. M. Okada and Y. Arata, *Nippon Kinzoku Gakkai-Si*, 1955, **19**, 186.
10. E. C. Roberts, *Trans. Met. Soc. A.I.M.E.*, 1950, **188**, 1210.
11. D. V. Wilson, *J. Iron Steel Inst.*, 1952, **170**, 248 (discussion).
12. J. P. Senateur, R. Fruchart, and H. Michel, *Compt. Rend.*, 1962, **255**, 1615.
13. J. P. Senateur and R. Fruchart, *ibid.*, 1963, **256**, 3114.
14. L. J. E. Hofer, E. M. Cohn, and W. C. Peebles, *J. Amer. Chem. Soc.*, 1949, **71**, 189.
15. L. S. Palatnik, *Fizika Metallov i Metallovedenie*, 1966, **21**, 217.
16. J. Crangle, *J. Iron Steel Inst.*, 1952, **170**, 248 (discussion).
17. B. A. Apaev, *Fizika Metallov i Metallovedenie*, 1960, **9**, 400.
18. A. Bagaryatsky, *Doklady Akad. Nauk S.S.S.R.*, 1950, **73**, 1161.
19. N. J. Petch, *Acta Cryst.*, 1953, **6**, 96.
20. K. W. Andrews, *Acta Met.*, 1963, **11**, 939.

Research Note

A New Precipitate in the Al–Cu–Mg–Ag System

J. H. Auld and J. T. Vietz

Past work[1,2] has shown that small additions of silver (0·5 wt.-%) can modify the ageing characteristics of a range of Al–Cu–Mg alloys. In general, the silver additions accelerated the rate of ageing and caused increased hardening in the medium-temperature range (120–240°C). An electron-microscopy and X-ray-diffraction study of the alloy Al – 2·5% Cu – 1·5% Mg – 0·5% Ag aged at 200°C showed that silver stimulated the formation of a fine dispersion of T phase (body-centred cubic of the $Mg_{32}(Al,Zn)_{49}$ type) in preference to the more heterogeneous dispersion of lath-shaped S (orthorhombic, Al_2CuMg) which normally precipitates in the ternary alloy at this temperature.[3]

Recently the effect of a similar addition of silver (0·5 wt.-%) to an alloy of lower magnesium content was investigated by electron-microscopy and X-ray-diffraction techniques. The alloy studied was Al – 2·5% Cu – 0·5% Mg with 0·5% Ag. The ternary alloy without silver lies in the $\alpha + S + \theta'$ region of the phase diagram for long ageing times at 190°C. Alloys aged to peak hardness at ~ 200°C contained G.P.B. [2] zones, S', and θ' precipitates.[4]

Transmission electron microscopy of the quaternary Al – 2·5% Cu – 0·5% Mg – 0·5% Ag alloy aged for various times in the range 150–350°C showed the principal precipitating phase to be in the form of thin hexagonal-shaped plates lying on the {111} aluminium planes. The diameters of the plates were extremely large compared with their thickness in the ⟨111⟩ aluminium direction (Fig. 1). For example, after solution-treating the alloy at 500°C, cold-water-quenching, and ageing at 150°C for 1 day, followed by ageing at 200°C for one day, the plates were 2000–3000 Å in dia. and their thickness was measured as 15–25 Å; after ageing at 250°C for 0·7 day they were 6000–8000 Å in dia. and between 50 and 70 Å thick.

Electron and X-ray-diffraction patterns showed the precipitate to have a hexagonal unit cell with $a_0 = 4{\cdot}96$ Å, $c_0 =$

Manuscript received 3 July 1968. J. H. Auld, M.Met., F.I.M., and J. T. Vietz, B.E., are in the Australian Defence Scientific Service (Aeronautical Research Laboratories), Department of Supply, Melbourne, Australia.

Fig. 1 Electron micrograph of the Al – 2·5% Cu – 0·5% Mg – 0·5% Ag alloy aged at 225°C for 2 days; [110] zone axis showing two sets of plates edge on.

8·48 Å, oriented with $[00.1]_{Hex} \parallel [111]_{Al}$ and $[10.0]_{Hex} \parallel [1\bar{1}0]_{Al}$. With this a_0 the {10.0} hexagonal interplanar spacing of the precipitate is exactly three times the {200} aluminium interplanar spacing, which suggests that coherency in this direction enables the plates to grow to such large diameters in the {111} aluminium plane.

As the precipitates are so thin there is considerable streaking of the diffraction spots perpendicular to the basal plane of the precipitate (Fig. 2). In fact, in the peak-aged condition at the lower ageing temperatures the streaks on the electron-diffraction patterns were virtually continuous and any indication of intensity maxima was further complicated by double-diffraction effects, making an accurate determination of the c_0 parameter very difficult. This parameter was found from the peak positions of 00.l streaks in X-ray photographs using a microphotometer to plot the intensity distribution. The same c_0 value was found by measurements on electron-diffraction patterns of the alloy in overaged conditions.

Interpreting the broadening of the streaks in the X-ray-diffraction patterns as being entirely due to size effects gave excellent agreement with measurements of the thickness of the plates directly from the electron micrographs. From these measurements it can be seen that in the early stages of ageing, including peak hardness, the precipitates were only two or three unit cells thick and were only six to ten unit cells thick in well overaged specimens. The thinness would appear to be due to the very large misfit in planes parallel to the plates. This is +19% if the (00.1) precipitate spacing is compared

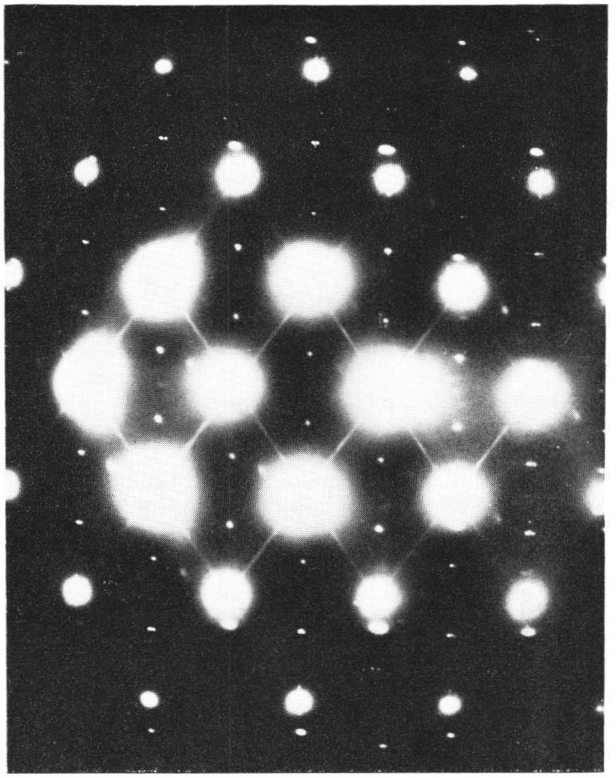

Fig. 2 Electron-diffraction pattern of the alloy aged at 150°C for 1 day, then at 200°C for 1 day; [110] zone axis.

with the repeat distance of the f.c.c. matrix (three (111) spacings), or −10% compared to four (111) spacings.

The precipitate appears to be very stable, as even after ageing at 350°C for 3 days the diffraction patterns show that the structure is identical to that produced at the lower ageing temperatures, though by this stage the plates are very coarse and the distribution quite sparse owing to the low solute supersaturation. Thus, it may well be an equilibrium precipitate though this has not so far been verified.

In addition to the hexagonal precipitate, a fairly small amount of lath-shaped *S* precipitate has been observed under almost all ageing conditions examined. At 150°C it is sparsely distributed and possibly homogeneously nucleated, while at higher temperatures (200–250°C) it is fairly coarse, being up to 6000 Å in length after ageing at 250°C for 0·7 days, and is apparently dislocation-nucleated as in the ternary alloy.

The structure of the new precipitate has not been established as yet. The lattice parameters, being similar to the commonly occurring $MgZn_2$-type Laves phase, initially suggested that it might have this structure. However, there are considerable differences in intensities between a number of reflections: for example, the 200 reflection of the unknown is very strong, while that of $MgZn_2$ is very weak; the 201 reflection, absent in the unknown, is very strong in $MgZn_2$. Although different atoms are involved and changes in atomic parameters can cause changes in intensities, it is considered that it is very unlikely to have the $MgZn_2$ structure.

A more likely possibility is found in the Al–Cu–Li system. Hardy and Silcock[5] detected an equilibrium compound of approximate composition Al_2CuLi, called T_1, having a hexagonal unit cell with $a_0 = 4{\cdot}97$ Å, $c_0 = 9{\cdot}35$ Å. Comparison of the reflections from the unknown with the X-ray powder data for T_1 indicated general intensity agreements

Since precipitates of T_1 had the same habit and epitaxy as found in the present work, an Al – 2·0% Cu – 1·7% Li alloy was prepared. Electron microscopy of aged alloys showed similar precipitates to the quaternary alloy except that the plates of T_1 were larger in diameter and thicker for the same ageing treatments; however, they had a similar high dia.: thickness ratio.

X-ray photographs of aged single crystals of the Al–Cu–Li alloy showed the same arrangement of T_1 diffraction spots with intensities fairly similar to those of the hexagonal precipitate in the Al–Cu–Mg–Ag alloy. Thus, it is quite probable that this precipitate is isostructural with T_1. Unfortunately the structure of T_1 has not been determined so that its similarity does not greatly assist in postulating a structure for the new precipitate. Work is in progress on this and other aspects associated with the ageing of this alloy.

References

1. I. J. Polmear, *Trans. Met. Soc. A.I.M.E.*, 1964, **230**, 1331.
2. J. T. Vietz and I. J. Polmear, *J.Inst.Metals*, 1966, **94**, 410.
3. J. H. Auld, J. T. Vietz, and I. J. Polmear, *Nature*, 1966, **209**, 703.
4. J. M. Silcock, *J.Inst.Metals*, 1960–61, **89**, 203.
5. H. K. Hardy and J. M. Silcock, *ibid.*, 1955–56, **84**, 423.

Research Note

Excess Vacancies and the Mechanism of the Slow Reaction in an Aluminium–4% Copper Alloy

J. Okamoto and H. Kimura

Several mechanisms have been proposed to explain the long lifetime of excess vacancies during the slow reaction in low-temperature ageing of Al–Cu alloys: (*a*) that an excess vacancy concentration exists in equilibrium with dislocation loops or voids formed by condensation of vacancies;[1] (*b*) that vacancies are trapped at G.P. zones;[2] (*c*) that a long-range stress field of G.P. zones retards the decay of vacancies;[3] and (*d*) that a surface oxide film prevents vacancies from escaping or pumps them into the crystal.[4] The activation energy for the diffusion of copper should be greater than that in the fast reaction (the initial stage of ageing where the excess vacancy concentration is independent of the ageing temperature) for mechanisms (*a*) and (*b*), whereas it should be almost equal to that in the fast reaction for mechanisms (*c*) and (*d*). The activation energy of the slow reaction was determined as ~ 1eV by Turnbull and Cormia.[5] For a more detailed discussion of the mechanism, the activation energy for copper diffusion must be determined as a function of the ageing time. The purpose of the present note is to report a result for the activation-energy determination and to discuss the mechanism of the slow reaction.

Specimens in the form of wire 0·5 mm in dia. were drawn from an alloy containing 4·04 wt.-% Cu, 0·005 wt.-% Si, and 0·002 wt.-% Fe. They were first heated at 530° C for 10–12 h and quenched into water at 0° C. They were held at 0° C for 10 sec and then transferred into a liquid-nitrogen bath where the resistance of the specimens was determined. The pre-ageing, 10 sec at 0° C, was performed to ensure nucleation of any vacancy clusters likely to be formed. Once the vacancy clusters reach a certain size at 0° C, they are stable at subsequent ageing temperatures.[6]

Ageing kinetics was followed by the resistivity change measured at liquid-nitrogen temperature. The sensitivity of the measurement, $\Delta\rho/\rho$, was 5×10^{-5}. The activation energy of the ageing process was determined by the slope-change method. The ageing temperature is changed at a fixed time of ageing from T_1 to T_2, the rate of ageing (the resistivity change) is determined at this time for both the temperatures,

Manuscript received 3 July 1968. Professor H. Kimura, Ph.D., D.Eng., is at the Research Institute for Iron, Steel, and Other Metals, Tohoku University, Sendai, Japan, where the work was carried out. J. Okamoto, B.Eng., M.Eng., is now with Japan Air Lines.

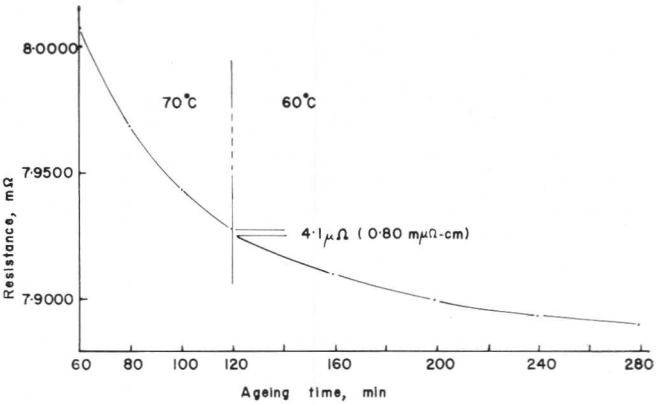

Fig. 1 Slope-change method to calculate the activation energy. An activation energy of 0·47eV is obtained. Ageing temperature was changed from 70 to 60° C at 120 min.

and the ratio of the rates gives the activation energy. If the activation energy so obtained is to be compared with the activation energy of copper diffusion, any structural change upon altering the ageing temperature must be avoided or properly corrected for, except of course for any change in the factors controlling the diffusion of copper atoms. For example, variations in the number of G.P. zones and in the degree of supersaturation of copper atoms should be avoided or corrected for.

It is of critical importance to change the temperature from high to low, thus avoiding the partial reversion of G.P. zones. Fig. 1 shows an example of the measurement; the rate of ageing is calculated numerically from the measured values. The value of the resistance at the time of the temperature change extrapolated back from the second ageing curve is slightly smaller than the value from the first ageing curve. This difference is due partly to the increase in the concentration of vacancy–copper atom complexes by the removal of free vacancies and partly to the increase in the number of G.P. zones. The concentration of vacancy–copper atom complexes is a factor controlling the diffusion of copper atoms and hence no correction need be made. The correction for the change in the number of G.P. zones and any other

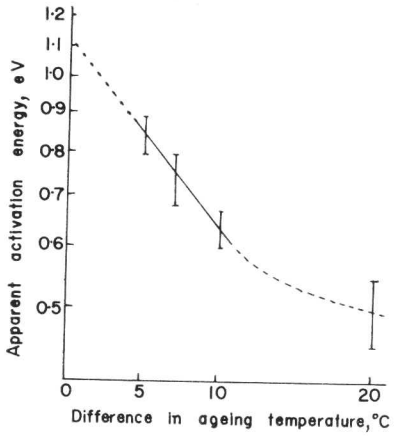

Fig. 2 Extrapolation of the apparent activation energy obtained by the slope-change method to the temperature change of 0° C.

possible structural changes is made by extrapolating the apparent activation energies obtained as a function of the temperature change to the temperature change of 0° C. The effect of the change in the degree of supersaturation of copper atoms is also corrected for. Fig. 2 is the result of these corrections; the extrapolated activation energy is 1·1eV (for an ageing treatment of 120 min at 70° C).

Similar but less extensive measurements were made for other ageing times and temperatures; 5 min at 30° C is the earliest ageing condition investigated and 120 min at 70° C is the latest. The activation energy for the diffusion of copper atoms becomes > 1eV by ageing for several hundreds of minutes at 40° C.

The large activation energy, 1·1eV, rules out mechanisms (*c*) and (*d*). Mechanism (*a*) explains the kinetics of ageing more reasonably than mechanism (*b*).

The concentration of vacancies, C_v, in equilibrium with the line tension of a dislocation loop is given by

$$C_v = C_v^0 \exp\left(\frac{\Delta E}{kT}\right) \qquad \ldots (1)$$

where C_v^0 is the thermal equilibrium concentration of vacancies and ΔE the increase in the energy of a dislocation loop upon absorbing a vacancy. From the energy expression of a dislocation loop,[7] ΔE is calculated to be approximately

$$\Delta E = 0{\cdot}45\,\frac{Gb^4}{r}$$

for a perfect loop lying in a {111} plane. For aluminium ($G = 2{\cdot}8 \times 10^{11}$ dynes.cm^{-2} and $b = 2{\cdot}86$ Å), $\Delta E = 5{\cdot}2\text{eV}/r$ (r in Å). The activation energy for the diffusion of copper with a vacancy concentration given by equation (1) is $E_D - \Delta E$, where E_D is the usual activation energy of diffusion of copper in aluminium, 1·3eV.[8] Observation gives $E_D - \Delta E$ as 1·1eV and hence ΔE is 0·2eV; this energy gives $r = 26$ Å. From the ageing-time-dependence of the activation energy, the lifetime of excess vacancies is estimated to be 1 min at 40° C. This time and the diffusion constant of vacancies (associated with copper atoms) gives an average distance between loops of $2{\cdot}4 \times 10^{-6}$ cm. Hence, the loop density should be 7×10^{16} cm^{-3}. The concentration of vacancies condensed in the loops is calculated to be 3×10^{-4}, which is quite reasonable for the concentration of thermal vacancies in this alloy at 530° C. From isothermal ageing, the concentration of vacancies during ageing from 500 to 1000 min at 40° C is estimated to be 10^{-8}. This is in good agreement with the value calculated from equation (1) with $\Delta E = 0{\cdot}2$eV and the formation energy of vacancies = 0·76eV.[9]

The possibility of mechanism (*b*) is ruled out if the activation energy for the diffusion of copper is > 1·0eV. With the accuracy of the present investigation, however, mechanism (*b*) still cannot be ruled out completely.

Acknowledgement

Grateful acknowledgement is made to the Light Metal Educational Foundation for financial support of this work.

NOTE ADDED IN PROOF: Further analysis gave the activation energy of the slow reaction as 1·0eV (rather than 1·1eV). The conclusions, however, remain essentially unchanged.

References

1. D. Turnbull, H. S. Rosenbaum, and H. N. Treaftis, *Acta Met.*, 1960, **8**, 277.
2. T. Federighi and G. Thomas, *Phil. Mag.*, 1962, **7**, 127.
3. W. G. Grupen and G. Sines, *Acta Met.*, 1965, **13**, 527.
4. S. Kritzinger, R. S. Dobson, and R. E. Smallman, *Phil. Mag.*, 1967, **16**, 217.
5. D. Turnbull and R. L. Cormia, *Acta Met.*, 1960, **8**, 747.
6. M. Kiritani, *J. Phys. Soc. Japan*, 1965, **20**, 1834.
7. D. J. Bacon and A. G. Crocker, " Lattice Defects in Quenched Metals ", p. 667. **1965:** New York and London (Academic Press).
8. M. S. Anand, S. P. Murarka, and R. P. Agarwala, *J. Appl. Physics*, 1965, **36**, 3860.
9. R. O. Simmons and R. W. Balluffi, *Phys. Rev.*, 1960, **117**, 52.

Research Note

The Effect of 0·24% Si upon the Initial Stages of Ageing of an Al–2·5%Cu–1·2%Mg Alloy

R. N. Wilson

Sen and West[1] have described how the mode of precipitation in an Al–2·7% Cu–1·3% Mg alloy may be altered by the addition of 0·5% Ag. The purpose of this note is to describe two effects resulting from the addition of a small quantity (0·24%) of Si to the same precipitation-hardening system. It was reported previously[2] that the Si addition reduced the density of vacancy loops in the quenched alloy and also reduced the rate of hardening at room temperature. At 190° C the plateau hardness due to G.P.B. zone formation and peak hardness due to the precipitation of the *S* phase were both higher in the Si-bearing alloy. Comparison of the

Manuscript received 3 July 1968. R. N. Wilson, M.Met., A.I.M., A.Inst.P., is at the Royal Aircraft Establishment, Farnborough, Hants.

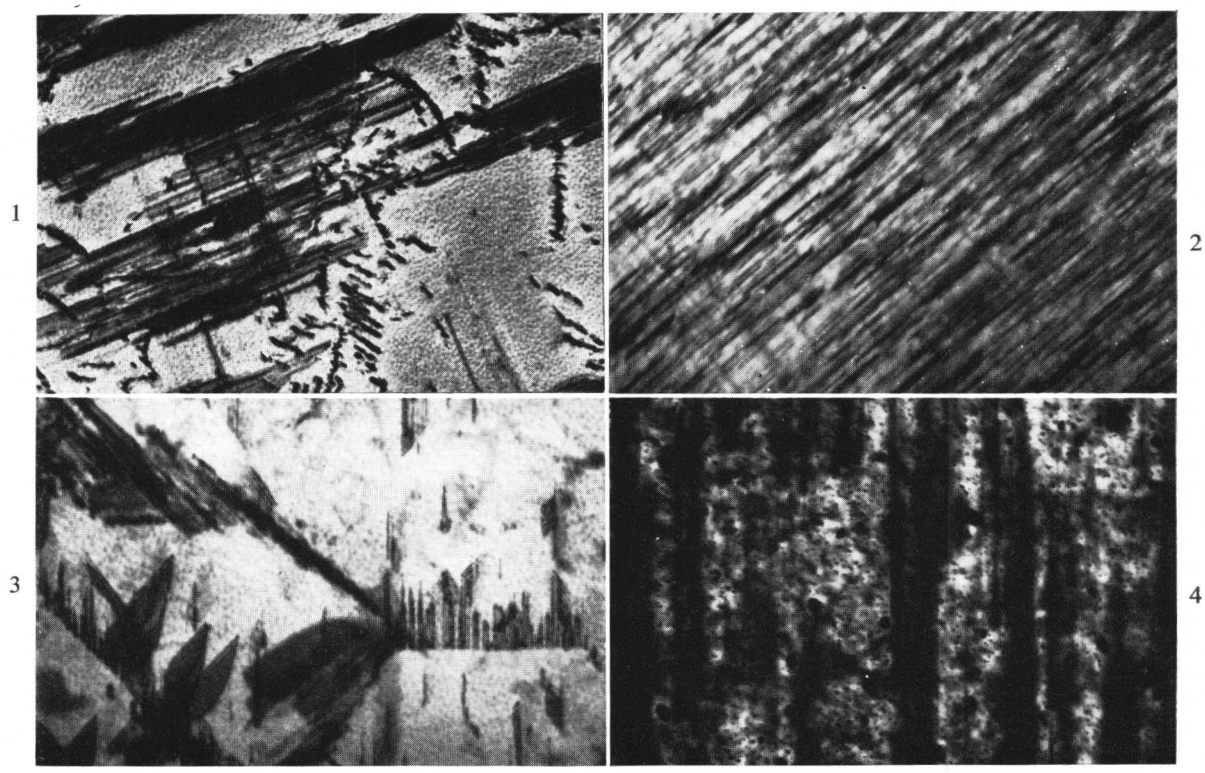

Fig. 1 *Al–*2·5% *Cu–*1·2% *Mg alloy. Solution-treated* 1 *h* 530° *C, directly quenched to* 160° *C, and aged* 2 *months at* 160° *C. Showing the heterogeneous precipitation of the* S *phase.* × 20,000.

Fig. 2 *Al–*2·5% *Cu–*1·2% *Mg–*0·24% *Si alloy. Solution-treated* 1 *h* 530° *C, directly quenched to* 250° *C, and aged* 5 *min at* 250° *C. Showing homogeneous distribution of* S *precipitates.* × 30,000.

Fig. 3 *Al–*2·5% *Cu–*1·2% *Mg–*0·24% *Si alloy. Solution-treated* 1 *h* 530° *C, directly quenched to* 300° *C, and aged* 5 *min at* 300° *C. Showing precipitation of both* S *laths and* θ′ *platelets.* × 30,000.

Fig. 4 *Al–*2·5% *Cu–*1·2% *Mg–*0·24% *Si alloy. Solution-treated* 1 *h* 530° *C, directly quenched to* 160° *C, and aged* 2 *months at* 160° *C. Shows presence of both* S *precipitates and G.P.B. zones* (*cf. Fig.* 1). × 60,000.

microstructures showed that the *S* precipitation was homogeneous in the Si-bearing alloy, but that *S* nucleated heterogeneously on dislocations in the Si-free alloy. This observation could be interpreted in terms of the effect of trace-element additions upon the G.P. zone solvus temperature, as proposed for the effects of Ag upon precipitation in the Al–Zn–Mg system by Lorimer and Nicholson[3] and for the effects of double-ageing treatments upon precipitation in the Al–Mg_2Si system by Pashley *et al.*[4] The microstructures developed in the Al–Cu–Mg alloys by ageing at several temperatures in the range 100–300° C have been studied in an attempt to determine the effects of silicon upon the G.P. zone solvus temperatures of the alloy. As pointed out by Sen and West[1] the G.P. zone solvus temperature of the Al–Cu–Mg alloy was shown to be ~ 265° C by Beton and Rollason,[5] using hardness-reversion techniques. However, after direct-quenching the Al–2·5% Cu–1·2% Mg alloy to temperatures as low as 160° C, the *S* phase precipitated heterogeneously on ageing (Fig. 1), although G.P.B. zones were found by hardness tests to be stable at much higher ageing temperatures (e.g. 240° C). Double-ageing treatments of 7 days at 140° C followed by 16 h at 190° C have also failed to produce a homogeneous distribution of *S* precipitates in the alloy. By comparison, after solution-treatment and cold-water-quenching, the Si-bearing alloy developed a homogeneous distribution of precipitates on ageing at temperatures up to 300° C. Ageing temperatures up to 250° C from a direct quench also produced a homogeneous distribution as shown by Fig. 2. A comparison of the microstructures at higher ageing temperatures after direct-quenching was impossible owing to the simultaneous precipitation of *S* and θ′ precipitates (Fig. 3). Although the zones in the Si-free alloy were difficult to detect, the zones in the Si-bearing alloy were readily resolved, as shown in Fig. 4, and it would therefore seem that both the size and the temperature stability of the G.P.B. zones are widely different in the two alloys.

The second effect of Si in the alloy, which may provide some insight into the reasons for its effect upon the mode of precipitation, was its influence upon the nucleation and growth of vacancy loops. Westmacott *et al.*,[6] discussing the distribution of defects in quenched binary Al alloys, related the difficulty in forming such loops to the solute–vacancy binding energy, E_b in the alloy. They showed that in an Al–1·2% Si alloy a higher quench-bath temperature was required to produce a similar loop distribution to that in an Al–1·2% Mg alloy. The present results on the Al–2·5% Cu–1·2% Mg–0·25% Si alloy differ from those of Westmacott *et al.* in that no quench-bath temperature could be found in the range 20–200° C that would give a distribution of vacancy loops similar to that produced by quenching the Si-free alloy into cold water. Moreover, loops were not nucleated in the Si-bearing alloy on holding at the various quench-bath temperatures for several days.

The distribution of vacancies between the different solute

elements present has been estimated by means of the Lomer equations as used by Westmacott *et al.*[6] and also applying the equation due to Kimura and Hasiguti.[7] Assuming that no interaction between solute elements has occurred, the residual vacancy concentration available for the diffusion of Cu and Mg atoms has been calculated to be 20–40% of the quenched-in vacancy concentration. The values of binding energies used in the calculations were E_b(Cu) = 0·1, E_b(Mg) = 0·1, and E_b(Si) = 0·2 eV. These may be higher than the actual values in the light of more recent calculations[8] but a general reduction in them would only increase the concentration of vacancies available for the diffusion of copper and magnesium. Both the observations and the calculations indicate that no simple association of silicon atoms to vacancies could have controlled the solute mobility in the present alloy, and a more complex interaction between all the solute elements present and the vacancies must have occurred.

The concept of solute–vacancy binding energy has been extended by Federighi and Thomas[9] to the interaction of vacancies and zones. They suggest that in zone-forming alloys, the duration of the slow reaction is governed by the binding energy of the vacancies to the zones. If this binding energy is zero the vacancies move through the zones as easily as through the parent lattice. If the binding energy is infinite the vacancies, once they have transported solute to the zones, become fixed permanently in them and no longer aid solute diffusion. Both these extreme values would give a rapid decay of the ageing reaction. Intermediate values would control the acceptance and the emission of vacancies by the zones, and so control the concentration of free vacancies in the lattice and consequently the rate of solute clustering. The effects of Si agree well with this model if one considers that the binding energy between the vacancies and the G.P.B. zones is increased when Si is present and that the affinity of the zones for vacancies increases as the zones grow. This may result from the direct association of Si atoms with the vacancies or perhaps by Si becoming a component of the structure of the zones. This model would account for the increased hardening associated with the zones, their slower formation at room temperature,[2] and their increased temperature stability in the Si-bearing alloy. Weatherly[10] has shown strong evidence by transmission electron microscopy for the *in situ* transformation of the G.P.B. zones to *S* precipitates at 190° C in an Al–2·7% Cu–1·5% Mg–0·2% Si alloy to produce the homogeneous distribution of precipitate. It would appear from the present work that Si stabilizes the G.P.B. zones to such a degree that their solvus temperature approaches the temperature of the $(\alpha + S)/(\alpha + \theta + S)$ phase boundary in the directly quenched Si-bearing alloy and so provides nuclei for homogeneous precipitation at temperatures as high as 250° C.

Acknowledgement

This paper is published by permission of the Controller, H.M. Stationery Office.

References

1. N. Sen and D. R. West, this vol., p. 49.
2. R. N. Wilson, D. M. Moore, and P. J. E. Forsyth, *J. Inst. Metals*, 1967, **95**, 177.
3. G. W. Lorimer and R. B. Nicholson, *Acta Met.*, 1966, **14**, 1009.
4. D. W. Pashley, M. H. Jacobs, and J. T. Vietz, *Phil. Mag.*, 1967, **16**, 51.
5. R. H. Beton and E. C. Rollason, *J. Inst. Metals*, 1957–58, **86**, 79.
6. K. H. Westmacott, R. S. Barnes, D. Hull, and R. E. Smallman, *Phil. Mag.*, 1962, **7**, 127.
7. H. Kimura and R. R. Hasiguti, *Acta Met.*, 1961, **9**, 1076.
8. D. R. Beaman, R. W. Balluffi, and R. O. Simmons, *Phys. Rev.*, 1965, **137**, (3A), A917.
9. T. Federighi and G. Thomas, *Phil. Mag.*, 1962, **7**, 127.
10. G. C. Weatherly, Ph.D. Thesis, Univ. Cambridge, **1966.**

Research Note

Trace Elements and Precipitation in Aluminium–Copper Alloys

G. B. Brook and B. A. Hatt

Trace elements are known to influence precipitation in aluminium–copper alloys in two ways.[1] First, they change the redistribution of vacancies at ambient temperatures after quenching from 530° C and the consequences of this can be seen in the formation of G.P. zones, the kinetics of which depends on the vacancy-aided diffusion of Cu atoms. Additions of up to 0·02 at.-% of Cd, In, Sn, and Mg reduce or inhibit G.P. zone formation for considerable periods at ambient temperature and this has been attributed to the stronger interaction of vacancies with the trace element than with the Cu atoms.[2] Additions of up to 0·1% silver have a similar effect but the Ag–vacancy complex does not appear to be as stable and increases in hardness can be detected after relative short times at 30° C, i.e. 20-60 days compared to 100-300 days in the case of In. Where the trace elements form part of the G.P. zone structure, as in the case of magnesium when present in excess of ~ 0·05 at.-%, ternary G.P.B. zones also form and this is again associated with an increase in binary G.P. zone intensity.[3]

The second influence of trace elements in this system is the specific nucleation of the θ′ phase, which then supersedes the θ″ phase on ageing at elevated temperatures, e.g. 130-190° C, in the most favourable conditions. The dense precipitation of trace-element-nucleated θ′ provides the highest strength in these alloys, whereas θ″ is associated with maximum strength in binary Al–Cu alloys, softening being a consequence of the transformation to coarse and rapidly growing θ′.

A feature of θ′ nucleated by trace elements is the appearance of additional diffractions in X-ray or electron-diffraction photographs. These *P* diffractions represent a structural feature of the same thickness and orientation as the θ′ phase and appear at about the same time. They have been inter-

Manuscript received 3 July 1968. G. B. Brook, M.Sc., A.Inst.P., and B.A. Hatt, B.Met., A.I.M., are with the Fulmer Research Institute, Ltd., Stoke Poges, Bucks.

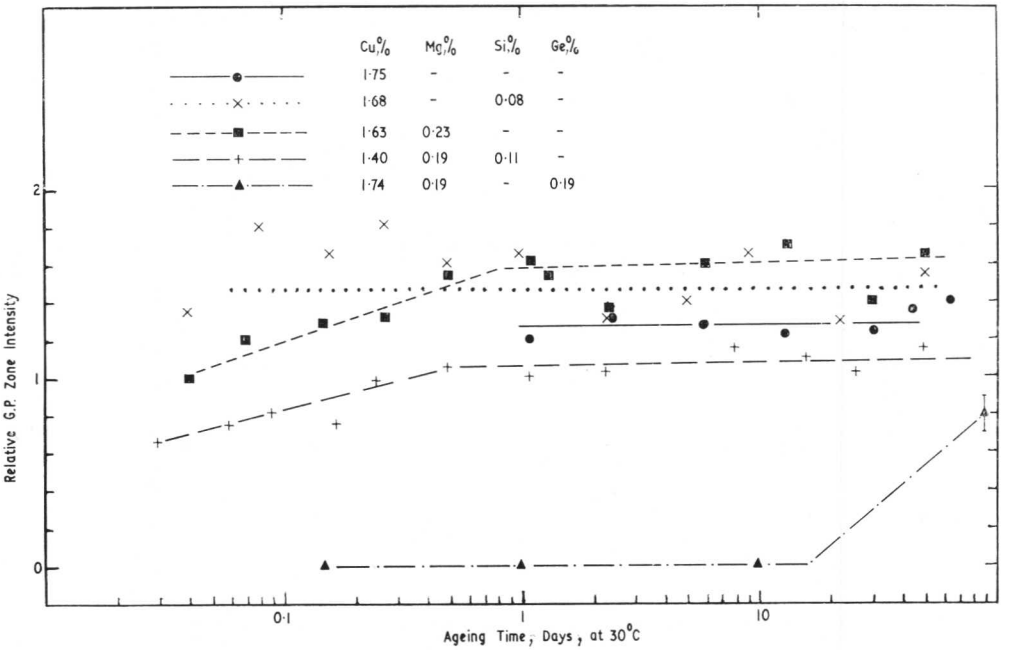

Fig. 1 Ageing response for various alloys at 30° C.

preted as an interfacial structure at the α/θ' interface parallel to $[001]_{\theta'}$. While they are present, θ' coarsens only slowly. Their disappearance follows the precipitation of the trace element and leads to the rapid coarsening of the θ' phase. Of the elements that interact strongly with vacancies, only Cd, In, and Sn cause specific nucleation of θ'. The ageing characteristics of alloys with Ag or small amounts of Mg are similar to those of the binary alloy, except that the rate of reaction is reduced.

Investigation of some anomalous results on ageing Al–Cu alloys containing Mg made from Al of different purities has led to the discovery of two combinations of trace elements that affect G.P. zone growth and also specifically nucleate θ', but at very different rates. High-purity Al–Cu alloys with 0·20 at.-% Mg hardened appreciably at 30°C by formation of both G.P. and ternary G.P.B. zones but precipitated θ'' at peak hardness at 165° C. A comparable alloy but containing 0·11% Si formed fewer G.P. zones and no G.P.B. zones at 30° C. On ageing at 165° C, θ'' first precipitated, as in the binary Al–Cu alloy, but after ~ 16 h θ' appeared with strong *P* diffractions in the same positions as those produced by In. No such effect was obtained with either Mg or Si alone and these two experiments provide strong evidence that an Mg/Si interaction can exist in solid solution in Al. Such an interaction is consistent with the high enthalpy of formation of the binary phase Mg_2Si. Thus, it was reasonable to expect that additions of Mg and Ge should have a similar effect because of the high enthalpy of formation of Mg_2Ge. Lutts[5] had already shown that the Al–Mg_2Ge pseudo-binary system existed and that the greater scattering factor of Ge made its detection easier. Alloys with 1·7 at.-% Cu and 0·19 at.-% Ge and of the same composition with 0·19 at.-% Mg have been compared. (Similar results have since been obtained for alloys with Mg : Ge ratios of 2 : 1).

Fig. 1 shows the effect of the various combinations of Mg, Si, and Ge on the amount of G.P. zones formed at 30° C after quenching 0·02-in.-thick specimens from 530° C into acetone. The curve for the ternary Al–Cu–Mg alloy does not include the G.P.B. zones that were also present. Despite the lower Cu content, additional zones were formed and greater hardening was obtained. Si also increased the intensity of G.P. zones, but the results were erratic. The combined addition of Mg and Si reduced the amount of zones below that of the binary alloy but, allowing for the lower Cu content, it is probable that Mg and Si mutually cancelled the effect of one another.

The effect of Mg + Ge was quite remarkable in that no G.P. zones could be detected at all in the first few days and the intensity of G.P. zones was still very low after 100 days. This was reflected in the hardness, which remained constant before increasing slowly from 20 days. Thus, it can be concluded that Mg interacts strongly in solid solution with Si and Ge. After quenching from 530° C, there appears to be little redistribution of vacancies to Mg–Si complexes but, at the other extreme, the Mg–Ge complexes interact so strongly with the vacancies that little diffusion of free Cu occurs. However, the increase in hardness and zone intensity after ~ 20 days indicates that the Mg–Ge–vacancy complexes may not be stable for long periods at 30° C.

The behaviour of the Al–Cu–Mg–Ge alloys was equally striking on ageing at 165° C. After 2 h, weak streaks in the *P* diffraction positions were detected with no evidence of θ' or θ''. These streaks are similar to those found by Lutts[5] in Al–Mg–Ge alloys. In electron micrographs of polycrystalline specimens aged for the same time a distribution of very fine precipitates of ~ 50 Å dia. was formed. Both strong *P* diffractions and weak θ' were identified in the electron-diffraction patterns. After 4 h, fine θ' (~ 350 Å dia. and 27 Å thick) had precipitated fully with very strong *P* diffractions visible in both X-ray and electron-diffraction photographs. This was associated with maximum hardnesses of 145-150 HV after 4 h (Fig. 2) compared with 120 HV after 24-48 h in the Al–Cu–Mg–Si alloy and ~ 130 HV for In-bearing alloys of this Cu content. While the *P* diffractions were present, the θ' precipitate increased in size only slowly but, as in Al–Cu–In alloys, prolonged ageing brought about an increase in the rate of coarsening as the *P* diffractions faded and diffractions due to Mg_2Ge appeared, confirming the de-

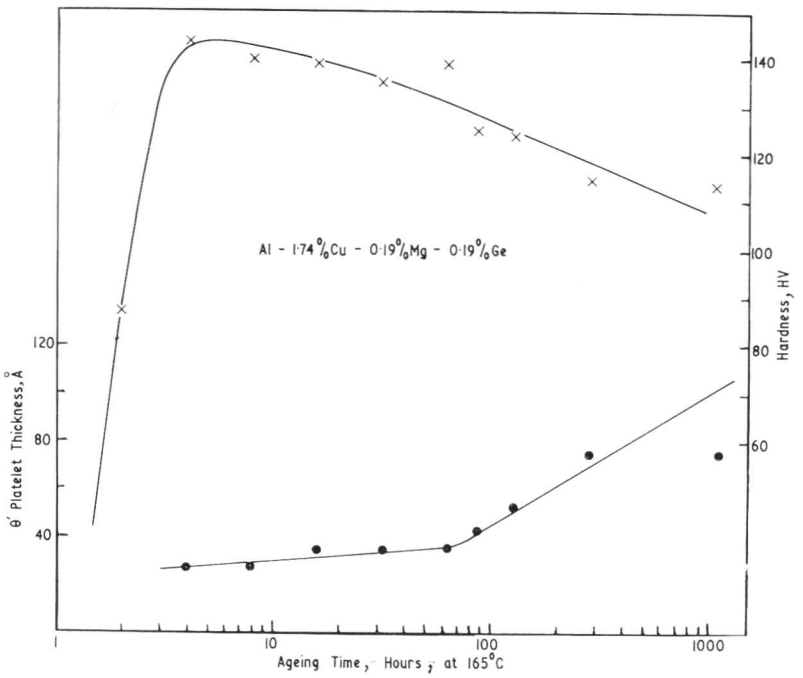

Fig. 2 Ageing response of Al–Cu–Mg–Ge alloy at 165° C.

pendence of the stability of θ′ on the presence of the trace-element substructure. The onset of overageing could be delayed by reducing the trace-element concentration.

These experiments have shown that the more strongly the trace additions interact with vacancies after quenching, the more rapidly is θ′ nucleated on ageing at 165° C, and the finer is the precipitate. The efficiency of nucleation of θ′ decreases in the order Mg + Ge, Sn, In, Cd, and Mg + Si (using the maximum solute content, i.e. ~ 0·2 at.-% Mg, Si, and Ge, 0·02% Cd, and 0·01% In or Sn).

This correlation indicates that the controlling factor is the rate at which trace-element complexes can diffuse and stabilize θ′ embryos. The strong interaction of the Mg–Ge complexes with vacancies accounts for the rapid nucleation and growth of θ′, as it is probable that the Mg–Ge complexes release their vacancies at the θ′ embryos, thus aiding Cu diffusion. There is evidence from the work of Lutts on Al–Mg_2Ge alloys that vacancies are released when Mg–Ge zones form and it is feasible that this also occurs on nucleation of θ′ by these elements. The free-vacancy concentration is probably very low and little Cu diffusion precedes stabilization of the θ′ embryos. At the other extreme, the Mg–Si complexes nucleate θ′ only after a relatively long incubation period during which vacancy-aided diffusion of Cu to form G.P. zones and θ′ takes place. This is consistent with the behaviour of this alloy after quenching and confirms that the Mg–Si complexes do not interact preferentially with vacancies, so that there are sufficient free vacancies available for Cu diffusion. With the intermediate trace elements such as In and Cd the first precipitate to form depends on the heating rate to the ageing temperature. At low rates, θ′ with attendant *P* diffractions is obtained but at high rates G.P. zones and θ″ appear briefly before trace-element nucleation of θ′ takes place. This again shows that the rate-controlling factor is the diffusion of the trace element rather than that of Cu.

The effect of cold work before ageing at elevated temperatures on the efficiency of nucleation by trace elements, can now be understood more clearly. θ′ can be nucleated on dislocations introduced by cold work or during quenching from the solution-treatment temperature and this appears to be a process dependent on the rate of Cu diffusion at the ageing temperature. This occurs more rapidly than nucleation by Sn, Cd, In, or Mg + Si and the resulting distribution of θ′ can be finer or coarser than that normally nucleated by the trace additions, depending on the dislocation density and the trace element considered. Nucleation on dislocations is infrequent in alloys containing Mg + Ge and their properties are almost unaffected by cold work before ageing at 165° C.

The other consequence of nucleation by trace elements is that the size of the θ′ phase is controlled by the presence of the trace-element substructure at its periphery. The efficiency of a trace element does not appear to depend on its interaction with vacancies, i.e. the stability does not arise from inhibition of Cu diffusion by the maintenance of a low vacancy concentration by the trace element. This is apparent from the observation that nucleation by Mg + Si provides better stability than Mg + Ge. The supersaturation of the trace element(s) and the kinetics of precipitation of the equilibrium phase appear to be more significant.

Finally, it is possible to use several trace elements to obtain specific responses, e.g. Ge can partially replace Si and as little as 0·02% will accelerate nucleation, while 0·2% will produce a fine θ′ precipitate but with the stability associated with Mg + Si nucleation.

Likewise if Si partially replaces Ge, G.P. zone formation at 30° C can be introduced. These factors are of technical importance in that properties can be controlled to produce various combinations of strength, creep-resistance, and response to age-hardening at ambient temperature, e.g. after welding.

References

1. G. B. Brook, *Fulmer Research Inst. Special Rep.* (**3**), 1965.
2. J. M. Silcock, *Phil. Mag.*, 1959, **4**, 1187.
3. B. A. Hatt, unpublished work.
4. M. Ohta and F. Hashimoto, *Trans. Japan Inst. Metals*, 1965, **6**, 9.
5. A. Lutts, *Acta Met.*, 1961, **9**, 577.

The Effect of Deformation on Precipitation in Ni-Base Alloys

I. Kirman and D. H. Warrington

A fine dispersion of a body-centred tetragonal phase, γ^*-Ni_3Nb, may be used to harden nickel-base alloys.[1] It is metastable[2] to a Cu_3Ti-type orthorhombic β-Ni_3Nb in a similar manner to the behaviour of γ' and η-Ni_3Ti in Ti-bearing alloys.[3] The aim of the present work was to discover the cause of an acceleration of the transformation in Nb-bearing alloys which in the analogous situation in Ti-bearing alloys had been attributed to changes in matrix stacking-fault density[3] or increased matrix-vacancy concentration.[4]

Thin strips (0·005 in. thick) of a Ni–25% Fe–15% Cr–5% Nb–0·05% C alloy were solution-treated for 1 h at 1150° C, water-quenched, and aged in argon-filled silica capsules at 750 or 800° C. The as-quenched dislocation density was low, consisting of isolated dislocations and occasional arrays around massive particles of Nb(C,N).

Complex deformation introduced by rolling or by large tensile strain has failed[3,4] to demonstrate any effect on the precipitate *distribution*. In this investigation, restriction of the deformation of foils to 2–3% in tension revealed plainly that in grains which had deformed on predominantly one slip system the subsequent precipitate structure was clearly aligned along the active slip planes.

The γ^* phase precipitates as small square platelets on $\{100\}_\gamma$ planes.[1] The γ/γ^* misfit is a maximum (2·7%) normal to the plate along the c_{γ^*} axis and a minimum (0·8%) in the plane of the platelets. Undeformed, quenched, and aged specimens show a random distribution of orientation with an enhanced density of particles on quenched-in dislocations or at occasional extrinsic stacking faults (generated by NbC precipitation).[2]

Prior deformation produced structures in which on ageing at 750° C virtually all the γ^* was distributed along the effective slip planes (Fig. 1), though the effect was less noticeable at lower ageing temperatures where a considerably greater volume fraction of γ^* precipitates. The distribution of γ^* may be explained in terms of the strain-relief mechanism proposed for θ' in Al–Cu alloys.[5] Nucleation is aided if the maximum misfit vector of the precipitate has a component parallel to the Burgers vector of the dislocation. Consequently as the γ^* misfit is concentrated in $\langle 100\rangle_\gamma$ only two orientations nucleate in association with one $a/2\langle 100\rangle$ slip system. This was rigorously obeyed in practice. It was also noted that in the early stages the γ^* plates grew from one side of the dislocation and did not accommodate it in their structure.

The precipitate in specimens aged for 240 h at 750° C was half transformed to β plates which lay equally on all four $\{111\}_\gamma$ planes. Deformation before ageing speeded the transition to non-aligned β, probably by increasing the density of the initial γ^* nuclei.

However, if after ageing for 10 h to a random structure the foil was deformed and reaged a further 230 h the structure shown in Fig. 2 was observed; no γ^* is visible and generally only orientation of β precipitates in any one area. Small deformations of γ^* dispersions do produce arrays of dislocations along one slip system,[2] hence the β nucleation is affected by the slip dislocations.

The independent effect of the dislocations on the dispersions of γ^* and β is neatly demonstrated by the structure shown in Fig. 3. A foil of the structure of Fig. 1 was deformed a further 2% about an axis ~ 60° from the original tensile axis so as to activate a second slip system. Reageing for 70 h produced a structure similar to that of Fig. 2, but reageing for 30 h

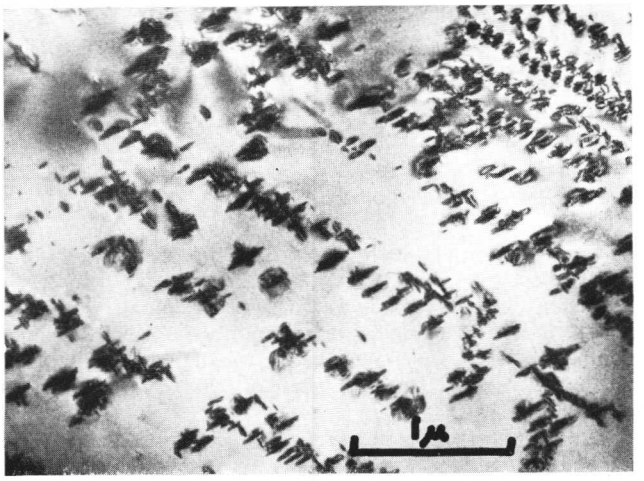

Fig. 1 Nb alloy deformed 2% and aged for 10 h at 750° C. × 19,000.

Fig. 2 Nb alloy aged for 10 h at 750° C, deformed 2%, and reaged for 230 h. × 10,500.

Manuscript received 3 July 1968. I. Kirman and D. H. Warrington, Ph.D., are in the Department of Metallurgy, University of Sheffield.

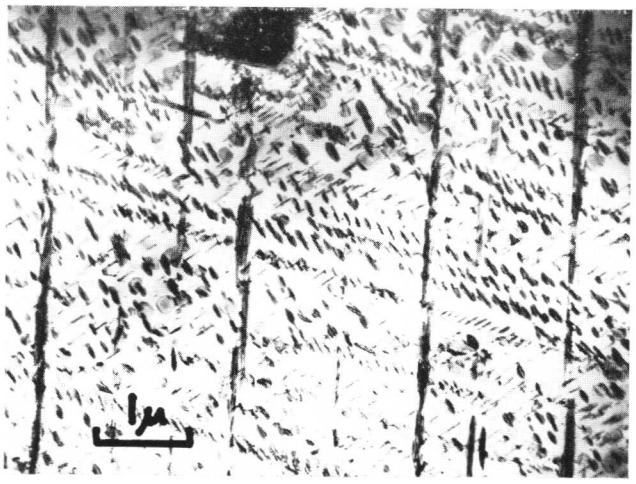

Fig. 3 Nb alloy deformed 2%, aged for 10 h at 750° C, deformed 2% about new axis, and reaged for 30 h. × 11,000.

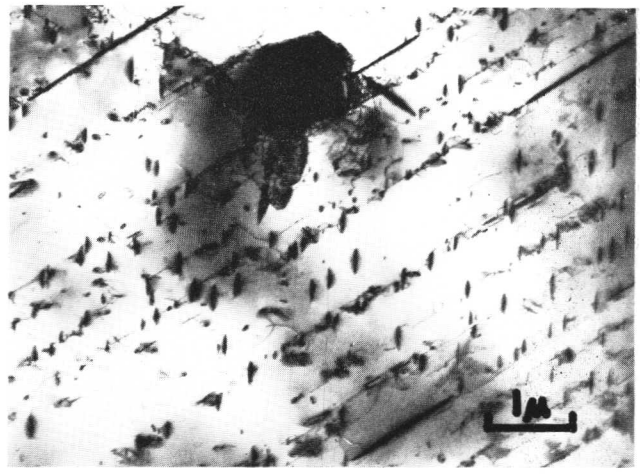

Fig. 4 Nb alloy deformed 2% and aged for 12 h at 800° C. × 10,500.

gives a structure in which the γ^* and β are distributed along different sets of $\{111\}_\gamma$ planes.

Ageing at 800° C gives a wider separation of γ^* on the dislocations, and a single dislocation in a deformed specimen contains both γ^* and β nuclei (Fig. 4); the latter grow to an aligned β structure, whereas ageing at 750° C would produce a non-aligned structure.

The structure of β is nearly h.c.p. stacking ordered to form an orthorhombic phase; it could nucleate on dislocations, on stacking faults similarly to γ' in Al–Ag alloys,[6,7] or on deformation faults within the γ^* structure.

If β forms independently from γ^*, it is necessary to postulate that at 750° C all possible nucleation sites are occupied by γ^*, and β forms a non-oriented structure on edge dislocations emitted by growing γ^* particles. The oriented nature of the β after intermediate deformation suggests that the dissociation of the slip dislocations is important. On the other hand an intrinsic stacking fault in γ^* produces the correct stacking for β nucleation and is expected to have a low energy. Faults are formed in γ^* as it precipitates[2] so that deformation is not necessary for β nucleation. However, deformation could introduce many more faults, and succeeding dislocations could cross-slip to produce a nucleus of γ^* of any required thickness. Thus, the restriction that many of the grown-in faults in γ^* do not grow[2] can be overcome.

Repeating the present experiments with an alloy in which the Nb is replaced by 3% Ti shows that alignment of η may be produced by prior deformation. γ' is not preferentially nucleated on dislocations which are responsible for η nucleation either directly or by dissociation within a γ' particle or series of γ' particles.

References

1. I. Kirman and D. H. Warrington, *J. Iron Steel Inst.*, 1967, **205**, 1264.
2. I. Kirman and D. H. Warrington, paper presented at Fourth European Regional Conference on Electron Microscopy (Rome, 1968); also unpublished work.
3. J. R. Mihalisin and R. F. Decker, *Trans. Met. Soc. A.I.M.E.*, 1960, **218**, 507.
4. H. F. Merrick, Ph.D. Thesis, Univ. Cambridge, **1963.**
5. G. Thomas and M. J. Whelan, " Proceedings of the Second European Regional Conference on Electron Microscopy, Delft 1960", p. 452., **1961:** (De Nederlandse Vereniging voor Electronen microscopie).
6. R. B. Nicholson and J. Nutting, *Acta Met.*, 1961, **9**, 332.
7. J. A. Hren and G. Thomas, *Trans. Met. Soc. A.I.M.E.*, 1963, **227**, 308.

Research Note

Theoretical Calculation of the Rhombohedral Distortion of the Transition Phase in Al–Zn Alloys

Ryszard Ciach

Decomposition of the supercooled α phase in Al–Zn alloys involves numerous transition precipitates before the formation of the final aluminium and zinc phases.[1–6] Of special interest is the phenomenon of the rhombohedral distortion of the G.P. zones[3–6] and the appearance of the rhombohedral transition phase.[2–6] The lattice parameters of these precipitates are given by various authors[2–6] and are shown in Table I.

The data are difficult to compare, because different compositions and transformation temperatures were used. The present paper will attempt to explain the difference in these results and to make theoretical calculations of the degree of rhombohedral distortion.

It has been assumed that the appearance of the transition phases is due to the decomposition of the supercooled α phase

Manuscript received 3 July 1968. R. Ciach, D.Sc., Institute of Metals, Polish Academy of Sciences, Cracow, Poland, at present holds a N.R.C. Fellowship in the Physical Metallurgy Division, Mines Branch, Department of Energy, Mines, and Resources, Ottawa, Ontario, Canada.

TABLE I

Values of c/a_h and α_r

Authors	G. & L.[2]	S. & S.[3]	M.&G.[4]	K., H., & P.[5]	C.&G.[6]
c/a_h	2·42	2·345*	2·35	2·379	2·38
α_r	60°34′18″	61°59′–62°4′† 62°8′–61°50′ ‡	61°46′	61°17′	61°12′

* Given by Ref. (5). † Range at decomposition temperature of 175° C. ‡ Range at decomposition temperature of 225° C.

into two α-type f.c.c. transition phases, compositions of which are determined by the Al- and Zn-rich boundaries of the metastable α–α′ miscibility gap.[7] This assumption was based on the present author's research,[7,8] as well as the results of other workers.[1,6,9]

The formation of the rhombohedral structure is due to the difference in the parameters between the matrix and the precipitates, and also to the changes in the character of the bond between them. In the case of the plate-like G.P. zones the bond is related to the anisotropy of the coherency strains around the zones.[3,4,6] The subsequent stage of the semi-coherent precipitates is characterized by the maintenance of the coherency in the (111) habit planes only.[3–6] This type of bond between the precipitates and the matrix affects the continuity of the {100} planes across the precipitate and thus the interatomic distances in the ⟨100⟩ directions of the {100} planes within the precipitates are almost the same as those in the matrix. However, the concentration of the zinc atoms within the precipitates causes their contraction, which is then manifested by a reduction in the distances between (111) planes. These phenomena are responsible for the rhombohedral structure, the a_r of which is $< a_m/\sqrt{2}$ (where a_m is the parameter of the matrix), whereas a_h (in hexagonal symmetry), defined by the atomic distance in the (111) habit plane, is proportionally $> a_m/\sqrt{2}$. Thus to, determine the rhombohedral structure it is necessary to know:

a_m, which may change during the decomposition process from the value governed by the composition of the supercooled α phase to that governed by the Al-rich boundary of the metastable equilibrium.

$C_{\alpha}'_t$, the parameter c (in hexagonal symmetry) of the Zn-rich f.c.c. transition phase which limits the rhombohedral contraction in the [111] direction and is not affected by the alloy composition.

The changes in the parameters caused by the change in composition of the α-type phases has been found by extrapolation of the parameters[10,11] and by the thermodynamic analysis of this metastable equilibrium.[12]

The values a_r, a_h, and c_h for various rhombohedral angles α_r and the constant parameter a_m have been calculated according to the equations:

$$a_r = \sqrt{\frac{a_m^2}{4\sin^2\frac{\alpha_r}{2} + 1}} \qquad \ldots (1)$$

$$a_h = \sqrt{a_m^2 - a_r^2} \qquad \ldots (2)$$

$$c_h = 3\sqrt{a_m^2 - \frac{4}{3}a_h^2} \qquad \ldots (3)$$

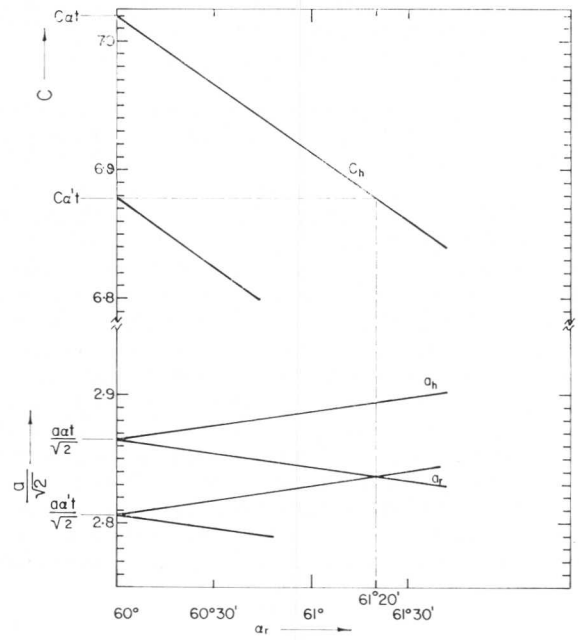

Fig. 1 The changes in a_r, a_h, *and* c_h *at the various rhombohedral angles* (α_r) *for the alloy containing 29 at.-% zinc and the decomposition temperature 75° C. The* $a_{\alpha t}$ *and* $a_{\alpha' t}$ *denote the parameters of the f.c.c. transition phases defined by the Al and Zn boundaries of the metastable α–α′ miscibility gap.*

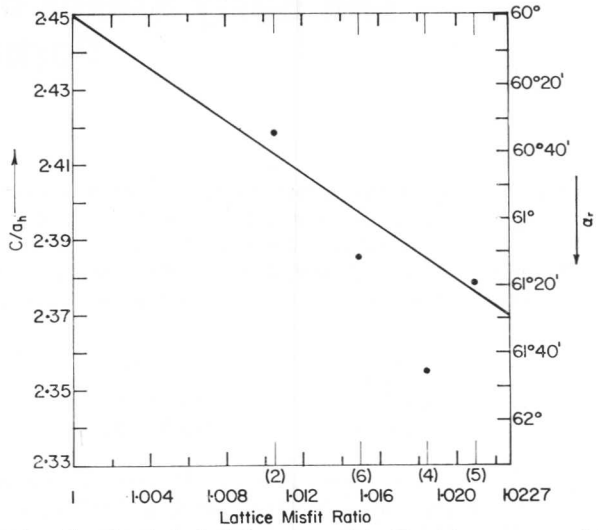

Fig. 2 The rhombohedral distortion of the Zn-rich α-type transition phase vs. the lattice-misfit ratios. The α_r *experimental results* (●) [2, 4–6] *are also plotted.*

These are shown in Fig. 1 for the alloy containing 29 at.-% zinc and the decomposition temperature of 75° C. The decrease in c_h (using a_m determined by the parameter of the Al-rich f.c.c. phase denoted $a_{\alpha t}$) to the value of $C_{\alpha}'_t$. (Fig. 1) gives the maximum degree of rhombohedral distortion, which for this case is $\alpha_r = 61°20'$ and $c/a_h = 2{\cdot}378$.

The calculated α_r values are plotted vs. the ratios of the parameters of matrix and precipitates in Fig. 2 as a straight line. The corresponding c/a_h values are shown and are plotted vs. α_r according to the equation

$$\sin\frac{\alpha_r}{2} = \frac{3}{2\sqrt{3 + (c/a_h)^2}} \qquad \ldots (4)$$

The extreme values of the ratios of the parameters denote a value of 1·0 for the f.c.c. structure, and a value of 1·0227 for the degree of the rhombohedral distortion at room temperature.

The values for α_r obtained experimentally[2,4–6] are plotted as points in Fig. 2 and are substantially in agreement with calculated results.

According to some authors the solvus curve of the G.P. zones is below the metastable equilibrium[13,14] and approaches the spinodal curve.[15,16] This may lead to a decrease in the degree of the rhombohedral distortion of the G.P. zones by comparison with transition phases. An additional decrease in the rhombohedral distortion of the G.P. zones results because, in this case, it is necessary to carry out the calculations using the matrix parameter a_m, which is smaller than the Al-rich transition phase parameter $a_{\alpha t}$. Thus, the gradual conversion of the distorted G.P. zones in the high-zinc alloy is much easier than for aluminium-rich alloys, where the G.P. zones have a higher degree of the rhombohedral distortion (Fig. 2). This may explain the considerable increase in the decomposition time for the transition structures with the increase in the aluminium content of the supercooled α phase.[5,6,17]

References

1. R. D. Garwood, A. L. Davies, and G. L. Richards, *J. Inst. Metals*, 1959–60, **88**, 375.
2. R. Graf and M. Lenormand, *Compt. Rend.*, 1964, **259**, 3494.
3. M. Simerská and V. Syneček, *Acta Met.*, 1967, **15**, 223.
4. W. Merz and V. Gerold, *Z. Metallkunde*, 1965, **57**, 607.
5. K. Krishna Rao, H. Herman, and E. Parthé, *Mat. Sci. Eng.*, 1966, **1**, (3), 162.
6. G. J. C. Carpenter and R. D. Garwood, *Metal Sci. J.*, 1967, **1**, 202.
7. R. Ciach, D.Sc. Thesis, Inst. Basic Tech. Problems, Polish Acad. Sci., Warsaw, Poland, **1964.**
8. R. Ciach, " Proceedings of the 5th Physical Metallurgy Conference " (Cracow, Poland, 1968), to be published by Polish Acad. Sci.
9. V. Gerold and W. Schweizer, *Z. Metallkunde*, 1961, **52**, 76.
10. E. C. Ellwood, *J. Inst. Metals*, 1951–2, **80**, 217.
11. R. Ciach, *Scripta Met.*, 1968, **2**, 575.
12. A. Krupkowski, R. Ciach, and J. Kröl, *Bull. Acad. Polon. Sci., Ser. Tech.*, 1967, **XV**, (11), 25, 975.
13. G. Borelius, *J. Metals*, 1951, **3**, 477.
14. A. A. Johnson, E. J. Hughes, and P. W. Barton, *J. Inst. Metals*, 1966, **94**, 186.
15. K. B. Rundman and J. E. Hilliard, *Acta Met.*, 1967, **15**, 1025.
16. J. Lašek, *Czech. J. Physics*, 1965, [B], **15**, 848.
17. R. Ciach, " Proceeding of the 7th Conference of Metallurgists " (Met. Soc. of Canad. Inst. Mining and Metallurgy) (Vancouver, Canada, 1968).

Research Note

The Early Stages of Precipitation of Some Group IV Carbides and Nitrides in Molybdenum

N. E. Ryan and J. W. Martin

A range of ternary molybdenum alloys has been prepared by introducing a Group IVA element and carbon or nitrogen into molybdenum such that ~ 1 vol.-% of the relevant carbide or nitride was present. Classical precipitation-hardening by quench-ageing treatments has been demonstrated in the following systems:[1]

Mo–Ti–C	Mo–Ti–N
Mo–Zr–C	Mo–Zr–N
Mo–Hf–C	Mo–Hf–N

The alloys were solution-treated for 1 h at 2100° C, quenched to room temperature at > 200 degC. sec^{-1}, and subsequently aged at 1200, 1350, or 1500° C. Structural changes occurring during ageing were studied using transmission electron microscopy.

In as-quenched alloys, defect clusters were observed (Fig. 1) in the size range 50–150 Å, which have been identified as prismatic interstitial defects on $\{100\}_{Mo}$ in the ZrC, ZrN, HfC, and HfN alloys. In the quenched TiN alloy the defects were largely of the vacancy type with no apparent rational habit plane. Increased concentrations of these defects were detected during the early stages of ageing, though wide precipitate-free zones (Fig. 2) eventually developed adjacent to sub-boundaries, grain boundaries, and other substructural features.

Manuscript received 3 July 1968.

N. E. Ryan, A.I.M., and J. W. Martin, M.A., Ph.D., F.I.M., are in the Department of Metallurgy, University of Oxford.

This effect has usually been attributed to vacancy depletion in f.c.c. metals, but no convincing evidence for the formation of high vacancy supersaturations has yet been obtained in quenched high-purity b.c.c. metals because the high energy of formation (E_f) and high mobility (low E_m) of vacancies precludes the formation of high vacancy supersaturations. In the presence of interstitial impurities, however, phenomena analogous to those produced by vacancy supersaturation in f.c.c. metals have been detected. The activity of carbon in molybdenum exhibits a marked positive deviation from ideality,[2] which indicates repulsive interaction between these atoms, but the addition of the reactive Group IVA metal substitutional solutes should introduce attractive interactions between solute and carbon, to produce clustering effects in the solid solution. Thus, the interstitial prismatic defects observed might be considered as complex aggregates of vacancy–interstitial element–substitutional element clusters, i.e. embryo precipitate particles.

With prolonged ageing, the carbides and nitrides of zirconium and hafnium were found to precipitate on $\{100\}_{Mo}$ habit planes with the orientation relationship: $\{100\}_{Mo} \parallel \{100\}_{ppt}$; $\langle 100\rangle_{Mo} \parallel \langle 110\rangle_{ppt}$; $\langle 110\rangle_{Mo} \parallel \langle 100\rangle_{ppt}$. Trace analyses suggested that TiC and TiN precipitate on $\{130\}_{Mo}$ habit planes.

It has generally been accepted that the $\{100\}_{matrix}$ habit plane commonly observed for precipitates in f.c.c. alloys and in α-iron arises from the accommodation of strain due to differences in specific volume of matrix and precipitate in the direction of minimum elastic modulus. In molybdenum,

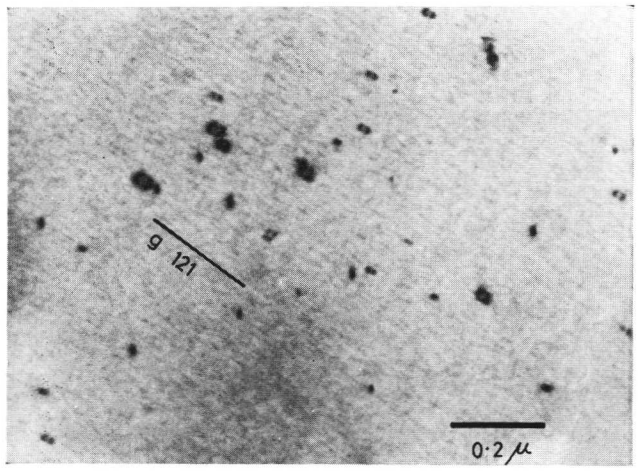

Fig. 1 Interstitial prismatic defects on $\{100\}_{Mo}$ *in quenched alloys.*

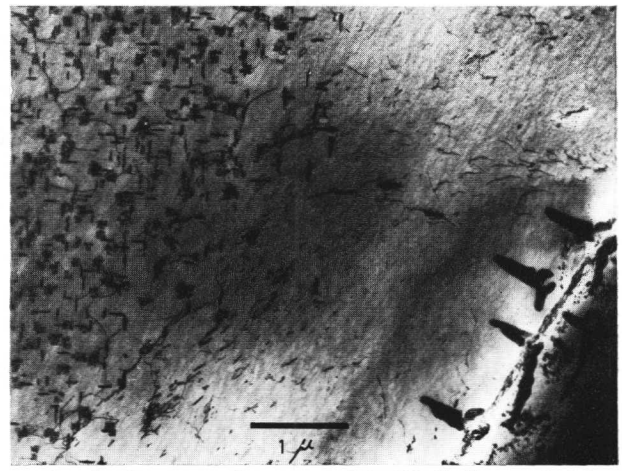

Fig. 2 Precipitate-free zone in Mo–Hf–C alloy aged 15 h at 1350° C.

TABLE I

Values of Strain Energy Associated with Precipitation of Group IV$_A$ Carbides and Nitrides on $\{100\}_{Mo}$ and $\{310\}_{Mo}$

Habit-Plane Relationship	Strain Energy (W) Contained Wholly in Molybdenum Matrix, cal/cm^3					
	TiC	TiN	ZrC	ZrN	HfC	HfN
$\{100\}_{Mo} \parallel \{100\}_{ppt}$	108·8	308·8	361·4	74·1	237·8	28·9
$\{310\}_{Mo} \parallel \{311\}_{ppt}$	0·45	37·2	741·6	311·2	573·8	236·9

however, $\langle 100 \rangle$ is the direction of maximum modulus; to rationalize this and also the different habit planes exhibited by the different compounds a new approach has been made by considering the strain energy/unit volume (W) associated with the formation of coherent precipitates of the various structures.[3]

Fig. 3(*a*) shows that the mismatch parameters between matrix and precipitate are least for zirconium and hafnium carbides and nitrides along directions contained in the cube plane. Mismatch parameters for titanium carbide and nitride (Fig. 3(*b*)) are least along directions other than those contained in the cube plane, namely between: $\langle 113 \rangle_{Mo}$ and $\langle 112 \rangle_{TiC,TiN}$; $\langle 331 \rangle_{Mo}$ and $\langle 310 \rangle_{TiC,TiN}$; $\langle 221 \rangle_{Mo}$ and $\langle 210 \rangle_{TiC,TiN}$.

Using calculated mismatch data and the known elastic constants of the molybdenum matrix, the local strain energy/unit volume (W) on a number of possible habit planes was calculated,[3] which involved computing the appropriate transformed tensor of the elastic constants C_{ijkl}, when

$$W = \tfrac{1}{2} C_{ijkl}\, \varepsilon_{ij}\, \varepsilon_{kl}$$

(ε_{ij} and ε_{kl} = principal orthogonal strains contained in the habit plane, obtained from the mismatch data). The results are given in Table I, and the very low strain energies associated with precipitation of TiC and TiN on the $\{310\}_{Mo}$ habit plane thus explain its selection. Values for ZrC, ZrN, HfC, and HfN are least on the $\{100\}_{Mo}$ plane, which confirms the experimental observations.

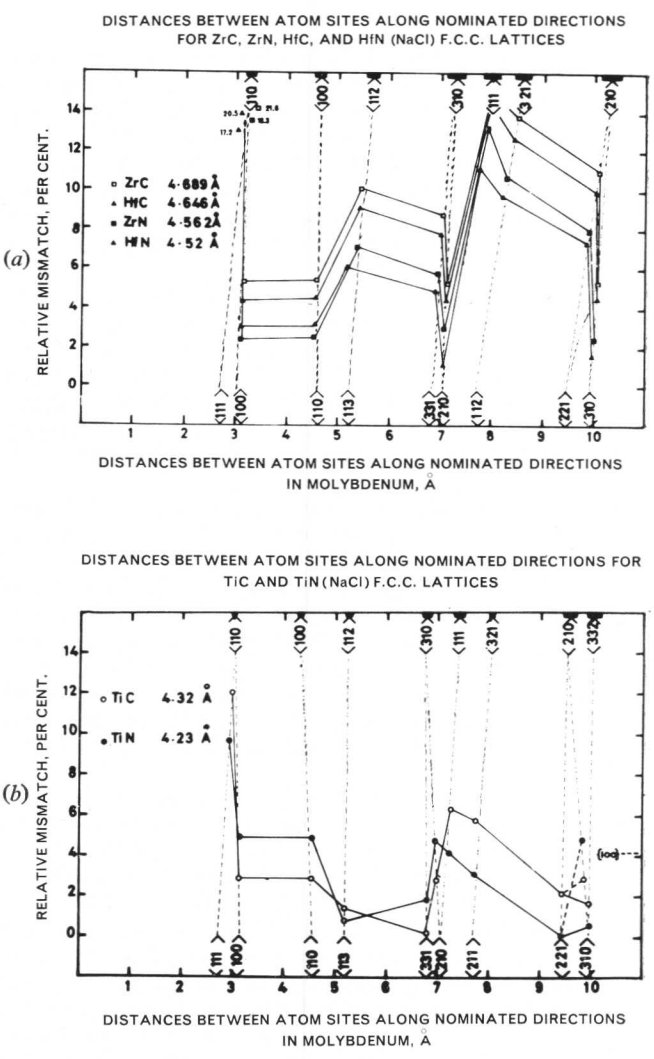

Fig. 3 Graphical representation of mismatch data along various nominated directions in Mo and the Group IV$_A$ carbides and nitrides. (a) *Mo–ZrC, ZrN, HfC, and HfN;* (b) *Mo–TiC and TiN.*

Acknowledgements

The authors wish to express their appreciation to Professor P. B. Hirsch, F.R.S., for the provision of laboratory facilities. One of them (N.E.R.), on leave from the Aeronautical Research Laboratories, Australia, is indebted to the Commonwealth Public Service Board for the award of a Post-Graduate Scholarship.

References

1. N. E. Ryan and J. W. Martin, Proc. 6th Plansee Seminar (1968), to be published.
2. A. C. Huang, P. P. Bansal, and L. Seigle (State University, New York), *U.S. Nat. Aeronaut. Space Admin. Rep.* (**NASA CR83391**) (Metallography), 1968.
3. N. E. Ryan, W. A. Soffa, and R. C. Crawford, to be published.

Research Note

Nucleation and Growth of α Rods from Pre-Existing α_1 Plates in Some Copper–Zinc Alloys

P. E. J. Flewitt

Various investigations[1–6] into the transformation of copper-zinc alloys during isothermal treatment have identified the phases formed and determined the influence of temperature and the time necessary for their formation. Metastable β-phase alloys containing 39–45% Zn, held isothermally just below the B_s temperature, develop a microstructure consisting of α_1 plates and α rods.*[4,5] The α_1, unlike the f.c.c. α, exhibits characteristics of the sub-zero martensite[7] but differs in that growth is diffusion-regulated.[1–4]

Although classical nucleation theory takes into account volume-, surface-, and strain-energy considerations, it does not include specifically the influence of pre-existing sites such as the precipitate/matrix interface which may from the aspects of composition and crystallography be suitable for nucleation of a second phase. In this note results are presented to show the importance of such considerations for nucleation of α from pre-existing α_1.

Experimental techniques have been described previously.[4] Fig. 1(*a*) shows α growing from the leading edges of an original α_1 pair reacted at 250° C, which is just below the B_s temperature for this composition.[4] At X (Fig. 1(*a*)) the plane of section $(110)_\beta$ is approximately parallel with the faulting within the α_1 and the change of habit corresponds with a change from the $(\bar{2}\,11\,12)_\beta$ habit plane of α_1[1,4] to the $[\bar{1}11]_\beta$ habit direction of α.[2] At Y cross-sections of rods are visible. To obtain more precise information, electron microscopy was carried out on thin foils prepared[7] from a 42·3 at.-% zinc alloy reacted at 250° C.

The $\alpha_1 + \alpha$ mixture (Fig. 1(*b*)) corresponds to Y in Fig. 1(*a*). Regions within the α_1 where non-regular annihilation of stacking faults has resulted are visible at A, (Fig. 1(*b*)), together with cross-sections of rods at B and C, and α that has nucleated independently in the adjacent matrix. Selected-area diffraction from the unfaulted region within the α_1 (A) and from α (B and C) nucleated at the α_1 edge, give similar patterns (Fig. 1(*b*)). Analysis of these shows unambiguously that the product and the unfaulted regions of the original plate are f.c.c. with a $[2\bar{3}1]$ normal to the foil. Since the β matrix normal is $[3\bar{1}1]$, (Fig. 1(*b*)), which is within 3° of the $[2\bar{3}1]_\alpha$

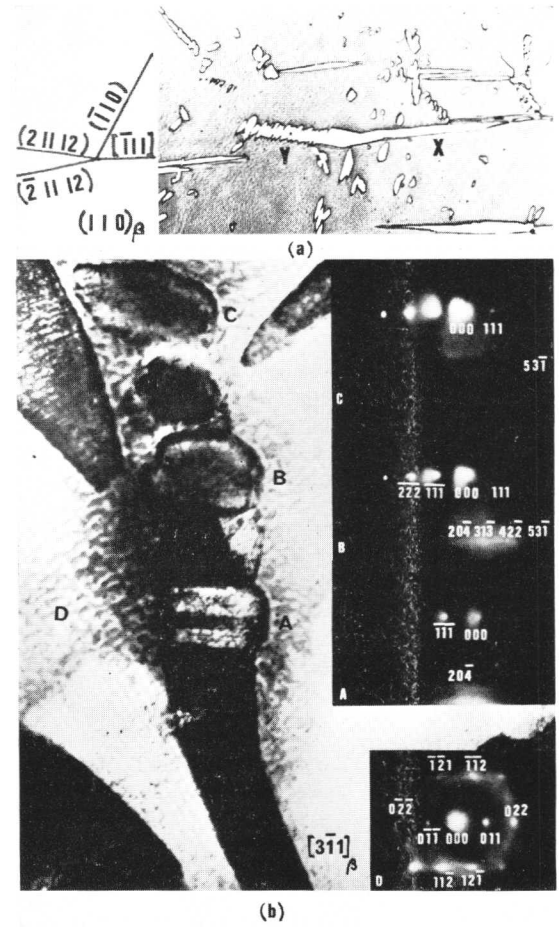

Fig. 1 (a) *Cu–42·3 at.-% Zn alloy isothermally transformed at* 250° *C for* 48 *h. The plane section is* $(110)_\beta$ *and* α *rods have grown from the leading edges of the pair of* α_1 *plates. Etched with alcoholic ferric chloride.* × 650.
(b) *Cu–42·3 at.-% Zn alloy isothermally transformed at* 250° *C for* 20 *h. The thin foil shows* α *rods in cross-section (B and C) growing from the original plate which contains regions relatively free of faulting (A). The* β *matrix (D) normal is* $[3\bar{1}1]_\beta$. × 20,000.

* Henceforth referred to simply as α_1 and α.

Manuscript received 3 July 1968. P. E. J. Flewitt, B.Sc., Ph.D., is in the Department of Metallurgy, University of Sheffield.